Deciphering the impact of lipid metabolism in breast cancer cells

Thesis

Deciphering the impact of lipid metabolism in breast cancer cells

Roberta Vazzana
OU Personal identifier: F8759767

Director of studies (Supervisor): **Dr. Kristina Havas**
External Supervisor: Prof. Tom Owen-Hughes

Registered degree: Doctor of Philosophy
Programme: Fundamentals of Cancer Biology
Discipline: School of Life, Health and Chemical Sciences
Registration owner: Affiliated Research Centre programme
Affiliated Research Centre: IFOM – FIRC Institute of Molecular Oncology
Submission: May 2021

ABSTRACT

Breast cancer represents the most common cancer among women and, despite increased early detection and improved therapeutic approaches, it also remains among the deadliest cancer worldwide. Accumulating evidence has shed light on the correlation between oncogenic signalling and metabolic reprogramming in cancer cells, and ten years ago metabolic reprogramming has been included among the hallmarks of cancer. In breast cancer a de-regulated metabolism has been described both in patients previously untreated and in treatment-resistant populations. Relapses are believed to arise from residual cancer stem cells that survive the initial therapeutic treatment. Tumour relapse still represents the main cause of breast cancer related death. Therefore, a comprehensive understanding of cancer stem cell biology and metabolism is needed to eventually impair the formation of tumour relapses and obtain more effective therapies.

In my Ph.D. research activity, I first investigated the correlation between lipid metabolism and breast cancer stem cells. Focusing specifically on lipid droplets (LD), the lipid storage organelle of the cell, I investigated the role of LD in breast cancer stem cells and tumorigenesis. Mammosphere assays and gene expression profiling, revealed a strong correlation between lipid droplet number and stemness in a panel of 4 different breast cancer cell lines. Furthermore, *in vivo* studies revealed the role of lipid droplets as a marker of cell harbouring increased tumorigenic capacity.

The accumulation of lipid droplets in cancer cells is part of a more general metabolic reprogramming characterizing breast tumours. Indeed, from a metabolic perspective, breast cancer cells show high glycolytic rates, intense anabolic growth and an up-regulation of de-novo fatty acid synthesis. Historically, a competitive relationship between glucose and fatty acid usage at the level of tissue metabolism was reported, with the cells ultimately relying upon only one of the two energy sources. In order to better dissect the role of lipid metabolism in breast cancer onset at a molecular level, I sought to investigate the previously described, but never elucidated, biochemical interplay between lipid and glucose metabolism. With a particular focus on the glycolytic enzyme Pyruvate kinase M2 (PKM2), which has been correlated also with the promotion and maintenance of the stemness traits, I focused my attention on the role of lipids as direct possible regulators of glycolysis and glycolytic enzymes. Medium and long-chain fatty acids are involved both in energy metabolism and in signalling pathways. Here, I show a new possible level of regulation, where fatty acids could act as allosteric regulators of PKM2. Using fatty-acid pull-down and *in vitro* binding assays, I demonstrate that PKM2 is able to directly interact with fatty acids. Particularly, my results suggest that it is the glycolytically inactive, dimeric form of PKM2

that preferentially interacts with FAs. To better dissect the functional implications of this regulation, finally I decided to characterize structurally the PKM2_K422E dimer mutant. Crystallization studies revealed a different conformation of the protein, compared to the wild type enzyme, that could correlate with the fatty acid binding capacity observed in my *in vitro* assays. Moreover, the structural characterization of the complex formed by PKM2_K422E and oleic acid is still under investigation.

Although further investigations are required to deeply characterize the molecular mechanism underpinning the correlation between altered lipid metabolism, LDs accumulation and stemness traits, the possibility that targeting lipid metabolism and LDs formation could impact on tumorigenesis, opens important scenarios for the development of new therapeutic strategies. My findings pave the way for new possible mechanisms by which deregulated lipid metabolism can impact on cellular proliferation and cancer progression, via the regulation of one of the key metabolic players and glycolytic enzyme PKM2.

Acknowledgments

I would like to express my gratitude and my deepest appreciation to all these people who have supported me during this study.

First of all I would like to thank my supervisor Kristina Havas, for the possibility she gave me to be enrolled in the Ph.D. Programme. She supported me with her constant presence, I greatly appreciated the knowledge she gave me, the technical and personal skills I developed thanks to her, the time she dedicated to me.

I would also thank my external supervisor Tom-Owen Hughes for his scientific support during these past years and my internal advisor Ylli Doksani for his presence and advices during this journey.

I would like to thank Sebastiano Pasqualato, who taught me all I know about the structural and the crystallography part of my project, for the interesting discussions and his constant support and help. I would also like to thank his friendly team, especially Valentina Cecatiello and Silvia Monzani, for their help in the sample preparation and their assistance. A special thanks goes to Janine Weber, for her help, assistance and interesting results discussion about the crystallization part of my Ph.D. project.

Thanks also to the present and past members of Kristina's group, in particular Ben, for his help and support during our days in the lab, and Deborah. My special thanks belong to all people contributed to my experimental work for practical, mental and theoretical support, in particular I would like to thank all my present and past lab mates, Paulina N., Chiara B., Alessandro P., Fabrizio P., Floriana A., Andrea D., Stefano M., Camilla G., Andrea G., Michele C., Tania D., Vanessa S. and Salvatore C. I am very grateful to all of you, thanks for being very often friends more than colleagues.

I am deeply grateful to Giorgio Scita and Simona Polo, for their intellectual contribution and advises throughout my PhD research as well as for their immense knowledge. Your lab meetings contributed greatly to my scientific knowledge and intellectual growth.

My special thanks belong to all members of the IFOM, and the head of the Institute for making an immense place to work. I am also very grateful to all the technical staff of the institute, their support was crucial for all my lab activities. A special thanks goes to Mio for her constant support, and the Open University U.K. that gave me the possibility to be part of their family during these years.

A huge thank to my wonderful family for their love and support.

Last but not least, I would like to thank my best friend and husband, Roberto, who has been my rock during these years. I deeply appreciate him for his enduring support, patience and scientific assistance. He inspired and encouraged me to be the best that I can.

Table of contents

List of tables:

List of Figures:

ABBREVIATIONS

ACC	Acetyl-CoA Carboxylase
ATP	Adenosine Triphosphate
BC	Breast Cancer
CD	Cluster of Differentiation
CE	Cholesterol Esters
CPT-1	Carnitine Palmitoyl Transferase 1
CSC	Cancer Stem Cells
DDR	DNA Damage Repair
EGF	Epidermal Growth Factor
EGFR	Epidermal Growth Factor Receptor
EMT	Epithelial Mesenchymal Transition
ER	Endoplasmic Reticulum
ER	Estrogen Receptor
F-1,6-BP	Fructose 1,6 Biphosphate
F-2,6-BP	Fructose 2,6 Biphosphate
FAO	Fatty Acid Oxidation
FASN	Fatty acid Synthase
FAT	Fatty Acid Translocase
FGFR-1	Fibroblast Growth Factor Receptor 1
GFAP	Glial Fibrillary Acidic Protein
HIF-1	Hypoxia-Inducible Factor 1
HK	Hexokinase
hnRNP	Heterogeneous Nuclear Ribonucleoprotein family
LD	Lipid Droplets
MFE	Mammosphere Formation Efficiency
mTOR	Mechanistic Target of Rapamycin
MUFA	Mono-Unsaturated Fatty Acids
NADPH	Nicotinamide Adenine Dinucleotide Phosphate
NF-kB	Nuclear Factor Kappa B
OXPHOS	Oxidative Phosphorylation
PDH	Pyruvate Dehydrogenase
PEP	Phosphoenolpyruvate
PFK	Phosphofructokinase

PFKFB	6-Phosphofrukto-2-kinase/fructose-2,6-biphosphatase
PK	Pyruvate Kinase
PKL	Pyruvate Kinase Liver type
PKM1	Pyruvate Kinase Muscle 1 type
PKM2	Pyruvate Kinase Muscle 2 type
PKR	Pyruvate Kinase Red blood cells type
PLIN2	Perilipin 2
PPP	Pentose-Phosphate Pathway
PR	Progesterone Receptor
RFS	Relapse Free Survival
ROS	Reactive Oxygen Species
SAICAR	Succinyl-Amino-Imidazole- Carboxamide-Ribose-5'-phosphate
SCD1	Stearoyl CoA Desaturase 1
SE	Stearyl Esters
SEC	Size Exclusion Chromatography
SLS	Static Light Scattering
SREBP-1	Sterol Regulatory Element Binding Protein 1
TAG	Triacylglycerols
TCA	Tricarboxylic Acid
TEM	Mesenchymal Epithelial Transition
TOFA	5-tetradecyloxy-2-furoic acid

1. INTRODUCTION

The research activities of my Ph.D. are dedicated to the dissection of the lipid metabolic role in breast cancer cells, with a particular emphasis on the implications in cancer stemness. Moreover, I focused my attention on the biochemical characterization of the role of lipids in Pyruvate kinase M2 regulation, a glycolytic gatekeeper enzyme involved in cancer onset and progression. Thus, this introductive chapter will illustrate the role of lipid metabolism in cancer stemness and in the metabolic reprogramming observed in cancer cells, with a particular focus on the interplay between lipid and glucose metabolism.

1.1 Breast Cancer

Breast cancer (BC) remains the most commonly diagnosed cancer among women worldwide (1), representing 24.5% of all new cancer cases diagnosed in 2020 **(Figure 1.1)**. Despite increased early detection and improved therapeutic approaches, it also remains among the deadliest, with over 50,000 women succumbing to breast cancer every year. Highlighting the need for more effective diagnostic and therapeutic strategies. There are both genetic and environmental factors that can contribute to the development of breast cancer. Most notably, germline mutations in tumour suppressors BRCA1 and BRCA2 correlate with an increased risk of developing breast and ovarian cancers. In addition, epidemiological studies have suggested that obesity, alcohol consumption, use of contraceptives and hormone replacement therapy can all correlate with an increased risk of breast cancer (2).

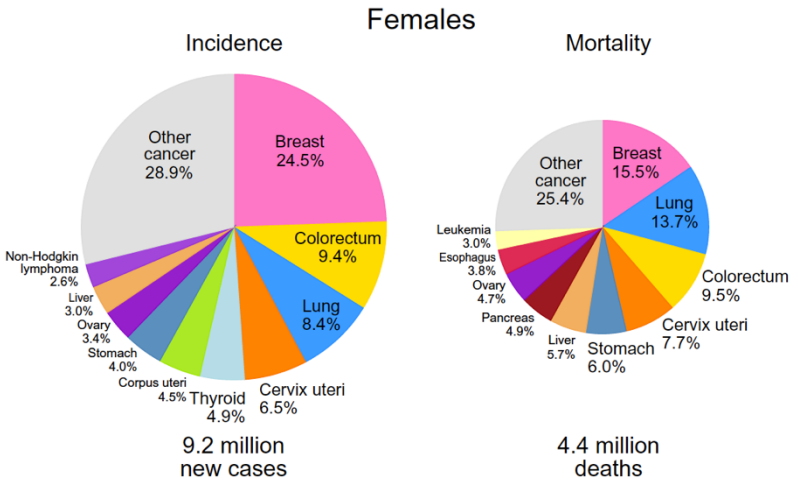

Figure 1.1 Percentage of new cases and mortality for the most common cancers in 2020 for women (1).

BC is not one disease, but can be classed into at least four different subtypes with a range of histopathological features, molecular alterations and a highly variable response to

therapeutic treatments. In order to better classify the subtypes, histopathological criteria, including tumour grade, tumour stage, lymph node and metastasis, are the most widely used features and have both diagnostic and prognostic relevance (3). In addition, the status of hormone receptors like oestrogen receptor (ER), progesterone receptor (PR), epidermal growth factor receptor 2 (HER2/neu), are also used to stratify BC tumours. Their expression has been shown not only to have a prognostic value but also drive the choice of therapeutic regimen (4). Receptor expression levels are used to stratify breast cancer into four mains: luminal A (ER+, PR+, HER2-, lowKi-67), luminal B (ER+, PR+, HER2-/+, highKi-67), HER2 overexpressing (ER-, PR-, HER2+) and triple negative (ER-, PR-, HER2-) (5).

Common molecular features of breast cancer include impaired DNA damage repair (DDR) resulting in genomic instability, mutations, chromosome rearrangements (6) and up-regulation of signalling pathways that promote cellular growth and proliferation. Recent studies have also shed light on the correlation between oncogenic signalling and metabolic reprogramming in cancer cells.

Metabolic reprogramming has been included among the hallmarks of cancer (7). The most studied metabolic pathways in cancer, such as aerobic glycolysis, nucleotide and fatty acids synthesis, and glutamine metabolism, are essential to support the higher cellular proliferation rates and growth. These pathways are regulated by oncogenic signalling networks and recent evidences have illustrated that, although all tumors undergo metabolic reprogramming, perhaps unsurprisingly, metabolic profiles differ among tumours. This observed heterogeneity also explains the varying efficacies of metabolism targeting therapies. For example, the use of antagonists of folate metabolism has been shown to highly effect most of the haematological cancers but not solid tumours (8). Moreover, also in the context of the same tumour, an intra-tumoral heterogeneity has been described that supports tumour evolution from primary site to the metastatic lesion, suggesting a scenario in which tumour metabolism is highly flexible and context-specific. In breast cancer dysregulated metabolism has been described both in untreated and in treatments-resistant populations. In most of the cases, the failure of the therapeutic approach is caused by the acquisition of secondary resistances (9). Resistant populations of cells have been shown to be, in part, characterized by a rewired metabolism (10, 11). This is particularly the case for HER2+ and triple negative breast cancers (12), which represent the BC subtypes most prone to development of therapeutic resistance (13, 14). The intense study of cancer metabolism has recently led to the recognition that cancer is not only a genetic disease but it also represents a metabolic disease (15). In this context, it becomes clear that a deep comprehension of the specific metabolic addictions observed in cancer cells is crucial, since they represent potentially important therapeutic targets.

1.2 Cellular metabolism as a hallmark of cancer

Metabolism is a fairly recent addition to the list of factors required for the transition to malignancy. But, the study of cancer metabolism began nearly a century ago in 1927 with Otto Warburg's seminal observation that tumour cells converted glucose to lactate in the presence of oxygen, and as such it represents one of the oldest fields of cancer biology (16). Although, Warburg hypothesized that this phenomenon was due to a respiratory impairment in mitochondria, further studies revealed that, in most of the cases, mitochondria were not defective in oxidative phosphorylation. Instead, the increased lactate production was the consequence of a general metabolic reprogramming required to sustain the increased energy requirements in cancer cells. Indeed, quiescent and proliferating cells differ considerably in their metabolism. The most prominent difference is the fate of the carbon sources (17). While in non-proliferating cells glucose is mostly converted into pyruvate and used in the tricarboxylic acid cycle (TCA cycle) to generate acetyl-CoA and ATP, in active proliferating cells glucose is used to sustain the pentose phosphate pathway, cholesterol and non-essential amino acid generation (18) (**Figure 1.2**).

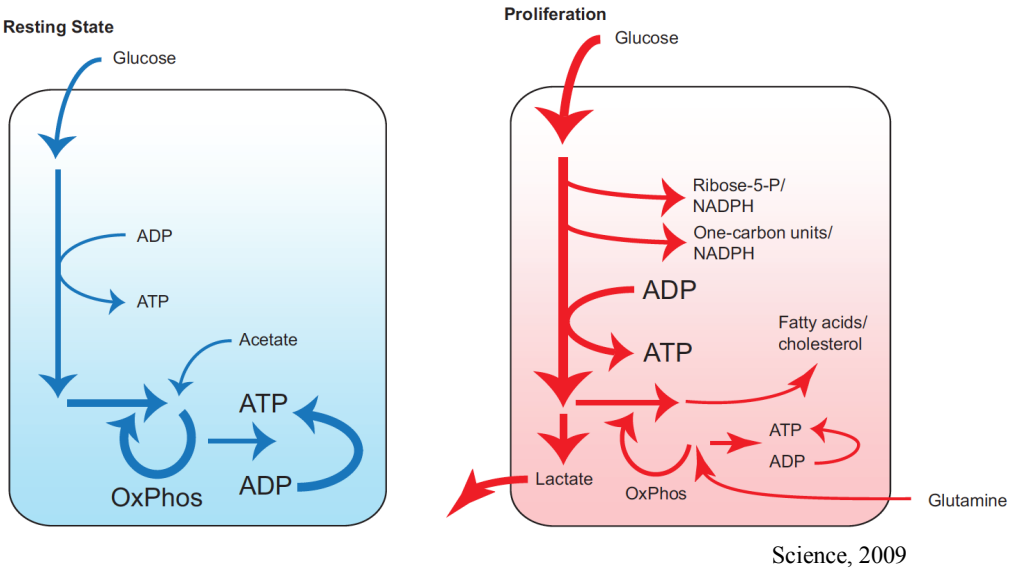

Figure 1.2. Glucose metabolism in quiescent and proliferating cells (17).

Recently, it has become evident that tumour cells are characterized not only by aerobic glycolysis, but by increased uptake of glucose and amino acids along with dysregulation of nucleotide bio-synthesis and lipid metabolism. Collectively, this phenomenon is referred to as the "metabolic reprogramming" of cancer cells (19). The metabolic reprogramming that accompanies the transition to malignancy encompases nearly every aspect of cellular

metabolism. Given the breadth of the field I will now focus on reviewing the contributions of lipid and glucose metabolism in supporting tumour metabolism.

1.3 The role of glycolytic enzymes in cancer

The best characterized aspect of tumour metabolic reprogramming is the aerobic lactate production associated with increased glucose uptake referred to as aerobic glycolysis or the Warburg effect (20). The shuttling of glucose derived pyruvate into lactate production comes at the expense of efficient mitochondrial oxidative phosphorylation ATP production. To compensate for this, tumours uptake significantly higher amounts of glucose, thus providing not only important intermediary metabolites but also sufficient ATP.

The increased flux of glucose through glycolysis is supported by the activity of three gatekeeper enzymes that catalyse three (nearly) irreversible reactions: Hexokinase, Phosphofructokinase and Pyruvate kinase (**Figure 1.3**).

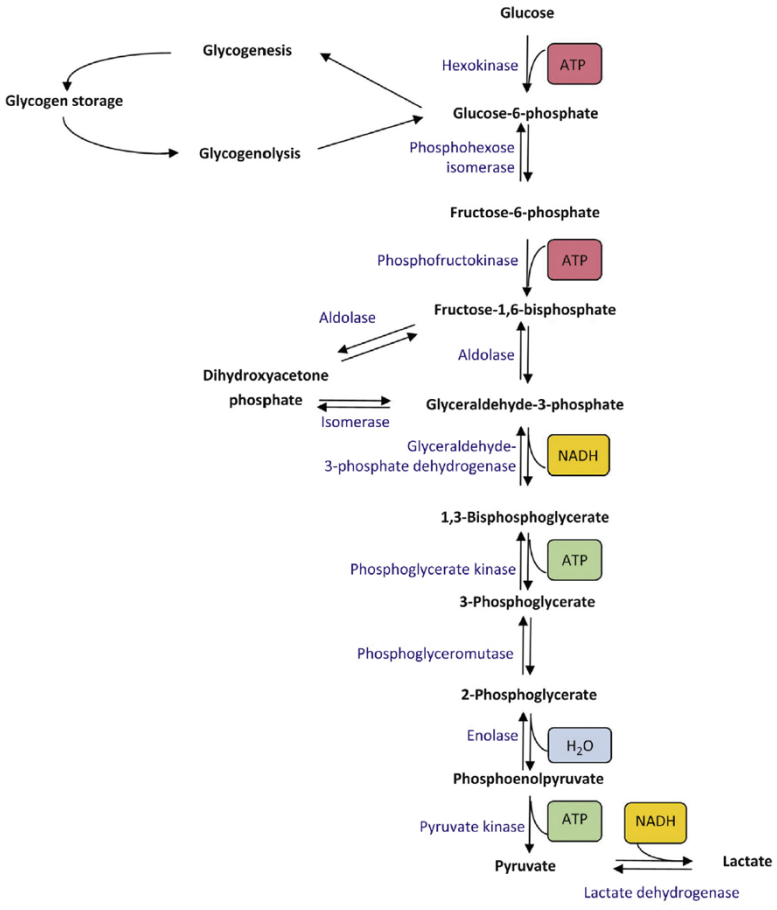

Figure 1.3. The glycolytic pathway (Werner, Doenst et al. 2016).

The first enzyme involved in the glycolytic pathway is Hexokinase (HK), that catalyses the conversion of glucose to glucose-6-phosphate (**Figure 1.3**), thus trapping it inside the cell.

There are five reported isoforms (I, II, III, IV, V) in human, and HKII overexpression has been observed in many tumours and linked with a more aggressive phenotype (21, 22). Moreover, in HKII knockout mice models of KRas-driven lung cancer and ErbB2-driven breast cancer, it was shown the key role of HKII for tumour development (23).

In ovarian cancer HKII overexpression has been shown to be involved in the resistance to cisplatin treatments, by increasing cisplatin-induced autophagy mediated by ERK1/2 phosphorylation (24). Moreover, in human glioblastoma it was shown that its deletion associates with a higher apoptotic index (25). The next glycolytic enzyme that catalyses an irreversible reaction, is Phosphofructokinase (PFK). PFK converts fructose-6-phosphate to fructose 1,6 bisphosphate (F-1,6-BP). It has been shown that the most important PFK activator is fructose-2,6-biphosphate (F-2,6-BP) that is generated by 6-phosphofrukto-2-kinase/fructose-2,6-biphosphatase enzyme (PFKFB) (26) (**Figure 1.4**). Thus, creating a positive feedback mechanism: PFK activation is sustained by F-2,6-BP, that in this way supports the high glycolytic rate.

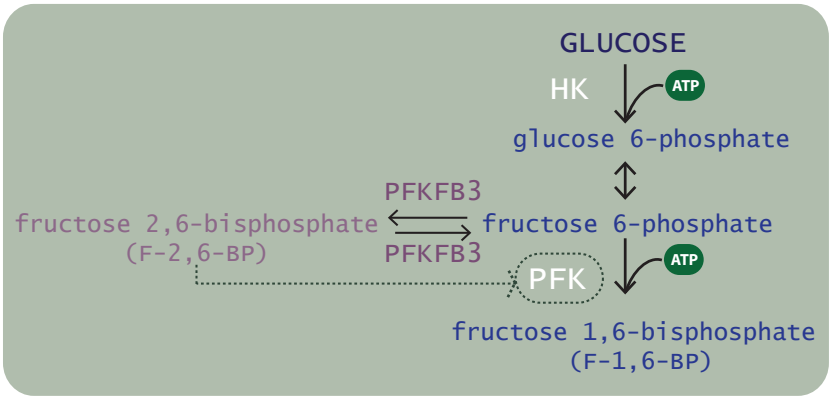

Figure 1.4. Schematic representation of the first three reactions in glycolysis and the role of PFKFB.

Pyruvate kinase (PK) catalyses the terminal reaction of the glycolytic cascade. In this step, PK enzyme is responsible for the conversion of phosphoenolpyruvate (PEP) to pyruvate, with the generation of ATP. In mammals, there are four different forms of Pyruvate Kinase (L, R, M1and M2) (27) encoded by two different genes: *PKLR* and *PKM*. By alternative splicing, PKL and PKR are produced from the *PKLR* gene transcripts, while PKM1 and PKM2 are produced by from *PKM* gene transcripts. The isoform expression is tissue-specific, with PKL and PKR predominantly present in liver and red blood cells respectively; PKM1 is present in most adult tissues, while PKM2 is expressed by embryonic cells and tumours (28). Indeed, during development, PKM2 is substituted by the tissue-specific form,

accordingly. Importantly, it has been shown that in tumour cells PKM2 is highly expressed, while the expression of the other forms is negligible (29).

The alternative spliced forms of PKM1 and PKM2, differ by only one exon. PKM1 includes exon 9 while excluding exon 10 and *vice versa* for PKM2 (**Figure 1.5A**). The two exons have the same length, but the sequence codifying for 56 amino acids differ by 23 residues (**Figure 1.5B**) (30). The alternative splicing of the PKM mRNA is regulated by members of the family known as heterogeneous nuclear ribonucleoprotein family (hnRNP), particularly hnRNP1-2-I, that are able to bind the sites flanking exon 9, thus excluding it and promoting the exon 10 inclusion with the consequent PKM2 expression (31). Interestingly, in some cancers, the oncogene c-Myc has been shown to upregulate those hnRNP proteins, inducing PKM2 expression (32).

A

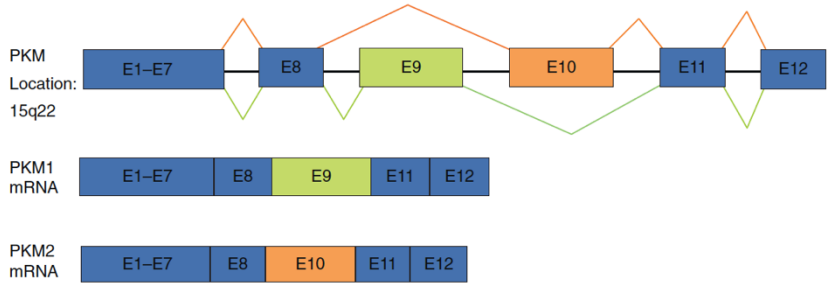

B

```
  1 MSKPHSEAGT  AFIQTQQLHA  AMADTFLEHM  CRLDIDSPPI  TARNTGIICT
 51 IGPASRSVET  LKEMIKSGMN  VARLNFSHGT  HEYHAETIKN  VRTATESFAS
101 DPILYRPVAV  ALDTKGPEIR  TGLIKGSGTA  EVELKKGATL  KITLDNAYME
151 KCDENILWLD  YKNICKVVEV  GSKIYVDDGL  ISLQVKQKGA  DFLVTEVENG
201 GSLGSKKGVN  LPGAAVDLPA  VSEKDIQDLK  FGVEQDVDMV  FASFIRKASD
251 VHEVRKVLGE  KGKNIKIISK  IENHEGVRRF  DEILEASDGI  MVARGDLGIE
301 IPAEKVFLAQ  KMMIGRCNRA  GKPVICATQM  LESMIKKPRP  TRAEGSDVAN
351 AVLDGADCIM  LSGETAKGDY  PLEAVRMQNL  IAREAEAAIY  HLQLFEELRR
401 LAPITSDPTE  ATAVGAVEAS  FKCCSGAIIV  LTKSGRSAHQ  VARYRPRAPI
451 IAVTRNPQTA  RQAHLYRGIF  PVLCKDPVQE  AWAEDVDLRV  NFAMNVGKAR
501 GFFKKGDVVI  VLTGWRPGSG  FTNTMRVVPV  P
```

Figure 1.5. PKM2 gene and PKM2 aminoacidic sequence. **(A)** Alternative spliced forms of PKM1 and PKM2 (33). **(B)** Aminoacidic sequence of human Pyruvate kinase M2. The underlined residues represent the 56 amino acids codified by exon 10 (27).

1.3.1 Pyruvate kinase M2: a glycolytic gatekeeper deregulated in cancer

While both the isozymes show the same catalytic activity, they are differently regulated. In fact, PKM1 is a constitutively active tetramer, while PKM2, thanks to the presence of the previous cited 22 amino acids, can be allosterically regulated. Indeed, PKM2 shows an

internal binding pocket necessary to host fructose-1,6-biphosphate (FBP), considered essential for the formation of the tetrameric structure (34). As a consequence of this, PKM2 can switch from a less active dimer to a more active tetramer. Christofk and collaborators demonstrated in 2008 that in cancer cells in which PKM2 was depleted and substituted with PKM1 isoform, there was a metabolic switch from aerobic glycolysis to the physiological coupled glycolysis/TCA cycle. Moreover, PKM1 expressing cancer cells, compared to the ones expressing PKM2, were not able to develop tumours upon xenotransplantation into mice (35). These results highlight the important role of PKM2 in sustaining cancer cell metabolism, making it an interesting molecular target for cancer therapy.

Through allosteric regulation PKM2 can switch from the highly active tetrameric form, able to sustain the production of pyruvate during glycolysis, to the lower active dimeric form (**Figure 1.6**). Despite being comprised of the same monomeric unit, the tetrameric and dimeric forms of PKM2 have very different functions. Compared to the dimer, the tetramer displays a higher affinity toward its substrate phosphoenolpyruvate and this correlates with the higher kinasic activity. Intriguingly, cytosolic association between the tetrameric form of PKM2 and glycolytic enzymes, such as hexokinase and enolase, has been reported, suggesting the role of metabolic factories in sustaining a processive glucose conversion to lactate (36).

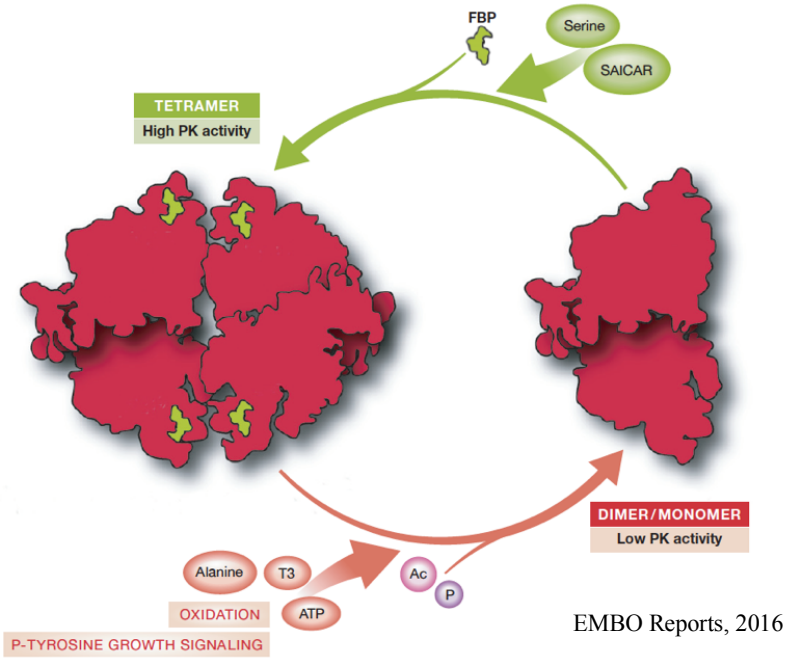

Figure 1.6. Possible conformations of Pyruvate kinase M2 and allosteric regulators (37). FBP: Fructose 1-6 bisphosphate; SAICAR: PhosphoribosylAminoImidazolesuccinoCarboxamide; Ac: acetylation; P: phosphorylation; T3: 3,3',5-triiodothyroxine; ATP: Adenosine triphosphate.

In tumours PKM2 exists primarily in its dimeric state (38) (39), meanwhile forced expression of tetrameric PKM2 has been shown to suppress tumorigenesis (40). The development of a ELISA has allowed researchers to discriminate the dimeric form of PKM2 in plasma from cancer patients (33). These studies suggested a role for dimeric PKM2 as a tumour marker for renal carcinoma and pancreatic cancer (41-43).

The accumulation of the dimer leads to a lower conversion rate of PEP to pyruvate, and subsequently to the accumulation of glycolytic intermediates (34) leading to increased flux through anabolic pathways such as the pentose-phosphate pathway (PPP) that sustains the growth and the proliferation of tumour cells (44, 45). For example, the production of ribose-5-phosphate, necessary for nucleic acid biosynthesis, depends upon glucose-6-phosphate flux through the pentose-phosphate pathway (PPP). Another important metabolite generated by PPP is nicotinamide adenine dinucleotide phosphate (NADPH), an important cofactor and electron donor essential for providing the reducing power to anabolic pathways and for preventing oxidative stress (46). Instead, another component of the glycolytic pathway, 3-phosphoglycerate, is an essential precursor for the biosynthesis of amino acids glycine and serine, whose synthesis was shown to be essential in breast and lung cancer (47, 48).

In addition to its well characterized role in glycolysis, there is mounting evidence to suggesting a non-canonical function of PKM2 in cancer cells. Dimeric PKM2 was recently reported to localize to the nucleus where it was shown to act as a protein kinase (49-51). Upon translocation into the nucleus, it has been proposed that PKM2 is able to phosphorylate multiple proteins including ERK1/2, STAT3, and histone H3 (45, 52, 53). STAT3 phosphorylation PKM2-mediated has been linked with tumorigenesis in anaplastic large cell lymphomas (54) and with enhanced cell migration in colon-rectal cancer (55). The role of PKM2 in tumorigenesis has been also shown in brain tumours, where the phosphorylation of another substrate, histone H3 at Threonine 11 residue, mediated by PKM2, leads to the activation of cyclin D1 and c-Myc, highlighting the role of the dimeric nuclear form of PKM2 as a novel regulator of cell-cycle progression and proliferation (53).

Additionally, nuclear PKM2 was also shown to regulate ß-catenin, Oct4 and HIF-1. Indeed, in glioma cells PKM2 nuclear translocation, regulated by the epidermal growth factor receptor (EGFR), leads to the activation of beta-catenin with the consequent expression of cyclin D1. This mechanism has been correlated with glioma malignancy, since PKM2-mediated beta-catenin transactivation has an impact on cell proliferation and tumorigenesis (56). In addition to this, PKM2 has been described as a novel interactor of Oct-4 transcription factor, whose trans-activation is important for the maintenance of the pluripotent state of stem cells (57). Recently, PKM2 transcription has been shown to be activated by the

hypoxia-inducible factor 1 (HIF-1). Moreover, once expressed, PKM2 contributes to the activation of HIF-1 factor, creating a positive feedback mechanism that sustains glucose metabolism reprogramming, angiogenesis and cancer progression (58).
Overall, the glycolytic and non-glycolytic protein kinase roles of PKM2 have been shown to play key roles in regulating the survival, pluripotency and the metabolic reprogramming observed in cancer cells.

1.3.2 PKM2 allosteric regulation in cancer

The allosteric regulation of PKM2 modulates the multimerization state of the protein (59). Glycolytic intermediate, fructose 1,6-biphosphate (FBP), was one of the first regulators described to induce the tetrameric active form of PKM2, and it remains the most significant, tying PKM2 activity to glucose availability (60). *In vitro* studies performed toward the middle and the end of the last century have shown that PKM2 activity could be also modulated by other macromolecules, such as amino acids or lipids (61-63). More recent work has identified serine as another allosteric activator of PKM2 able to induce the tetramerization of the protein, and has shown that serine deprivation correlates with a reduced activity of the enzyme (64). An additional PKM2 activator is an intermediate of the de novo nucleotide synthesis, SAICAR (succinylaminoimidazolecarboxamideribose-5'-phosphate). SAICAR was shown to induce PKM2 activity promoting cancer cell survival also under glucose deprivation (38) (**Figure 1.6**). In addition, several negative allosteric regulators of PKM2 have been described. Alanine, phenylalanine and tryptophan have been shown to inhibit tetramerization hence stabilizing the dimeric form or the so-called T-state, which represents an inactive tetramer (65).
Multiple post-translational modifications have been associated with the inhibition of PKM2 activity. For example, fibroblast growth factor receptor 1 (FGFR-1) can phosphorylate PKM2 on Tyr105 impeding FBP binding and hence the activation of the enzyme (66). In cancer cells, the oxidation of Cys358 mediated by increased Reactive Oxygen Species (ROS), inhibits PKM2 activity (67). This allows for up-regulation of the ROS detoxification process thanks to the boosted pentose phosphate pathway, and it is used by the tumour cells to resist in more hostile environments. The inhibition of PKM2 can also be mediated by acetylation. Indeed, as shown by Lei and collaborators, the acetylation of Lys433 leads to a lower PKM2 affinity towards its allosteric activator FBP and promotes PKM2 nuclear translocation (50). Furthermore, high glucose levels stimulate PKM2 acetylation at Lys305; this post-translational modification has been associated with a decreased PKM2 activity and with an increased protein degradation through a chaperone-mediated autophagic process

(68). In addition to this, PKM2 acetylation mimic mutant Lysine-305-Glutamine (K305Q) stably expressed in lung cancer cells, induces a massive accumulation of glycolytic intermediates and NADPH, and correlates with a higher proliferative phenotype of cancer cells, suggesting again the importance of PKM2 regulation in the cellular microenvironment.

1.4 The glucose-fatty acid cycle

Glycolytic enzymes are key players in the cellular metabolism. Several studies have highlighted the role of free fatty acids and lipids as regulators of glycolytic enzymes, such as phosphofructokinase and pyruvate kinase (69, 70), connecting the two main cellular pathways involved in energy production. The first description of the role of lipids in the regulation of glucose metabolism was reported in the 1960s. Indeed, in 1963 Philip Randle showed for the first time that there existed a hormone independent cross-talk between glucose metabolism and fatty acid oxidation (71). This interplay, later named "Randle Cycle" or "glucose-fatty acid cycle", describes a mechanism by which glucose metabolism is inhibited when high levels of fatty acids are available and, *vice versa*, fatty acid oxidation is inhibited when glycolysis proceeds with high processivity thanks to the accumulation of intra-cellular glucose. These observations generated interest in the field and some years later new studies emerged highlighting the role of short and long chain fatty acids in the inhibition of pyruvate kinase enzyme (72). Since then, many studies tried to better characterize, from a molecular point of view, the relationship between glucose and fatty acids usage. Some examples are the description of the role of citrate as allosteric inhibitor of phosphofructokinase that has been shown in heart and liver (73), and the role of pyruvate dehydrogenase (PDH) described more recently as a key regulator of glucose and lipid homeostasis (74) in *in vivo* studies of obese mice. Although, further studies are still required to better elucidate all the molecular mechanisms involved in the direct regulation of this complex network.

Despite the initial studies described above were focused on the role of glucose-fatty acid interplay in normal tissues, an antagonism between fatty acids oxidation and glycolysis has been described in many cancers. Indeed, the switch from the catabolic to the anabolic metabolism observed in cancer cells, represents part of the execution of the Randle cycle.

In non-Hodgkin lymphomas, a dysregulation of both fatty acids biosynthesis and glycolysis has been described in the context of a more general metabolic alteration, with human non-Hodgkin lymphomas B-cells showing an up-regulation of both fatty acid synthesis and the glycolytic flux in the comparison with primary B cells (75). Colon-rectal cancer and

glioblastoma are instead considered tumors highly dependent on glucose to sustain their proliferation but, while this description pretty well defines the primary tumor, in the metastatic lesions both tumors show a switch from glycolysis to fatty acid oxidation to fulfill their energy requirements and to survive in hostile microenvironments (76, 77). An important aspect to consider is that not all the internalized glucose is used to generate pyruvate; indeed, glucose is often re-directed to the pentose-phosphate pathway (PPP) where sustains nucleotide synthesis and NADPH production. Thus, even if the concept of cancer cells relying on glucose metabolism more than fatty acid oxidation seems to be counterintuitive, in the reality it is not about ATP generation but it is about the increased anabolic metabolism able to sustain cell growth.

Cancer metabolism is highly plastic. The regulation of the cellular metabolic behavior mediated by the nutrient accessibility, firstly described by Randle, can be important for the generation of novel therapeutic strategies. Deciphering the metabolic connections between the glycolytic pathway and fatty acids metabolism can inspire new approaches to better tackle cancer cells.

1.5 Dysregulated lipid metabolism in cancer

Lipids play an essential role within the cancer cell functioning as a component of cellular membranes, carbon sources, and as signalling molecules. As anticipated before, in order to fulfil their lipid requirements, cancer cells reprogram their lipid metabolism to increase both lipid uptake and de *novo* fatty acid synthesis. In healthy cells, lipid uptake from the bloodstream usually satisfies the cells demands for fatty acids. In contrast, in cancer cells, uptake of exogenous fatty acids is not sufficient to meet their needs and requires supplementation, which is achieved through upregulation of endogenous FA biosynthesis. This is realized by dysregulation of lipogenic enzymes, including Fatty Acid Synthase (FASN), the enzyme that catalyses the production of Palmitate starting from Acetyl-CoA and Malonyl-CoA. Many studies have reported the overexpression of FASN in multiple cancers, including breast cancer (78), prostate cancer (79), glioma (80) and melanoma (81). Targeting of FASN has been shown to be an effective anti-tumor strategy suggesting that *de novo* fatty acid biosynthesis plays a key role in sustaining cancer progression and survival (82) .

An important role in cancer lipogenesis is also played by the Acetyl CoA carboxylase (ACC) and stearoyl CoA desaturase 1 (SCD1) enzymes. The lipogenic pathway consists in the production of *de novo* fatty acids starting from acetyl-CoA, that is generated after glycolysis and the mitochondrial tricarboxylic acid cycle (TCA). Acetyl-CoA is converted into malonyl-CoA by ACC enzyme, and then malonyl-CoA with acetyl-CoA forms palmitic acid in a reaction catalysed by FASN enzyme. Afterwards, palmitic acid is transformed in stearic acid by the elongase ELOVL6 (83). The final products palmitoleoyl-CoA and oleoyl-CoA, generated from palmitoyl-CoA and stearoyl-CoA in a reaction catalysed by SCD1, are transformed in triglycerides or phospholipids for membrane generation or storage (**Figure 1.7**).

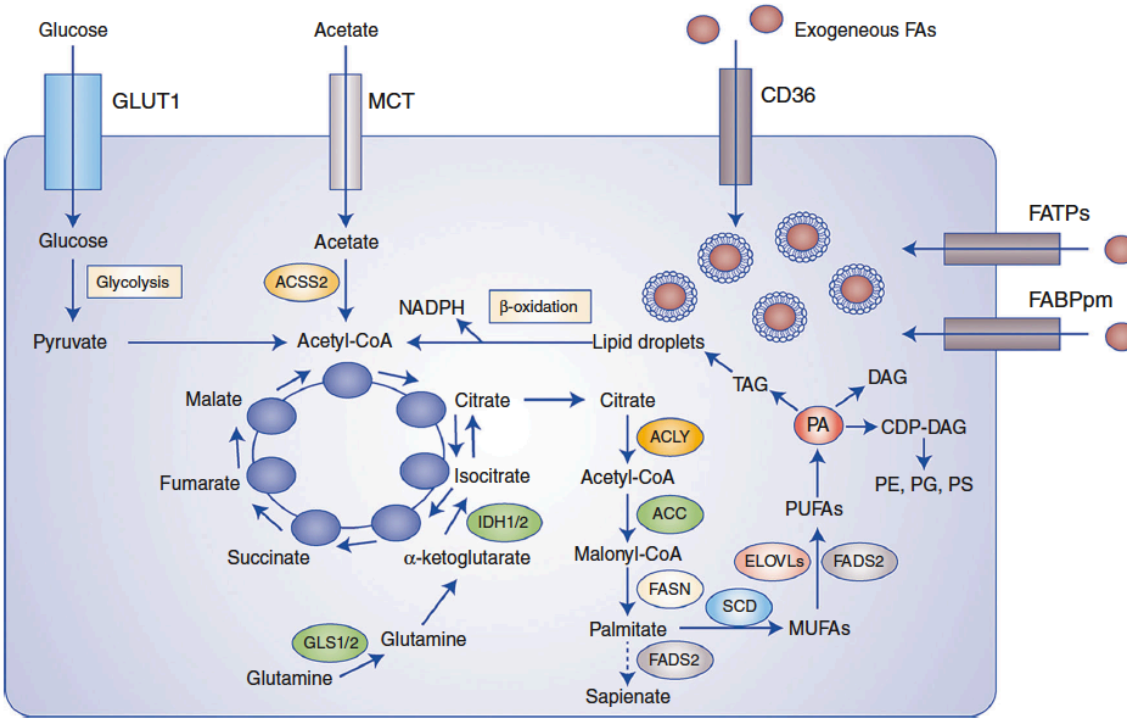

Br J Cancer, 2020

Figure 1.7. Fatty acids generation in cancer cells rely on *de novo* lipogenesis and exogenous uptake (84, 85).

ACC, FASN and SCD1 expression is regulated by signalling pathways. Among them, two of the most essential key regulators are: SREBP-1, sterol regulatory element-binding protein, important for lipid and cholesterol homeostasis, and mTOR, a major regulator of growth (86, 87). SREBP-1 is the most important transcription factor involved in the gene expression of lipogenic genes, such as *ACC*, *FASN* and *SCD1*. In cancer, the epidermal growth factor (EGF) activates the PI3-kinase/Akt pathway leading to the phosphorylation and activation of SREBP-1 (88). In glioblastoma, in particular, SREBP-1 has been correlated with tumor

growth and therapeutic resistance (89, 90). In SREBP-1 activation can also be involved the mechanistic target of rapamycin (mTOR).

mTOR is a Serine/Threonine kinase and is the catalytic subunit of two protein complexes mTORC1 and mTORC2 (91). The PI3K/AKT/mTORC1 dependent pathway strongly regulates SREBP1 activity, by inducing the activation of the transcription factor with the consequent expression of lipogenic genes (92). In addition, also mTORC2 is an important regulator of lipid metabolism. Upon SREBP1 activation, mTORC2 up-regulates *de novo* synthesis of glycerophospholipids and sphingolipids, and its overexpression has been associated with tumorigenesis in hepato-carcinoma (93).

Beyond synthesis cancer cells have been shown to uptake exogenous fatty acids. One of the major players in the uptake of exogenous fatty acid is CD36 receptor, cluster of differentiation 36, also known as Fatty Acid Translocase (FAT). Interestingly, CD36 overexpression has been associated with epithelial-mesenchymal transition in hepato-carcinoma (94) and with tumour dissemination and invasion in ovarian cancer (95). In ER+ breast cancer patients, high circulating free fatty acid levels and high CD36 expression correlate with tumor progression and aggressiveness by activating oestrogen receptors and mTOR signalling pathway (96).

It is broadly accepted that fatty acids, together with cholesterol, are fundamental to cancer cells for membrane biosynthesis and fluidity, and for providing energy under stressful conditions. One of the advantages conferred by *de novo* fatty acid synthesis is the generation of saturated fatty acids. Indeed, the higher level of membrane saturation in cancer cells has been correlated with a lower vulnerability to therapeutic drugs inducing oxidative stress (97). Saturated fatty acids are more stable than the unsaturated or polyunsaturated ones, since double bonds are usually subjected to peroxidation induced by reactive oxygen species (ROS). This phenotype has been mostly observed in primary tumors, while, epithelia to mesenchymal transition induces the acquisition of a more fluid membrane that sustains the cellular migration towards distant organs. Moreover, fatty acids are also necessary to form bioactive lipids that are essential secondary messengers that sustain signalling pathways involved in cell proliferation and survival. For example, phosphatidyl-inositol(3,4,5)-P_3, via AKT, is involved in the activation of mTORC1 and mTORC2 that, as described before, are master regulators of cell proliferation and survival (98). Together with phosphatidylinositols, fatty acids are also used as precursors of another class of bioactive lipids, eicosanoids. In fact, arachidonic acid is the key precursor of different eicosanoids such as prostaglandins and leukotrienes that have been associated with pro-tumorigenic events (99). Taken together these evidences suggest that dysregulated lipid metabolism is

not only necessary to support proliferation, but that increased lipid uptake and lipogenesis impart upon the cells a more aggressive phenotype.

1.5.1 Lipid droplets

Cancer lipogenesis contributes to the accumulation of neutral lipids and sterol esters that are stored within lipid droplets (LDs), the lipid cytosolic reservoir of the cells. The storage of neutral lipids inside these organelles protects cells from lipotoxicity, as well as functioning as an energy reserve (100). LDs have been described as important players for both cancer initiation and progression (101). Their accumulation in cancer cells relies upon a combinatorial effect of upregulated lipid uptake, increased fatty acid synthesis, and de-regulated lipolysis.

Lipid droplets (LDs) were long considered an inert organelle devoted to fat storage. Recently, it has become clear that their role is more complex and that they contribute to the regulation of multiple cellular processes, including cell signalling, inflammation, lipid metabolism and membrane biosynthesis (102). Lipid droplets are composed of a hydrophobic core of neutral lipids, containing primarily triacylglycerol (TAG) and cholesterol esters (CE), surrounded by a phospholipid monolayer. In addition to the lipid content multiple proteins have been shown to associated with LDs (**Figure 1.8**) (103, 104).

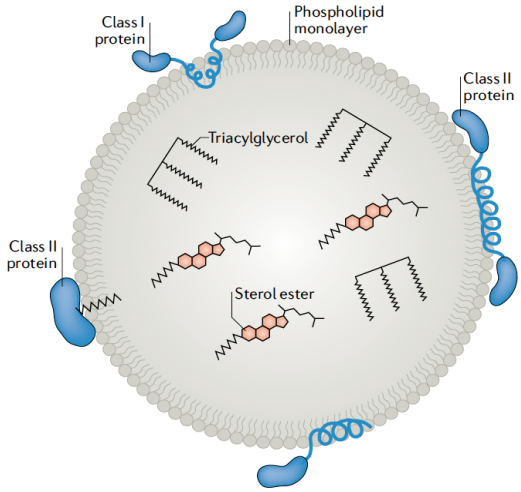

Nature Review Molecular Cell Biology, 2019

Figure 1.8. Lipid droplet structure and composition (105).

Lipid droplet size and composition are strictly regulated according to the cell type and to the metabolic state of the cells. LDs formation has been extensively studied and multiple models of lipid droplet biogenesis have been proposed (106-108). Although many of the details

remain unknown, the most widely accepted model describes a budding process of the endoplasmic reticulum (ER) towards the cytosolic environment (109). In this model, the biogenesis starts with the synthesis of neutral lipids, in particular triacylglycerols and stearyl esters (SE) in the ER, and their accumulation leads to the formation of a lens within the ER bilayer (110) (**Figure 1.9**).

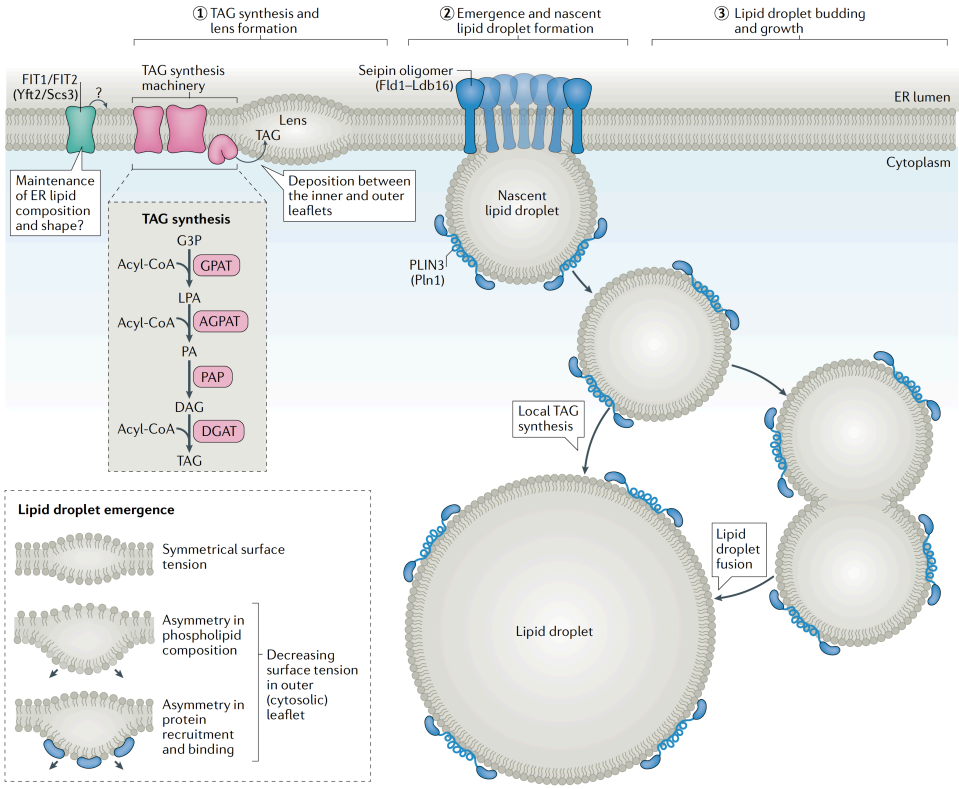

Nature Review Molecular Cell Biology, 2019

Figure 1.9. Lipid droplets biogenesis (105).

These neutral lipid lens extrude as buds from the Endoplasmic Reticulum membrane towards the cytosol at defined ER domains, where protein and lipid composition play an important role (111). It has also been suggested that LDs budding and size is influenced by chemical and physical membrane parameters, such as intrinsic curvature (112), ER phospholipid content and surface tension (113).

1.5.2 Lipid Droplets Accumulate in Tumours from Diverse Tissue Types

LDs accumulation has been reported in several tumours, including colon-rectal cancer (114, 115) glioblastoma (116), melanoma (117) and breast cancer (118-120). Their accumulation

in cancer cells is associated with cancer onset and progression. LDs formation, driven by TGFβ signalling, has also been associated with tumour acidosis, epithelial-mesenchymal transition (EMT) and mesenchymal-epithelial transition (TEM) in invasive phenotypes of cancer cell lines (121). Recently, it has been shown that epithelial and mesenchymal breast cancer cells are characterized by a different lipid profile. In particular, epithelial cells show an elevated fatty acid synthesis and mono-unsaturated lipid, while mesenchymal cells instead present a down-regulated lipogenic profile, together with an increased expression of genes necessary for LD formation (122). Although, the role of LDs in metastatic disease is still not properly characterized, accumulating evidence sustain that their accumulation in primary tumour cells act as a prognostic marker for metastatic potential (123).

A correlation between Perilipin 2 (PLIN2) expression, one of the most important LDs associated proteins, and tumour aggressiveness has been demonstrated. For example, in gastric cancer the overexpression of PLIN2 is linked with a malignant phenotype (124); similar results were previously shown in lung adenocarcinoma from Zhang and colleagues (125). In melanoma and in renal carcinoma, the overexpression of Perilipin 3, another member of the Perilipin family, was reported to correlate with a poor prognosis (126, 127). More in general, a negative correlation between PLIN protein expression and relapse free survival in patients was also shown in lung and renal carcinoma (128, 129). Considering the important role in lipid metabolism regulation, lipid droplets are now considered key organelles in many cancers. Unfortunately, while many studies have demonstrated a correlation between LD accumulation and a tumorigenic phenotype, the molecular mechanisms behind this phenomenon remain poorly investigated. Intriguingly they may represent an interest target for therapeutic intervention. It is known that their breakdown can be capitulated upon to protect cells in hostile conditions. Indeed, fatty acids deriving from lipid droplets are usually used to sustain cell proliferation in exogenous lipids deprivation and starvation (130). This process is regulated by AMP kinase, which activates lipid droplets re-localization to mitochondria and consequently fatty acid oxidation (131). Very recently, LDs have been also associated with cancer therapeutic resistance. Their hydrophobic pocket allows them to be an accumulation site for lipophilic drugs, thus decreasing treatment efficacy (132, 133). Due to the emerging evidences of LDs accumulation in cancer, they are now considered crucial components of the tumoral reprogrammed lipid metabolism and therefore an interesting therapeutic target.

1.6 Lipid droplets and breast cancer stem cells

1.6.1 Cancer stem cells origin and biomarkers

Cancer stem cells (CSC) are defined as a niche of cells responsible for tumour initiation and maintenance. These cells are characterized by "stem" traits such as multipotent differentiation and self-renewal capacity. Since they are usually not responsive to cancer treatments, they represent, in most of the cases, the main cause of therapeutic treatment failure, tumour relapse and metastatic dissemination (134, 135). Although, the origin of CSC is still debated there are two main hypotheses for the mechanism behind their emergence: (1) they arise from normal stem cells that have acquired oncogenic mutations; (2) they derive from cancer cells that have undergone a de-differentiation processes leading to the acquisition of stem properties (**Figure 1.10**). Due to their pivotal role in tumorigenesis, the search for biomarkers for CSC is a field of intense study.

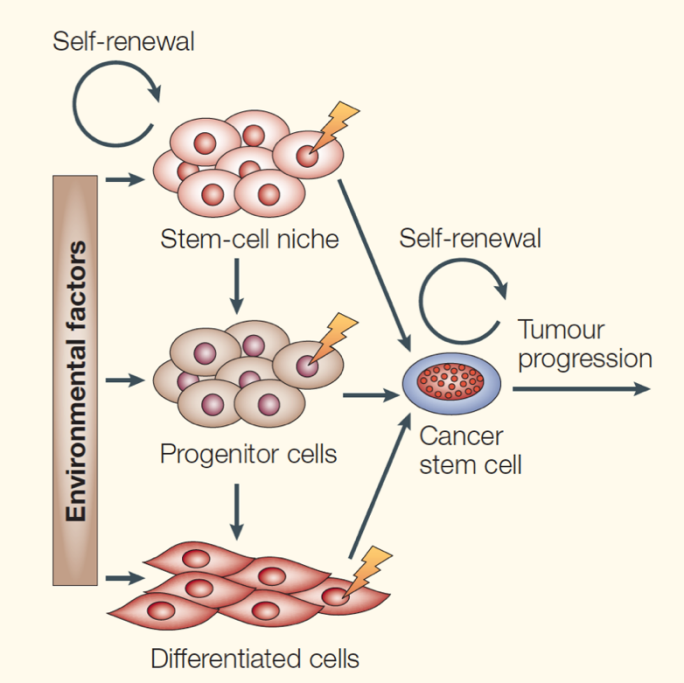

Nature Review Cancer, 2005

Figure 1.10. Cancer stem cells origins (136).

The identification of this small sub-population of cells usually relies on particular surface biomarkers that in some cases are shared by different cancer types. In breast cancer, several surface markers have been described, with several belonging to the Cluster of Differentiation (CD) family. One of the most frequently used is CD44, whose expression has been associated with self-renewal capacity and metastasis (137, 138). This marker shows both a

diagnostic and a therapeutic value (139). Another important marker described in breast cancer stem cells is CD133, which correlates with a poor prognosis (140). Its expression is usually associated with N-Cadherin and EpCAM expression (141, 142) whom recently were described to be associated with improved metastatic capacity (143). Yet, not all CD44 high cells are CSC. Therefore, in order to distinguish and isolate CSC it is a common practice to use a combination of surface markers together with intra-cellular proteins.

Together with the surface markers, several transcription factors have been associated with stemness properties. Among them we find Oct-3/4, Sox2, Notch and Nanog whose activation is correlated with higher expression of self-renewal genes and a down-regulation of differentiation genes (144, 145). In HER2 positive breast cancer patients, a correlation was observed between Oct4, Sox2 and Nanog overexpression and a worse prognosis (146).

Cancer stem cells share many features with normal stem cells, making their identification and isolation a complex task. In order to isolate CSC, several *in vitro* assays have been developed combining well-characterized stemness properties with cancer features. Among them we can find tumor initiating and self-renewal capacity in non-adherent conditions, studied through sphere-forming assays (147); the dye exclusion capacity of CSC due to their up-regulation of many transporters, analysed by the use of nuclear dyes like Hoechst (148); the expression of specific cell surface markers and genes, found to be key regulators of stemness (149) and known to be overexpressed in many cancers, analysed by FACS.

However, the lack of specific *in vivo* assays still represents a huge problem in the field, since they could improve our capability to identify and isolate these cells. A better characterization of this small sub-population of cells, which would allow us to selectively target these cells in clinics, is urgently needed.

1.6.2 Cancer stem cells metabolism and LDs

Recent evidence highlighting metabolic changes between normal stem cells and cancer stem cells, suggests metabolic profiling as a possible means to distinguish this sub-population of cells (150). For this reason, CSC metabolism is an active field of research that is starting to yield significant insights into the cancer cell biology field (151). Alterations of both glucose and lipid metabolism in CSC have been described (152). Yet, emerging evidence suggests that the metabolic profile of CSC could vary between tumours. Hepatocarcinoma cancer stem cells which are characterized by CD133 positivity have a glycolytic addiction, with inhibition of glycolytic enzymes leading to the down-regulation of specific stemness markers, like Sox2 and Oct4 (153), and spheroids-forming capacity *in vitro* (154). Furthermore, breast cancer cells which are characterized by $CD44^{+}/CD24^{-}/EPCAM^{+}$ show

a metabolic switch from oxidative phosphorylation to aerobic glycolysis that sustains the anabolic growth and is involved in a more general metabolic reprogramming, including higher ROS production, increased glucose uptake and oxygen consumption (155). The list of tumours showing that CSC, in comparison to the differentiated tumour cells, are characterized by a more glycolytic-based metabolism is growing. Indeed, it has been already described in glioblastoma (156), colon-rectal cancer (157), ovarian cancer (158) and nasopharyngeal carcinoma (159).

Instead, other findings, have reported a more OXPHOS dependency of CSC to fulfil their needs and to sustain their self-renewal capacity. This has been described for example in pancreatic ductal carcinoma, where $CD133^{+}$ CSC up-regulate mitochondrial biogenesis to adapt their metabolism to their energetic requirements (160). Also, in glioblastoma CSC have been shown a certain dependency on OXPHOS for the maintenance of the stemness traits (161). In leukaemia, CSC which are $CD34^{+}/CD38^{-}$ are able to reprogram their metabolism going from an OXPHOS-dependent when in a dormancy state, to a glycolytic-dependent metabolic profile when in a proliferative state. This switch is regulated by the apoptosis regulator BCL-2 that is involved in the up-regulation of OXPHOS (162). As shown above for glioblastoma, it seems that the same tumour can be characterized by different metabolic dependencies. Hence, emerging studies are now suggesting that CSC metabolic profile may depend on the cellular proliferative state, the tissue of origin and the metastatic preferential site. Actually, CSC allocated in hypoxic alcoves, like hematopoietic stem cells in the bone marrow, are truly dependent on aerobic glycolysis if compared to other tumor types (163).

In addition, a de-regulation of lipid metabolism has also been described in association with CSC phenotype. Low membrane fluidity, that is associated with a lower level of lipid unsaturation, correlates with a down-regulation of the stemness capacity and metastatic disease in breast cancer (164). Nevertheless, both leukaemia and hepatocarcinoma stem cells showed an addiction to fatty acid oxidation (FAO) that in the case of hepato-cells relies on the NANOG-mediated hyper-activation of FAO genes (165, 166). The increased FAO could also link with the observation that in leukaemia FAO is uncoupled from ATP generation, leading to continuous fatty acid biosynthesis (167), sustained also by FASN over-expression (168). FASN overexpression seems to play a key role in maintaining tumour-forming capacity and stemness traits also in glioma CSC. Indeed, in these cells, FASN inhibition led to the reduction of CD133 stem marker expression and to a lower invasiveness, while increasing the expression of the differentiation marker Glial Fibrillary Acidic Protein (GFAP) (169).

Another key player in lipid metabolism that has been associated with CSC is stearoyl-CoA desaturase 1 (SCD-1). SCD-1 overexpression has been reported both in lung CSC, where it stabilizes the nuclear localization of YAP/TAZ complex (170, 171), and in ovarian cancer, where it correlates with an higher tumorigenic capacity and its over-expression is regulated by the nuclear factor NF-kB (172). As described previously, SCD1 catalyses the conversion of saturated fatty acids to Mono-Unsaturated Fatty Acids (MUFAs), precursors of many lipids like triglycerides, diacylglycerols and cholesterol esters.

The up-regulation of lipid biosynthesis pathways may lead to the accumulation of lipid droplets, since excess lipids are stored in these organelles. Several studies have begun to link lipid droplet accumulation with stemness traits and invasion in colon cancer, ovarian cancer (172), glioblastoma (173) and prostate cancer (174). In colon cancer, a correlation between LD content and tumorigenic characteristics has been shown to be associated with the up-regulation of CD133 and the Wnt/beta catenin pathway (175). In some cases, it was observed that the accumulation of LD was employed by CSC as a reservoir of energy in form of lipids (176); in that case, the inhibition of lipolysis, led CSC to death. In this scenario, it appears clear that a better understanding of CSC metabolism can allow us to identify new strategies for evaluating CSC growth and target their peculiar features, thus preventing tumour relapses and metastasis formation.

1.7 Aims of my Ph.D. project

Breast cancer related death is usually caused by tumour relapses and metastasis development. The metastatic disease can rise from residual cancer stem cells (CSC) resistant to the therapeutic treatments (177). In particular, those sub-populations of cells accumulate lipid droplets (LD). Recently, it has become clear that lipid droplets play a role in the regulation of a variety of cellular processes, including cell signalling, inflammation, lipid metabolism and membrane biosynthesis (102). Interestingly, LD accumulation has been frequently observed in a variety of cancer types (116) (114). Consistent with the cancer stem cell theory, CSC have a role in both origin and tumour progression, as well as in tumour relapses. Thus, it becomes crucial to better characterize and target this population of cells during the diagnostic phase and the therapeutic approach (178). Unfortunately, to date, we still miss a detailed characterization of CSC in breast cancer and this is mainly due to the lack of specific markers. While a number of studies have shown the role of lipid metabolism in cancer stemness, the presence of lipid droplets in breast cancer stem cells has been never investigated. Based on these considerations, the first aim of my Ph.D. project was to:

1. *Assess the contribution of lipid droplets to CSC maintenance and their correlation with tumour onset, with the hope of revealing new therapeutic targets*

The accumulation of lipid droplets is part of a more general lipid metabolic reprogramming observed in breast cancer patients (179). Despite being a more recent concept compared to the Warburg effect, the importance of lipids in cancer metabolism has been fully recognized. The role of lipids as modulators of the activity and function of proteins and enzymes attracted scientists long time ago. Moreover, a decreased activity of some glycolytic enzymes, such as phosphofructokinase (PFK) and pyruvate kinase (PK), was also described caused by the increased levels of citrate (69, 180). The inhibition of glycolytic enzymes activity means a shift of the cellular metabolism from catabolism to anabolism, mechanism that is very often observed in cancer cells. Despite the increased interest in the field, there are still many gaps in the understanding this aspect that need to be covered. The more recent technologies allow us to better characterize the interplay of the two main cellular pathway, lipid and glucose metabolic pathways. Thus, the second aim of my Ph.D. project was to:

2. *Dissect the biochemical interplay between glucose and lipid metabolism in breast cancer cells*

Chapter II

Materials and Methods

2.1 Media

The growth media used for *Escherichia Coli* cultures were: Luria-Bertani (LB) broth containing Peptone 140, Yeast extract and Sodium chloride; Terrific Broth (TB) containing Yeast extract, Tryptone, Potassium hydrogen phosphate, Potassium dihydrogen phosphate and glycerol. TB media for Pyruvate kinase M2 purification was supplemented with kanamycin antibiotic 50 μg/ml.

2.2 Cell Lines and Culture Conditions

In this study were used the following human breast cancer cell lines: BT474, MCF7, T47D, MDA-MB 231, BT549, SUM-190, ZR-75-1, MDA-MB-468, SKBR3, and MDA-MB-453cells. BT474, MDA-MB-453 and SKBR3 cells were purchased from DSMZ; MCF7, T47D, MDA-MB 231, MDA-MB-468 and BT549 were purchased from the National Cancer Institute (NCI); SUM-190 cells were purchased from Asterand; ZR-75-1 cells were purchased from ATCC. All the cell lines were maintained in Roswell Park Memorial Institute 1640 RPMI (Lonza) supplemented with 10% fetal bovine serum and 2 mM L-Glutamine and cultured at 37˚C in a humidified atmosphere 5% CO_2 incubator.

2.3 Nile Red staining and Lipid droplets quantification analysis

The Nile Red staining was performed as previously reported (181) . Briefly, Nile red (Invitrogen, N1142) stock solution was made in DMSO at a concentration of 1 mg/ml. For the cellular staining cells were seeded on poly-lysine coated coverslips and then fixed in Paraformaldehyde 4% for 15 minutes. After washing, the cells were incubated for 10 minutes in Nile red (1 μl of 1 mg/ml Nile Red stock in 10 ml of 150 mM NaCl) protected from light. Nuclei were stained using Dapi and finally coverslips were mounted onto glass slides. For the Lipid droplets analysis quantification, a Fiji plug-in (developed by Martini E.) was used. Briefly, after manually delineating a ROI around the cells, the plugin identified lipid droplets using the ImageJ's Find Maxima2 algorithm on the maximum projection image after background removal (using the rolling ball algorithm3) and noise reduction (with a median filter).

2.4 RNA extraction and quantitative RT-PCR Analysis

In order to perform the RT-PCR analysis, total RNA was first isolated using Trizol-Chloroform extraction with TRIzol reagent (Life Technologies) and Chloroform (Carlo Erba). For the cells collected following cell sorting, RNA was extracted using the RNeasy Mini Kit (Qiagen). After the extraction, the RNA was quantified by NanoDrop to assess both concentration and quality. Reverse transcription was performed using the SuperScript III

Reverse Transcriptase kit (Invitrogen). Gene expression was analyzed using the TaqMan Gene expression analysis. Sample were amplified with primers for each gene and Actin B was used as housekeeping. The list of the assay ID used is shown in Table 2.

2.5 Mammospheres formation assay from cell lines

The primary mammospheres were produced as previously described (182). The mammospheres media used in this assay was DMEM-F12 (Biowest) supplemented with B27 supplement (Invitrogen) and EGF (20 ng/ml; Vinci Biochem). To prepare non-adherent plates, standard 6-well plates were coated with 1ml of 1% agarose solution in PBS. To produce the 1% agarose solution agarose powder was dissolved in PBS and autoclaved. Briefly, cells were centrifuged at 580 g for 2 minutes and resuspended in 2 ml PBS. To avoid cellular aggregates, a 22 G needle was used to syringe the cell suspension. We found out that 10^4 cells/well was a good seeding density for our cell lines. Cells were plated and incubated in a 5% CO_2 humidified incubator at 37˚C. After 5 days, all mammospheres larger than 50 μm were counted and the Mammospheres Formation Efficiency (MFE) % was calculated using the equation MFE(%)= (number of mammospheres per well/total number of cells seeded for well)x100.

2.6 BODIPY for staining and Fluorescence-Activated Cell Sorting

BODIPY™ 500/510 C_1, C_{12} (4,4-Difluoro-5-Methyl-4-Bora-3a,4a-Diaza-s-Indacene-3-Dodecanoic Acid) (Molecular Probes) stock solution (1mg/ml) was prepared in ethanol and kept at -20˚C until used. For the cellular staining cells were seeded on poly-lysine coated coverslips and incubated overnight with 1 μg/ml bodipy in the media. The day after cells were fixed in Paraformaldehyde 4% for 15 minutes. After washing, nuclei were stained using Dapi and finally coverslips were mounted onto glass slides.

For FACS sorting, the cells were incubated with 1 ug/ml BODIPY™, following an overnight incubation, they were washed twice, trypsinized, resuspended in PBS 2% FBS 0.3% Gentamycin and sorted on a MoFlo Astrios Beckman Coulter (Beckman).

2.7 Assessment of lipid droplet content using CD44/CD24 stem cell markers

MDA-MB-231 and BT474 cell lines were cultured in 6-well plate wells (Falcon, Ref no. 353046). On the night prior to FACS analysis cells were treated with BODIPY™ 500/510 C1, C12, as described in 2.6. Following incubation with BODIPY™ 500/510 C1, C12 the cells were harvested and incubated in 500μl of a 1X D-PBS, 5% BSA, blocking buffer for 45 min at room temperature. The cells were then stained with Alexa Fluor® 647 Mouse Anti-Human CD24 and CD44-VioBlue® mouse anti-human CD44 for 30min on ice

(antibodies details are listed in Table 1). The antibody concentrations recommended on the accompanying data sheets were used for the stain. Following staining the cells were pelleted and washed three times with a 1X D-PBS, 1%BSA solution, prior to resuspension in a 1% FBS, 1X D-PBS solution. The FACS was conducted using the Attune NxT (Thermofisher Scientific). FACS data depicted represents analysis done on single, propidium iodide negative, cell population. FlowJo Version 10.4.2 was used for the analysis.

2.8 5-(Tetradecyloxy)-2-furoic acid (TOFA) Treatments

TOFA (Sigma-Aldrich T6575) was resuspended in two milliliters of DMSO and stored at -20˚C. Experiments in which cells were treated with TOFA, unless otherwise specified, were cultured in the presence of 10 uM TOFA in their normal growth media for forty-eight hours prior to initiating measurements or assays.

2.9 FACS of fatty acid loaded and TOFA treated cells

FACS analysis of fatty acid loaded cells was done by culturing cells to 30-40% confluence. The normal growth media was then spiked with 100 uM Oleic acid (Sigma-Aldrich 01383) and 50 uM Palmitic acid (Sigma-Aldrich P5585) for forty-eight hours. Twelve hours prior to FACS cells were treated with Bodipy at 1ug/ml. Immediately before FACS, cells were then trypsinized and spin at 1200rpm for five minutes. The pellet was gently washed with D-PBS and resuspended in D-PBS containing 2%, 0.22um filtered, FBS. FACS was conducted using Attune NxT (Thermofisher Scientific). FACS data depicted represents analysis done on single, DAPI negative cell populations. FlowJo Version 10.4.2 was used for the analysis. The same workflow, with the exception of the fatty acid loading step, was used to assess the impact of TOFA treatment on the lipid droplet content of the experimental cell lines.

2.10 Fatty Acid Oxidation Assay

MDA-MB-231, MCF7, T47D and BT474 cell lines were seeded into 96-well plate wells (CostarTM) at $7x10^4$ cells per well and treated with either the vehicle, or 10 uM TOFA in DMSO. After approximately twenty hours the cells were assessed using a Fatty Acid Oxidation Assay (Abcam, ab217602) used in conjunction with an Extracellular O_2 Consumption Assay (Abcam, ab197243). The protocols accompanying the assays were followed to assess the cell lines after TOFA treatment. Experimental measurements were made using a Wallac EnvisionTM 2104 Multilabel Reader (Perkin-Elmer), maintained at 37˚C throughout the course of the experiment. Excitation filter, UV (TRF) 340 and Emission filter APC665 were used to assess the status of the oxygen sensing probe used for the assay.

A measurement of the oxygen sensing probe was made every ninety seconds for one and a half hours.

2.11 Growth Curves for 5-(Tetradecyloxy)-2-furoic acid (TOFA) sensitivity

BT474, T47D, MCF7 and MDA-MB-231 cell lines were seeded into five, 96-well plates (CostarTM) at $1.5x10^4$, $1.5x10^4$, $1x10^4$ and $0.5x10^4$ cells/well respectively. Three wells in each plate were seeded for each experimental condition. An additional set of three wells were filled with growth media alone to act as a plate blank. On the day of seeding, after the cells had adhered to the plate and begun to spread, a single plate was fixed. Fixation was done by removing the culture media and adding 100 ul of 4% paraformaldehyde solution, PFA (HIMEDIA), to each well for ten minutes. The PFA was then removed and 100 ul per well of Crystal Violet Solution (Merck KGaA) was added to each well. After twenty minutes all non-cell associated Crystal Violet was removed by washing the wells with water. The cells in the remaining four plates were treated with either: growth media, growth media containing 0.13% DMSO or growth media with 10 uM TOFA (Sigma-Aldrich) in DMSO. A subsequent plate was fixed and stained as described above every twenty-four hours for ninety-six hours. Once plates were completely dry, 100 ul of Acetic Acid Glacial (Carlo Erba) was added to each well and incubated for twenty minutes at room temperature. Then the log optical density of each experimental well was measured at a wavelength of 570nm using a Wallace Victor3TM Multilabel Reader (PerkinElmer Inc.). Reported OD values were generated by subtracting the average of the three experimental wells from the average of the three plate blank wells.

2.12 Transmitted light and fluorescence microscopy

Mammosphere images were acquired with EVOS FL imaging system (Thermo Fisher Scientific, Inc., Waltham, MA) transmitted light microscope. Fluorescent images were acquired with laser-scanning confocal microscopes: Leica TCS SP5 laser confocal scanner mounted on a Leica DMI 6000B inverted microscope equipped with motorized stage and HCX PL APO 63X/1.4NA oil immersion objective (Leica Mikrosysteme Vertrieb GmbH, Wetzlar, Germany) and Leica TCS SP2 AOBS laser confocal scanner mounted on a Leica DM IRE2 inverted microscope equipped with HCX PL APO 63X/1.4NA oil immersion objective (Leica Mikrosysteme Vertrieb GmbH, Wetzlar, Germany). For the excitation of fluorochromes dyes, 405 nm, 488 nm, 561 nm and 633 nm laser lines were used on Leica TCS SP5 and Leica TCS SP2 AOBS. The following settings were maintained for fluorescent images acquisition: digital zoom 2.5 and 1024x1024 scan format.

2.13 Kaplan-Meier Plotter

Kaplan-Meier plots were generated using the Kaplan-Meier plotter found at http://kmplot.com/analysis/index.php?p=background (183). With this online platform, using the Affymetrix ID 209122_at dataset, we assessed the prognostic values for PLIN2 mRNA expression for a cohort of 3951 breast cancer patients.

2.14 Statistical Analysis

All experiments were carried out at least 3 times unless otherwise indicated. Data were analyzed using GraphPad Prism version 8 statistical software. Experimental results are reported as Mean and Standard Deviation unless otherwise stated.

2.15 Animal models and in vivo studies

Mice experiments were performed in collaboration with Giorgio Scita group, in accordance with the national laws and institutional guidelines for animal care (directive 86/609/EEC). Animal work was started upon the approval of the Italian Istituto Superiore di Sanità (license number 614/16). The maintenance of the NOD/SCID mice was done under specific pathogen-free conditions in the research animal facility of the IFOM/IEO (Milan, Italy). Free access to food and water, a 12-hour light-dark cycle and constant temperature were provided for the animals. 3 weeks old NOD/SCID female mice were used for the in vivo studies. Briefly, total MDA-MB-231 cells pre-incubated overnight with 1 µg/ml BODIPY were sorted for BODIPY intensity and 1.5 million cells from each subpopulation (5% $BODIPY^{low}$, 5% $BODIPY^{high}$, 5% $BODIPY^{ave}$) were mixed with Matrigel and Trypan blue and then injected into the mammary gland of the mice. Electron caliper was used every three days to measure the tumor size and the volume was calculated by multiplying [large diameter x $(\text{small diameter})^2$ x $\pi/6$]. Animals were sacrificed when first clinical signs of illness became apparent and tumors were collected.

2.16 SDS-PAGE and Western blot analysis

Cells were collected in PBS and lysed in RIPA Lysis Buffer (150 mM NaCl, 50 mM Tris pH7.6, 1% NP-40, 0.5% Na-deoxycholate, 5 mM EDTA plus protease inhibitors) for one hour on ice. 30 ug of lysate were then subjected to SDS-PAGE on 4-12% precast gradient gels (Invitrogen). Gels were run in running buffer at constant voltage of 120 V. Proteins were then transferred on Nitrocellulose membrane (Amersham 0.45 mm, GE Healthcare) in 1X transfer buffer 20% Methanol for 1.5 hours at 100V 4˚C. After the transfer, membranes were washed in water and stained with Ponceau solution to check the transfer quality. After three washes in 1X TBS-T 0.1% tween, membranes were blocked for 1 hour at room

temperature in 1X TBS-T 5% milk or 1X TBS-T 5% BSA according to the antibody datasheet. The incubation with the primary antibodies was performed by gently shaking the membranes at 4˚C overnight. The day after, membranes were washed three times for 10 minutes in 1X TBS-T and incubated for 1 hour at room temp. with the secondary antibody. Finally, membranes were washed thrice in 1X TBS-T and developed using ECL kit (Amersham) and images were acquired using Chemidoc (Bio-Rad, Molecular Imager Chemidoc XRS+). The list of antibodies is shown in Table 1.

2.17 Pyruvate kinase assay

Pyruvate kinase assay was performed following a published protocol from Worthington Biochemical. Phosphoenolpyruvate (PEP), Lactate dehydrogenase (LDH) and NADH were purchased from Roche. ADP and Fructose 1,6-biphosphate (FBP) were purchased from Sigma-Aldrich. In order to assess pyruvate kinase activity, a mixture containing 1300 units/ml of LDH, 45 mM ADP, 6.6 mM NADH, 45 mM PEP in a 0.05 M imidazole-HCl buffer pH 7.6 containing 0.12 M KCl and 0.062 M $MgSO_4$ was added to a 96-well plate in the presence or absence of FBP. To assess the pyruvate activity lysates or the recombinant protein were added to the mixture and then the reaction rate was calculated as the *Δ*-delta absorbance (Abs) read at 340 nm (25˚C) for minute.

2.18 Fatty acids pull-down assay

Fatty acid pull-down-assay was performed according to a previously published protocol (184). Shortly, Aminohexyl-agarose beads (SIGMA, A6017) were coupled to acyl chains with different length. The carboxygroups of the FA were activated by adding to a solution of 46 µmol dissolved lipids in 1ml dimethylformamide (DMF), 92 µmol N,Ndiisopropyl-ethylamine (DIEA) and 35 µmol O-(benzotriazol-1-yl)-tetramethyluronium tetrafluoroborate (TBTU). After stirring the solution for 6 hours at room temperature, 0.5 ml of ω-aminohexyl-agarose beads in DMF was added and the suspension stirred overnight at RT. The coupled beads were washed with 1 ml DMF and twice with 1 ml PBS. To test the completeness of amino acid coupling we performed a Kaiser-test (185) .Cells were then washed with PBS and cell pellets lysed in NP-40 lysis buffer (150 mM NaCl, 50 mM Tris-HCl pH 8, NP-40 1%, 2 mM DTT) containing protease inhibitors cocktail (Sigma-Aldrich for 30 minutes on ice. 50 µl lipid-beads were incubated with 50 ug pre-cleared lysate for 2 hours 30 minutes on a rotating wheel. Beads were washed 4 times with 1 ml cold lysis buffer. Samples were separated by SDS-PAGE, stained with Coomassie Brilliant Blue or transferred to PVDF membranes for immunoblotting.

2.19 In vitro binding assay

For the *in vitro* binding assay a chemically synthesized lipid probe *prop-2-yn-1-yl-2-(3-tridecyl-3-diazirin-3-yl) acetate* was used to study the protein-lipid interaction. Briefly, proteins were incubated with or without the lipid probe for 1 hour at 25 ˚C in dark conditions and then subjected to UV light at 345 nm for 10 minutes. Samples were then incubated with Alexa Fluor Picolyl Azide reagents (Molecular Probes, C10641) for Click-IT chemistry reaction for 1 hour at 25 ˚C for the detection and processed for SDS-page. Samples were visualized by Chemidoc fluorescent acquisition for Alexa Fluor 488 or stained with Instant blue (Expedeon).

2.20 Production of recombinant Pyruvate Kinase M2 enzyme in Escherichia Coli

2.20.1 Bacterial strains and preparation of competent bacteria cells

Escherichia coli TOP10 and DH5alpha strains were used for the amplification and preparation of plasmid DNA. BL21 cells were used for the production of the recombinant proteins. BL21 and TOP10 competent cells were prepared with the calcium chloride procedure. Briefly, an overnight starting culture (10 ml) of *E. coli* in LB media was inoculated into 1 L of LB and grown until the optical density O.D. reached 0.4. Then, the cells were put on ice for 30' and harvested by centrifugation at 3000g for 15' at 4˚C (Beckman Coulter Avanti J-20 XP, rotor JA-10). The cell pellet was then resuspended into 100 ml of ice-cold sterile $MgCl_2$ and harvested again by centrifugation at 2000g for 15' at 4˚C. Pellet was now resuspended in 200 ml ice-cold $CaCl_2$, incubated on ice for 20' and harvested again as described above. The pellet was resuspended in 50 ml ice-cold 85 mM $CaCl_2$ 15% glycerol and centrifuged at 1000g for 15' at 4˚C. Finally, 2 ml of ice-cold 85mM $CaCl_2$ 15% glycerol were used to resuspend the cell pellet that was then stored at -80˚C in 50 ul aliquots.

2.20.2 Generation of Pyruvate kinase M2 mutants through site-directed mutagenesis

In order to generate PKM2_K422E, PKM2_K422R and PKM2_R489L mutants, site-directed mutagenesis was performed using the Q5 High Fidelity DNA pol kit (BioLabs, M0491). Briefly,10 µl of 5X reaction buffer were mixed with 100 ng of pET-28a-hPKM2 plasmid (Addgene – Plasmid #44242) DNA template, 2.5 µl of 10 µM oligonucleotide primer forward, 2.5 µl of 10 µM oligonucleotide primer reverse, 1 µl of 10mM dNTP mix, 10 µl of 5X Enhancer solution and milli-Q H_2O (primers list is shown in Table 3). Finally, 0.5 µl of Q5 DNA polymerase was added before to start the PCR. After checking the DNA quality on a 1% agarose gel, the PCR product was subjected to DpnI digestion for 2 hours at 37˚C in order to remove the parental wild type plasmid.

2.20.3 Bacterial transformation

TOP 10 bacterial competent *E. coli* cells were transformed with 15 µl of the PCR product after digestion. Briefly, 50 µl of TOP-10 cells were thawed on ice prior to the addition of PCR product. Cells were incubated with DNA on ice for 20' and then subjected to heat shock for 45'' at 42˚C. After the heat shock, cells were incubated again on ice for 2'. 1 ml of SOC medium was then added to the reaction tube and cell suspension was incubated on a shaker at 37˚C for 1 hour before plating onto LB-kanamycin (50µg/ml) plates. Finally, plated bacterial cells were incubated overnight at 37˚C. Colonies were picked from the plates grown for minipreps in 5 ml LB medium containing kanamycin in shaking incubator at 37˚C overnight. Isolation of plasmid DNA was performed using Wizard Plus SV Minipreps DNA purification system kit (Promega, A1460). All the constructs were then validated by sequencing using the specific primers listed in Table 3.

In order to express PKM2 *wild type* and PKM2_K422E mutant, 50 µl of BL-21 bacterial competent *E. coli* cells were thawed on ice prior to the addition of pET-28a-hPKM2 plasmid DNA (Addgene – Plasmid #44242) or pET-28a-hPKM2_K422E plasmid. Cells were subjected to the same procedure described above and plated onto LB-kanamycin (50µg/ml)-chloramphenicol (50µg/ml) plates. Finally, plated bacterial cells were incubated overnight at 37˚C.

2.20.4 Production of recombinant PKM2 wild type and mutants

Single colonies were picked up from the LB-Kanamycin-Chloramphenicol plates and grown overnight into 40 ml Terrific Broth media (TB - tryptone, yeast extract, glycerol and potassium phosphate buffer) supplemented with 50µg/ml Kanamycin and 50µg/ml Chloramphenicol at 37˚C. Overnight culture was then diluted into 4 liters culture and grown until the optical density (O.D.) reached 0.9-1. Cells were then induced overnight at 18 ˚C with 0.5 mM IPTG at 225 rpm. The day after, the cultures were centrifuged and the pellet resuspended in Lysis buffer (10 mM HEPES pH 7.5, 300 mM KCl, 0.5% CHAPS, 12.5 mM imidazole, 5 mM MgCl2, 5% glycerol, 2.5 mM TCEP, in H_2O) and sonicated for 2 rounds of 9 minutes each, 1 sec on- 1 sec off. The sonicated cell solution was then centrifuged at 19'000 rpm for 30 minutes 4˚C (Beckman Coulter Avanti J-20 XP, rotor JA 25-50). The supernatant was immediately removed, filtered using 0.22 µm filter unit (Thermo Scientific Nalgene, 595-4520) and incubated with 400 µl/liter culture His-Select Nickel Affinity Gel (SIGMA, P6611) for 90 minutes on a rotatic wheel. Beads were then washed for 10' in lysis buffer and then the protein was eluted in elution buffer (10 mM HEPES pH 7.5, 300 mM KCl, 0.5% CHAPS, 200 mM imidazole, 5 mM MgCl2, 5% glycerol, 2.5 mM TCEP, in H_2O) using 10 ml Poly-Prep Chromatography Columns Bio-Rad (7311550).

2.21 Analytical Size Exclusion Chromatography (SEC)

For analytical SEC analyses 20 µM of PKM2_wt and PKM2_K422E mutant were loaded singularly on a Superdex 200 Increase 10/300 (GE Healthcare) equilibrated in 10 mM Hepes pH 7.5, 100mM KCl, 5 mM $MgCl_2$, 5% glycerol, 1 mM DTT, and eluted in 0.5 ml fractions. The presence of the proteins in the elution volume was monitored by absorbance at 280 nm (expressed as mAu), and subsequently checked by SDS-PAGE followed by Coomassie staining.

2.22 Static Light Scattering

Static Light Scattering (SLS) analyses of PKM2 wild type and PKM2_K422E mutant were performed on a Viscotek GPCmax/TDA (Malvern, UK) instrument. The system was equilibrated in a buffer containing 10 mM Hepes pH 7.5, 100mM KCl, 5 mM $MgCl_2$, 5% glycerol, 1 mM DTT and calibrated with BSA. PKM2 wild type and K422E mutants were loaded on the Viscotek GPCmax instrument equilibrated in a buffer containing 10 mM Hepes pH 7.5, 100mM KCl, 5 mM $MgCl_2$, 5% glycerol and 1 mM DTT. About 150 µl of the samples concentrated at about 3 mg/mL were loaded on the columns, and eluted.

2.23 Protein crystallization and structure determination

2.23.1 PKM2_WT and PKM2_K422E sample preparation and crystallization conditions

PKM2_wt and PKM2_K422E purified proteins were dialyzed overnight at 4 °C in 2 L 10 mM HEPES pH 7.5, 300 mM KCl, 5 mM MgCl2, 5% glycerol, 2.5 mM TCEP buffer using Slide-A-Lyzer Dialysis Cassette G2 (Thermo Scientific, 87723) and then concentrated at about 5 mg/ml using Vivaspin 2 membrane 5,000 MWCO PES (Sartorius, VS0211).

The proteins were subsequentially purified on a Hi-Load 16/60 Superdex 200 in 10 mM Hepes pH 7.5, 100mM KCl, 5 mM $MgCl_2$, 5% glycerol, 1 mM DTT. Eluted fractions were then collected and concentrated to a concentration of 9 mg/ml for PKM2_WT and 5 mg/ml for PKM2_K422E mutant. Initial crystallization trials of the PKM2_WT were performed with the commercial screen Peg/Ion (Hampton Research) using 10 mM Hepes pH 7,5, 100 mM KCl, 5 mM $MgCl_2$, 5% Glycerol and 1 mM DTT buffer. 100 nl protein solution were mixed with an equal volume of reservoir solution at 20 °C. Crystals appeared after 2 days in about 30% of conditions containing PEG. Initial crystallization trials of the PKM2_K422E samples were set up with the commercial screens Peg/Ion (Hampton Research) and JCSG-plus (Molecular Dimension) using a Mosquito nano-dispenser (TTP Labtech) in MRC 2 well crystallization plates (Swissci, Hampton Research), conducted in sitting-drop vapor-diffusion. Again, 100 nl protein solution were mixed with an equal volume of reservoir

solution at 20 °C. Crystals appeared after 3 days in about 30 % of conditions containing PEG.

2.23.2 Data collection, processing, and structure determination of PKM2_WT

The best crystals of PKM2_WT grew in 0.1 M Hepes pH 7.5, 10% PEG 8000, 8% ethylene glycol and diffracted at 2.87 Å, belonging to space group $P2_1$. Crystals were analysed by X-ray diffraction using the beamline PXIII of the Swiss Light Source (SLS), Villigen, Switzerland. Data processing, structure resolution and refinement were carried out by our collaborators of the Biochemistry and Structural Biology Unit of the European Institute of Oncology. The structure was solved by molecular replacement with *Phaser (186)*, using chain A of pdb entry 6b6u as search model, with 4 molecules per asymmetric unit. The model was progressively optimized by iterative cycles of manual building in Coot (187), and refinement in Phenix (186).

2.23.3 Data collection, processing, and structure determination of PKM2_K422E

PKM2_K422E was purified, dialysed, concentrated to 5 mg/ml and subsequentially purified on a HiLoad 16/60 Superdex 200 as described above. Eluted fractions were then collected and used to set up crystallization trials with or without the addition of fatty acid. Diffracting crystals were obtained only with protein incubated with Oleic acid (Sigma Aldrich, 01383) in a 1:10 molar ratio overnight at 18°C. The complex was concentrated to 5 mg/ml. Initial crystallization trials were performed with the commercial screen JCSG+ (Molecular Dimension), Peg/Ion (Hampton Research) and Hampton 1-2 (Hampton Research) using 10 mM Hepes pH 7,5, 100 mM KCl, 5 mM $MgCl_2$, 5% Glycerol and 1 mM DTT buffer. 100 nl complex solution were mixed with an equal volume of reservoir solution at 20 °C. Crystals appeared after 7 days, but shapes and morphology required optimization. In order to obtain larger crystals and to slow down their growth, we performed a series of grid screens around the initial condition. Diffracting crystals grew in two different conditions. The first one grew in the presence of 18% PEG-3350, 275 mM di-ammonium tartrate, 17% proline and 0.8 mM oleic acid. The second one, instead, in 21% PEG-3350, 275 mM di-ammonium tartrate, 12% glycine and 0.8 mM oleic acid. Crystals were analysed by X-ray diffraction using the beamline PXIII of the Swiss Light Source (SLS), Villigen, Switzerland. They belong to the space group $P1$ and $P2_1$, with, respectively, 8 and 4 molecules in the asymmetric unit. Structures were solved by molecular replacement with *Phaser* (186), using chain A of pdb entry 6b6u as search model. The models were then progressively optimized by iterative cycles of manual building in Coot (187), and refinement in Phenix (186).

TABLES

Table 1. List of antibodies and applications

Protein	**Primary antibody**	**Company**	**Application**
PKM2	Anti-human PKM2 (D78A4)	Cell Signaling	WB
TUBULIN	Anti-human TUBULIN (T5168)	Sigma Aldrich	WB
Secondary rabbit	Anti-rabbit	In house (IFOM)	WB
Secondary mouse	Anti-mouse	In house (IFOM)	WB
CD44	Anti-human CD44 VioBlue (130-112-899)	Miltenyi Biotec.	FACS
CD24	Anti-human CD24 Alexa Fluor 647 (561644)	BD Pharmingen	FACS

Table 2. List of Assay IDs

Oligo	**Sequence/Assay ID**	**Application**
Sox2	Hs01053049_s1	RT-qPCR
Pou5f1	Hs00742896_s1	RT-qPCR
Klf4	Hs00358836_m1	RT-qPCR
Aldh1a1	Hs00946916_m1	RT-qPCR
Aldh1a3	Hs00167476_m	RT-qPCR
ActinB	Hs99999903_m1	RT-qPCR

Table 3. List of oligos

Oligo	**Forward**	**Reverse**	**Application**
PKM2_K422E	ggcctccttcgagtgct-gcagtggggccataatcg	ccactgcagcacttgaag-gaggcctccacggc	Site-directed mutagenesis
PKM2_K422R	ggcctccttcaggtgct-gcagtggggccataatcg	ccactgcagcacctgaag-gaggcctccacggc	Site-directed mutagenesis
PKM2_R489L	gacgtggacctcctggtg-aactttgccatg	ttcacccagaggtccacg tc-ctcagcccag	Site-directed mutagenesis
PKM2_K422E	gtgaggcagaggctgc	cgtcctcagcccagg	Sequencing
PKM2_K422R	gtgaggcagaggctgc	cgtcctcagcccagg	Sequencing
PKM2_R489L	gtgaggcagaggctgc	cgtcctcagcccagg	Sequencing

Chapter III

Results I

Results I: Lipid droplets as a new marker of breast cancer stem cells

All the results discussed in this chapter are published in the Journal of Clinical Medicine (JCM). The title of the article in which I contributed as co-first author is: "*Lipid droplets define a sub-population of breast cancer stem cells*" (Hershey B., Vazzana R., et al. 2019) (188).

3.1 The correlation between lipid droplets content, breast cancer disease and stemness

In order to investigate whether lipid droplets accumulation could impact on breast cancer disease progression, I tested whether in a cohort of 3951 breast cancer patients there was any correlation between the expression Perilipin2 (PLIN2) at the mRNA level (Affymetrix ID 209122_at) and relapse free survival (R.F.S.). PLIN2, also known as adipophilin, is a well characterized lipid droplet structural protein, known to be important for LD biogenesis and is considered a LD specific marker. Using the Kaplan-Meier plotter, I estimated the probability of relapse free survival (183). As shown in the Kaplan Meyer survival curve in **Figure 3.1a**, the R.F.S. is significantly lower in patients with high PLIN2 expression compared to PLIN2 low expressing patients. Moreover, in the stratified analysis based on the four breast cancer subtypes, I observed that the significant negative correlation between PLIN2 expression and the survival rate is retained in all the subtypes, with the only exception of the HER2+ patients in which I could not observe any statistically significant difference (**Figure 3.1b**).

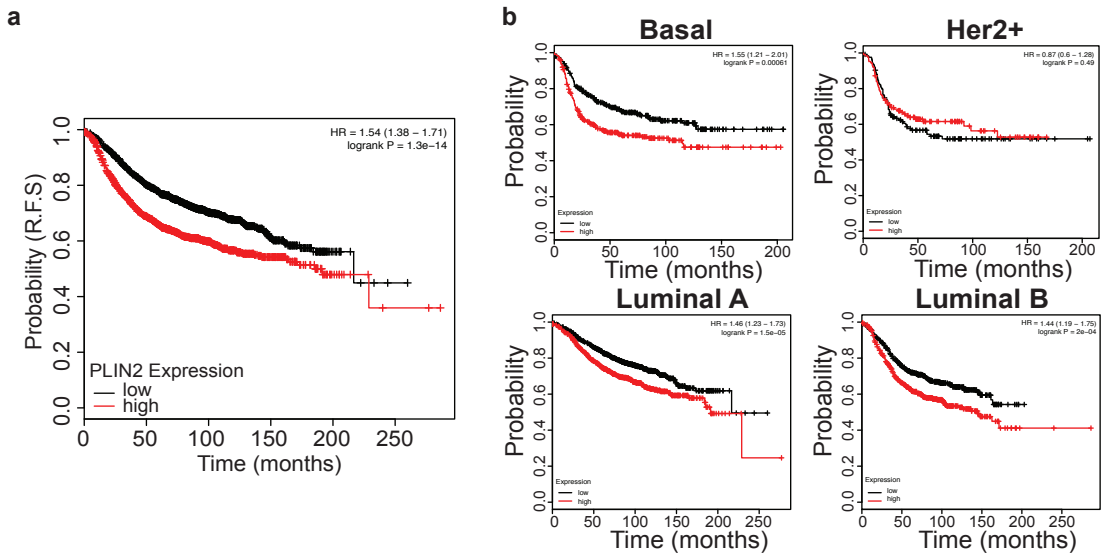

Figure 3.1. Lipid droplets content as a marker of cancer progression. a Kaplan-Meyer survival curve showing relapse free survival (R.F.S.) in breast cancer patients with low (black curve) and high (red curve) PLIN2 expression. ****P value = 1.3e-14. **b** Kaplan-Meyer survival curve stratifying the patients based on the breast cancer type. P values: Basal ***p=0.00061; Her2+ p=0.49; Luminal A ****p=1.5e-0.5; Luminal B ****p=2e-0.4.

I next sought to investigate whether the different breast cancer subtypes could be characterized by their lipid droplet content. With the attempt to have a panel of cells representing the most common breast cancer subtypes, I selected four different cell lines: BT474, belonging to the luminal B subtype (ER^+, PR^+, $HER2^+$), MCF7 and T47D luminal A cells (ER^+, PR^+, $HER2^-$), and MDA-MB-231 representing the triple negative (ER^-, PR^-, $HER2^-$) breast cancer cell line (**Table 4**).

Classification	ER	PR	HER2	Example Cell Lines [26,27]
Luminal A	+	+/-	-	**MCF7**, **T47D**, SUM185
Luminal B	+	+/-	+	**BT474**, MDA-MB-361
Claudin-low	-	-	-	**MDA-MB-231**, BT549
Basal	-	-	-	MDA-MB-468, SUM 190
HER2	-	-	+	SKBR3, MDA-MB-453

ER, estrogen receptor; PR, progesterone receptor; HER2, human epidermal growth factor receptor 2. The cell lines indicated in bold were used in this study.

Table 4. Classification of breast cancer cell lines based on receptors expression (183, 188-190).

In order to visualize the intracellular lipid droplets, I took advantage of the lipophilic dye Nile red 5H-Benzo[α]phenoxazin-5-one,9-(diethylamino). Nile Red allows for discrimination between neutral lipids, like triacylglycerols and sterol esters that form the lipid droplets' neutral core, that can be imaged using an excitation wavelength of 488 nm and an emission wavelength of 528, and charged lipids, like phospholipids included in all the organelle membranes whose excitation wavelength is between 515-560 nm and the emission > 590 nm (191). In line with this, I observed a robust lipid droplet staining in all four cell lines queried **Figure 3.2a.** The confocal images suggested that the lipid droplets content differed among the different cell lines. Therefore, using an ImageJ plug-in, I quantified the number of lipid droplets per cell for each cell line. This analysis revealed that in comparison to the other cell lines, BT474 and MDA-MB-231 were significantly enriched in lipid droplets **Figure 3.2b**.

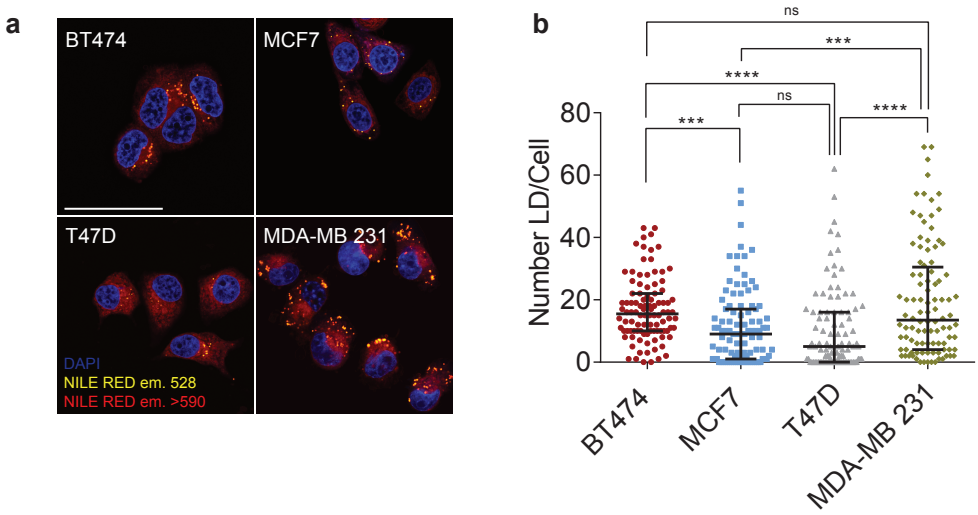

Figure 3.2. Lipid droplets content heterogeneity in cells. a Representative images of Nile red stainings in BT474, MCF7, T47D and MDA-MB231 cell lines. Nuclei were stained with Dapi (in blue). Images were acquired using the Sp5 inverted confocal microscope, 63x oil immersion objective, 2.5x magnification. Scale bar 50 µm. **b** Quantification of lipid droplets number for cell considering 100 cells for each cell line. Data are represented as mean ± standard error of the mean (SEM). P value: ***p < 0.001, ****p < 0.0001.

Intrigued by the observations about the accumulation of lipid droplets in the therapy resistant population of breast cancer patients (179), and the hypothesis by which the metastatic disease can be generated from the subpopulation of cancer stem cells that survive the therapeutic treatment (177), I wanted to investigate whether there was any correlation between the accumulation of these organelles and stemness traits. To do so, I started my study analysing the gene expression profile of different cancer stem cells markers. Particularly, I evaluated the expression of five genes: sex determining region Y-box 2 (Sox2), octamer binding transcription factor 4 (Oct4, also known as Pou5f1), Kruppel-like factor 4 (Klf4) and aldehyde dehydrogenase 1 family member 1 and 3 (Aldh1a1, Aldh1a3). Quantitative RT-qPCR data did not show consistent differences regarding the expression of these markers in our breast cancer cell lines panel, despite the increased expression of Sox2 in BT474 and MDA-MB-231 cells (**Figure 3.3**).

According to the cancer stem cell theory, tumours arise from a small population of cells capable to propagate, differentiate and with self-renewal properties. Due to the similarity with normal stem cells, we usually refer to them as Cancer Stem Cells (CSC). Recently, an *in vitro* approach was developed to isolate and characterize these cells in breast cancer. This system allows identification of CSCs based on their capability to survive and to form spheroids, in breast cancer called mammospheres, in non-adherent conditions (192). Further studies have shown that these mammospheres were enriched in progenitor cells able to

differentiate to several lineages and characterized by the expression of $CD44^{high}/CD24^{low}$, a marker of breast cancer stem cells (193).

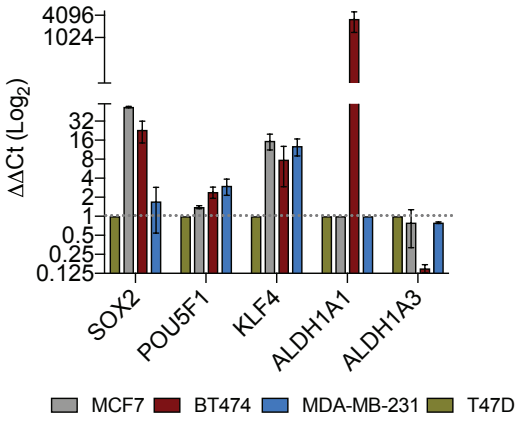

Figure 3.3. Relative mRNA levels normalized to T47D cell line and obtained from quantitative PCR analysis of a panel of five stemness related genes.

I decided to take advantage of this assay to test whether the four different cell lines harboured different capacities to form mammospheres. As shown in **Figure 3.4a**, I observed that all the cells were able to form mammospheres with varying efficiencies. Quantification of mammospheres formation efficiency, revealed a statistically significant difference between the cell lines (**Figure 3.4b**) that correlated with the previously quantified lipid droplet content **Figure 3.2b**.

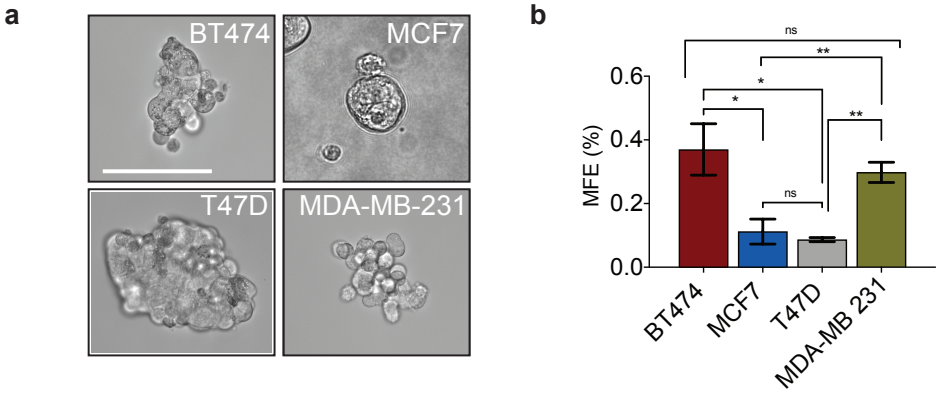

Figure 3.4. Lipid droplets accumulation correlates with stemness. a MDA-MB-231 Mammospheres from BT474, MCF7, T47D and MDA-MB-231 cells. Images were acquired using EVOS fluorescence microscope. Scale bar represents 200 µm. **b** Mammospheres formation efficiency for the four cell lines used in this study. Significance was calculated using two tailed t-tests; P value: *p<0.05, **p<0.01.

Since the lipid droplets enriched cells were also the ones more efficient in the mammospheres formation, I decided to use BT474 and MDA-MB-231 cells to test whether I could observe lipid droplets enriched cells inside the mammospheres. To do so, I generated second generation mammospheres, I fixed them and stained using Nile red, as previously described. Remarkably, within all the grew secondary generation mammospheres, there was one or maximum two cells highly enriched in lipid droplets, suggesting a correlation between LDs and stemness properties (**Figure 3.5**).

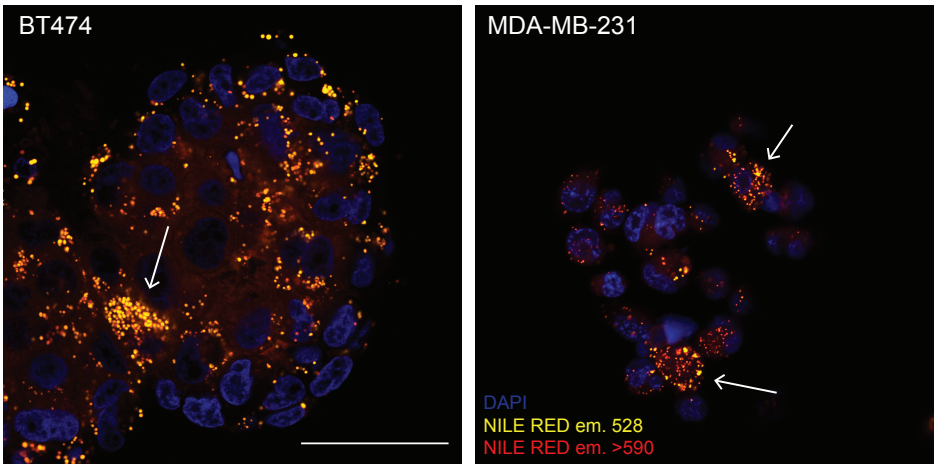

Figure 3.5. Second generation breast cancer mammospheres show lipid droplets enriched sub-population of cells. Representative images of BT474 and MDA-MB-231 mammospheres stained with Nile red. Nuclei were stained with Dapi (in blue). The white arrows call attention to the lipid droplets highly enriched cells. Images were acquired using the Sp5 inverted confocal microscope, 63x oil immersion objective. Scale bar 50 µm.

Despite not having registered significant differences for the expression level of some stem cell markers in the global population, I observed interesting differences between the cell lines in mammosphere formation capacity. Moreover, the confocal images of the second generation mammospheres revealed a marked lipid droplet accumulation localized only in few cells. Taken together these data suggest a potential role of these lipid droplets enriched cells as progenitors with stemness traits.

3.2 Cellular complexity is increased in lipid droplets enriched cells

The Nile red staining suggested an important heterogeneity in lipid droplet content between the cell lines. Along the same line, I also realized that the lipid droplets content was not homogeneously distributed inside the same cell line, with some cells highly enriched in lipid droplets and some others almost depleted.

In an attempt to better understand whether the more enriched cells were harbouring stemness traits, I developed a method to isolate the lipid droplets^{high} and lipid droplets^{low} subpopulations. To do so, I took advantage of a live cell marker of lipid droplets, BODIPY^{TM} 500/510 (Bodipy) that would permit us to isolate and collect the cells according to their lipid droplet content using a fluorescence activated cell sorting (FACS) based approach.

I first tested the internalization of the Bodipy, a fluorescent fatty acid analogue (194), by confocal microscopy. As shown in **Figure 3.6a** (upper panel), all the four cell lines were able to internalize Bodipy, and the accumulation was mainly observed at the level of the lipid droplet suggesting that when read in the green channel the amount of Bodipy internalized by all the other membranous compartments could be neglected. As an additional control, I treated cells with the exogenous fatty-acids palmitic acid (50 μM) and oleic acid (100 μM), prior to the addition of Bodipy. Palmitic and oleic acids represent the most abundant, saturated and unsaturated fatty acids in the human plasma, respectively. The amount of fatty acids that I used in my assays are in the range of the physiological levels quantified by metabolomic studies as reported in the Human Metabolome Database (195). Exogenous fatty acid uptake should enhance lipid droplet accumulation. Indeed, I observed an increase in the lipid droplets content, as shown in the lower panel of **Figure 3.6a**. Having established that Bodipy specifically stained lipid droplets, I was ready to use it in a FACS based protocol.

As I had previously used imaging to characterize the four cell lines for lipid droplet abundance, I then set out to determine whether I could confirm these results using a FACS based approach. Performing a FACS analysis on control (non-loaded) cells and Bodipy-loaded cells, I observed the expected shift of the fluorescein isothiocyanate (FITC)

Bodipy-signal in all four cell lines (**Figure 3.6b**). As appreciated in the histograms, we confirmed the differences in baseline levels of lipid droplets between the cell lines. Again, in order to ensure that the florescent signal could be attributed to lipid droplets we treated the cells with palmitic and oleic acids prior to the addition of Bodipy. As expected, pre-treatment with fatty acids resulted in a quantifiable shift in the mean florescence intensity (**Figure 3.6b**). Interestingly, in addition to the Bodipy specific signal, careful observation of the scatter plots revealed a shift in the Side Scatter (SSC) of the Bodipy^{high} populations. This shift was even more pronounced in the fatty acid loaded cells, suggesting an increase in the cellular complexity in lipid droplets enriched cells. Therefore, I decided to include this parameter in our analysis. Taken, together the combination of SSC and Bodipy provided me with an efficient method to identify and sort cells based upon lipid droplet abundance.

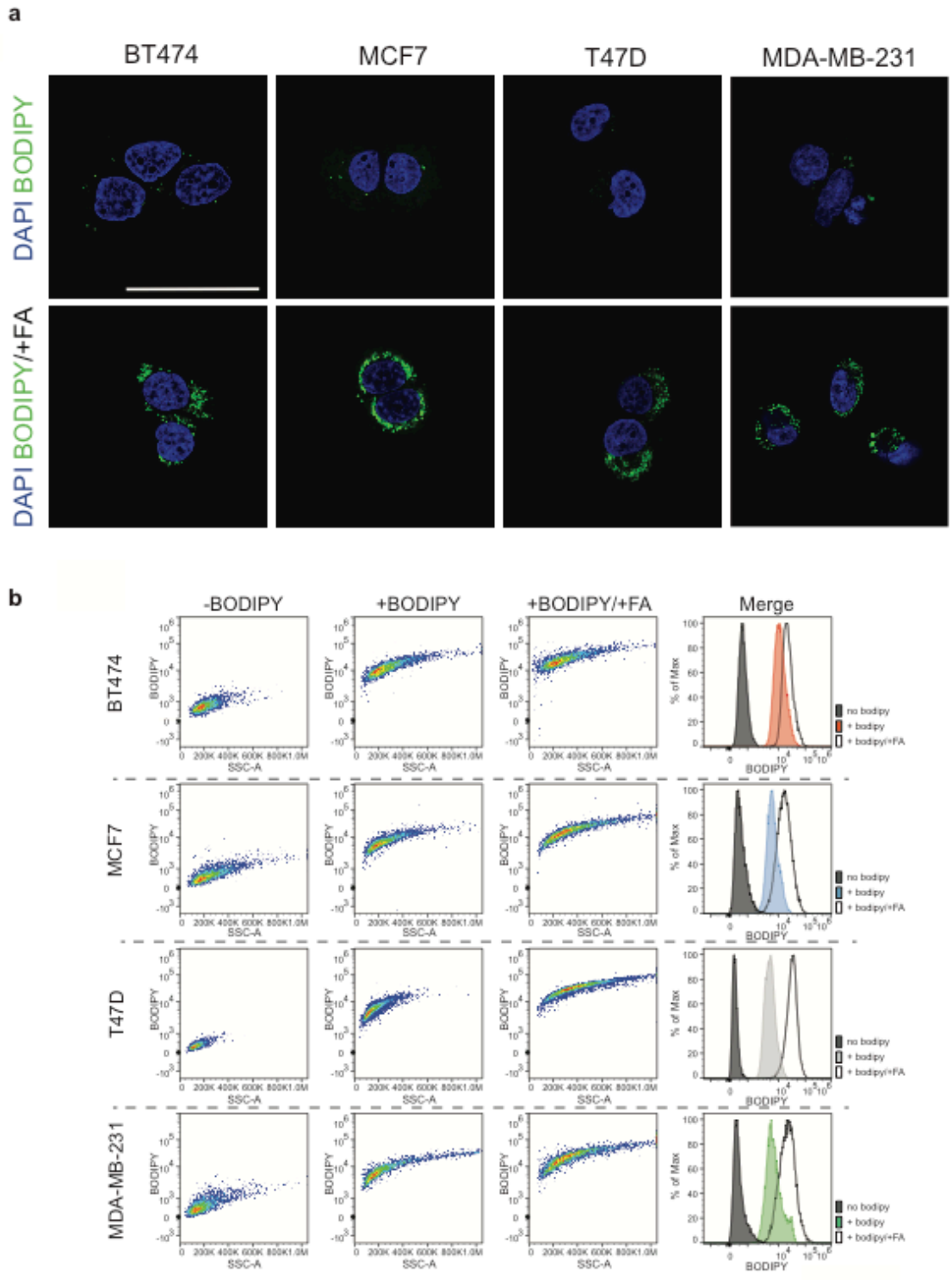

Figure 3.6. The fluorescent fatty acids analogue Bodipy as a tool to isolate lipid droplets enriched cells. a BODIPY 500/510 stainings of lipid droplets (in green) in BT474, MCF7, T47D and MDA-MB-231 cells. In the upper panel control cells and in the lower panel cells loaded with 50 µM palmitic and 100 µM oleic fatty acids. In both the conditions, cells were incubated for 12 hours with Bodipy. Images were acquired using the Sp5 inverted confocal microscope, 63x oil immersion objective. Scale bar 50 µm. **b** Side scatter vs forward scatter for total counted events in the absence of Bodipy, presence of Bodipy and Bodipy plus fatty acids loaded cells. The last panel merged panel represents the Bodipy signal for the three conditions.

3.3 Isolated lipid droplets^{high} cells are characterized by stemness markers and properties

The identification of the cancer stem cell population inside the tumour mass is still a limiting factor for effective therapeutic approaches. In breast cancer, a combination of markers is generally used to better distinguish and isolate the heterogeneous stem cell population. Among these markers, breast CSC have been shown to be particularly enriched in CD44 (Cluster of Differentiation) and depleted in CD24 surface markers, the subpopulation of cells characterized by this phenotype is usually referred to as CD44^{high}/CD24^{low} (196). In order to investigate whether there was a correlation between the CD44^{high}/CD24^{low} markers expression and the lipid droplet enrichment, I performed flow cytometry analysis taking advantage of the bodipy-FACS approach described above. I decided to apply this approach to the MDA-MB-231 and BT474 cell lines. The distribution of the bodipy signal corresponding to lipid droplets in the main population is represented by the grey curve in the histogram in **Figure 3.7a**.

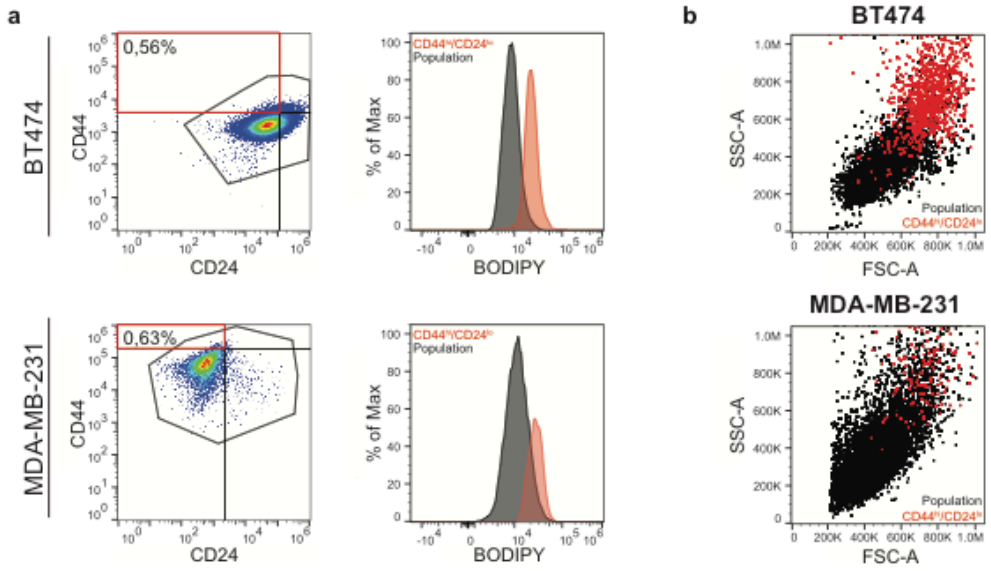

Figure 3.7. Stem cell marker CD44^{high}/CD24^{low} enriched cells show a higher lipid droplets content. a Flow cytometry analysis of CD44/CD24 cell surface markers in BT474 and MDA-MB-231 cells. Antibodies used include an anti-CD44 antibody conjugated to VioBlue and an anti-CD24 conjugated to Alexa Fluor 647. Left panels show representative dot plots of CD44-VioBlue versus CD24-AlexaFluor647 expression for BT474 and MDA-MB-231 cells. Cells which fell in the upper left quadrant we considered to express the CSC phenotype of interest (CD44^{high}/CD24^{low}). In the right panel, the histogram represents the Mean Fluorescence Intensity (MFI) for Bodipy in CD44^{high}/CD24^{low} cells (red) versus the total population (grey). **b** Flow cytometry scatter plots for side scatter (SSC) versus forward scatter (FSC) of BT474 and MDA-MB-231 cells show an increase in cellular complexity for CD44^{high}/CD24^{low} cells.

Interestingly, in comparison to the population, the CD44^{high}/CD24^{low} population represented by the red curve in the histogram, had a higher lipid droplet content in both cell lines. Moreover, CD44^{high}/CD24^{low} cells were also characterized by increased cellular complexity,

as shown in the side scatter (SSC) versus forward scatter (FSC) plot (**Figure 3.7b**). These data suggest that CSCs are enriched in lipid droplets.

In order to demonstrate with a more direct approach that lipid droplets enriched cells were characterized by stemness traits, I needed to isolate this population of cells from the total population. I decided to perform these experiments focusing our attention on BT474 cells, since they were showing a higher lipid droplets content together with a better mammospheres formation efficiency. Taking advantage of the BODIPY-FACS sorting previously described according to their bodipy intensity, I isolated the top and bottom 5% cells, and referred to them as lipid droplets^{high} and lipid droplets^{low}, respectively (**Figure 3.8a**). Moreover, I also collected a control group of cells, from the total population, called lipid droplets^{ave} sub-population. To be sure that the sorting procedure was efficient, I further checked the lipid droplets content in the sorted populations by Nile red staining and confocal microscopy. The Nile red staining confirmed that the Bodipy^{high} sub-population of cells was indeed highly enriched in lipid droplets compared to the counterpart Bodipy^{low} sub-population (**Figure 3.8b**).

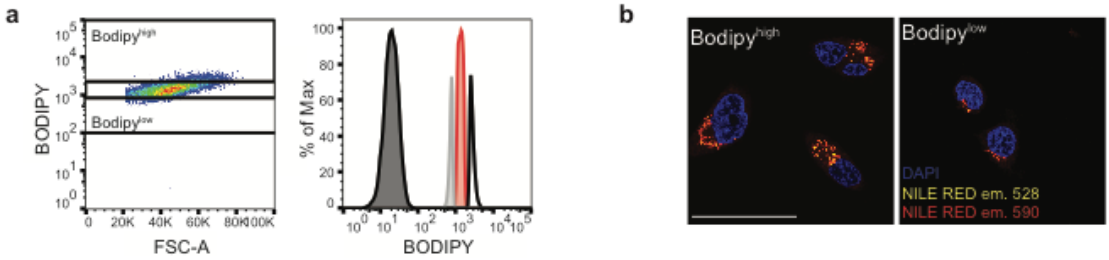

Figure 3.8. The BODIPY-FACS sorting as a strategy to isolate lipid droplets enriched cells. a Bodipy 500/510 FACS sorting analysis of BT474 cells. Left panels show representative dot plots of BODIPY-FITC versus forward scatter (FSC) plot and the gating strategy used to isolate the two different sub-populations, bodipy^{high} and bodipy^{low} cells. In the right panel, the histogram represents the Mean Fluorescence Intensity (MFI) for Bodipy in the sorted cells. **b** Representative confocal images of sorted cells stained with Nile red. Nuclei were stained with Dapi (in blue). Images were acquired using the Sp5 inverted confocal microscope, 63x oil immersion objective, 2.5x magnification. Scale bar 50 μm.

I wanted now to use the sorted cells to verify whether it was possible to score differences in the stemness traits among the three different sub-populations of cells. To do so, I evaluated the expression of several genes previously described as cancer stem cell markers. Interestingly, as shown in **Figure 3.9a**, the Bodipy^{high}/lipid droplets^{high} sub-population of cells shows a higher expression of all the analysed stem genes if compared to the Bodipy^{low} cells, suggesting that the lipid droplets^{high} population could be enriched in cancer stem cells.

Moreover, I also tested the capability of the sorted populations to form mammospheres. Importantly, also in this case, I observed a statistically significant increase in the mammospheres formation efficiency in the Bodipy^{high} population compared to the Bodipy^{low} (**Figure 3.9b**). All together these results demonstrate that the Bodipy-FACS based approach can be used to isolate sub-populations of cells according to their lipid droplets content. Moreover, my data demonstrate that the lipid droplets enriched cells have cancer stem cell features.

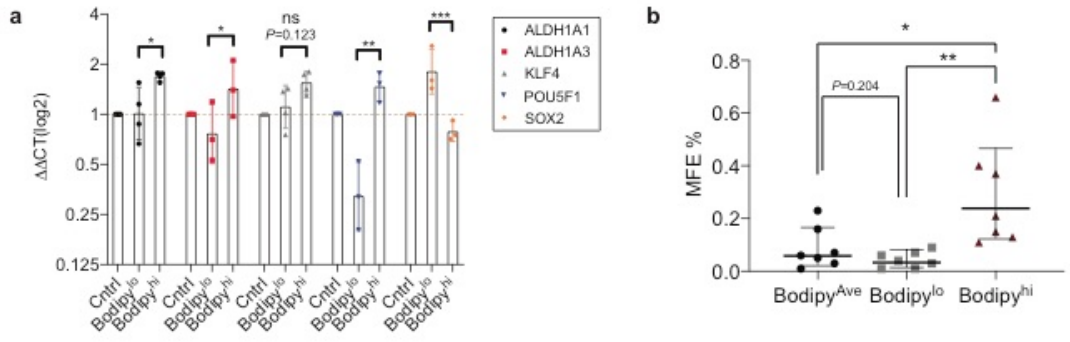

Figure 3.9. Lipid droplets^{high} sub-population shows stemness traits. a RT-qPCR of the indicated genes, marker of stemness, in BT474 cells following the BODIPY-FACS sorting. The three groups represent the Lipid droplets^{Ave}, Lipid droplets^{Low} and the Lipid droplets^{High} sub-populations. Data are shown as geometric mean ± standard deviation. **b** Mammospheres formation efficiency for the three different sub-populations of sorted cells. Significance was calculated using two tailed t-tests; P value: *p<0.05, **p<0.01, ***p<0.001.

3.4 In vivo tumorigenic potential of Lipid droplets^{high} cells

In order to determine whether the observed stem traits were associated with *in vivo* tumorigenic potential, I decided to inject the BODIPY-FACS sorted sub-population of cells into the mammary glands of immuno-compromised mice (**Figure 3.10a**). These *in vivo* studies were performed in collaboration with Emanuela Frittoli, from the IFOM Mechanisms of tumour cell migration laboratory headed by Giorgio Scita.

To do so, I firstly isolated the three different polulations of cells according to the lipid droplets content, LD^{high} (or Bodipy^{high}), LD^{low} and LD^{ave} cells; then I injected 300,0000 cells in each mammary gland and monitored tumor onset.

Despite the observation that all three populations, LD^{ave}, LD^{high} and LD^{low}, were able to form tumours, LD^{high} populations showed a more rapid onset compared to the LD^{low} or LD^{ave} populations (**Figure 3.10b**). These findings demonstrate that the lipid droplet enriched cells (LD^{high}) show an higher tumorigenic potential. Taken together these results demonstrate the role of lipid droplets as a marker of cells harbouring increased tumorigenic potential both *in vitro* and *in vivo*.

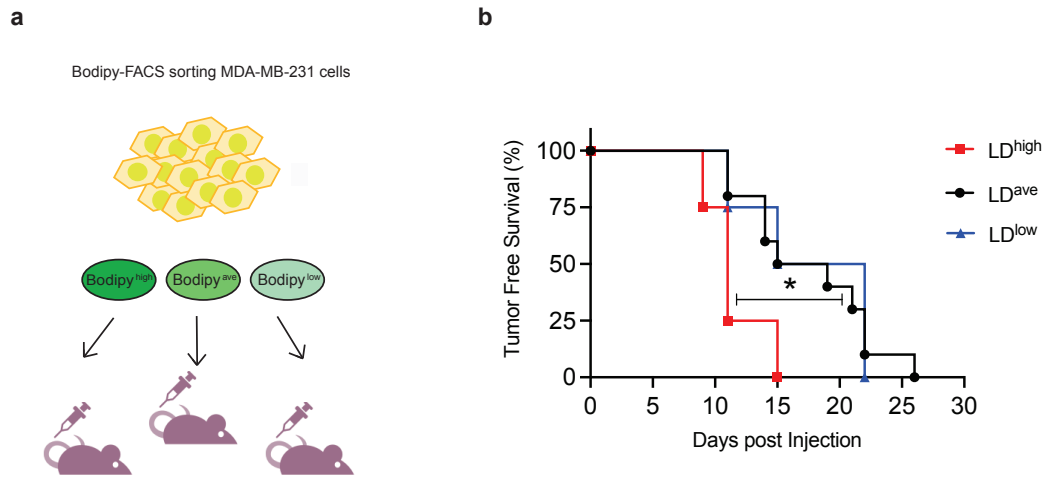

Figure 3.10. In vivo tumorigenic features of Lipid droplets^{high} cells. a Schematic representation of the strategy used for the in vivo studies. Triple negative MDA-MB-231 BODIPY-fluorescence activated sorted cells were injected into NOD/SCID mice. **b** Tumor Free Survival percentage for the in vivo studies of each group of mice injected with the Bodipy-sorted cells. 300.000 LD^{high} or LD^{low} cells were injected for mammary gland. The three groups of mice included n=4 mice for LD^{low}, n=9 mice for LD^{ave} and n=4 mice for LD^{high}. Significance was calculated using two tailed t-tests; P value: *p<0.05.

3.5 Breast cancer cell lines dependencies from the de novo fatty synthesis

These results suggesting increased cancer stem cell related traits in the lipid droplet enriched cells, led me to ask whether I could modulate the tumorigenic potential by interfering with lipid metabolism. One of the main dysregulated lipid metabolic pathways in cancer cells is the *de novo* fatty acids (FA) synthesis pathway. Starting from acetyl CoA, malonyl-CoA is generated in a reaction catalyzed by Acetyl CoA Carboxylase alpha (ACC-alpha) enzyme (197) (**Figure 3.11a**).

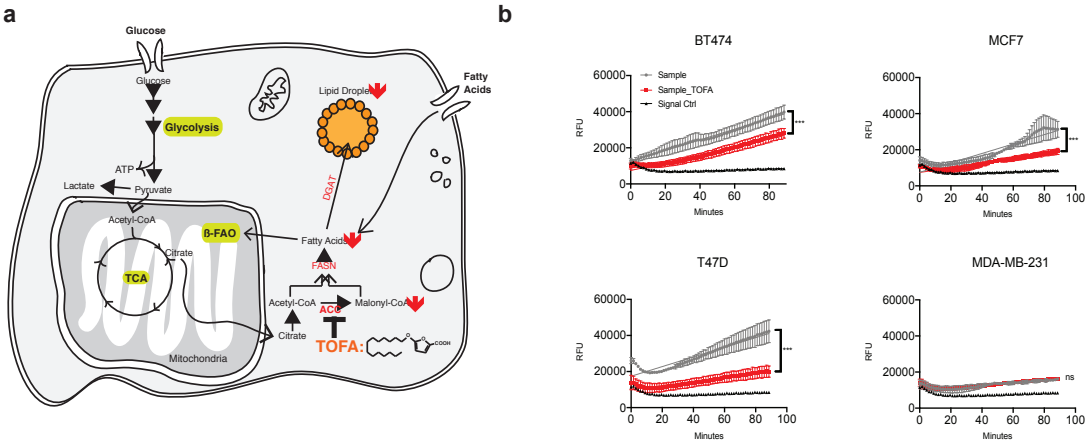

Figure 3.11. TOFA inhibits malonyl-CoA production and fatty acids beta oxidation. a Cartoon showing the effects of TOFA inhibitor on cellular lipid metabolism. **b** Fatty acid beta oxidation assay performed in the panel of breast cancer cell lines after 24 hours of 10 uM TOFA exposure. Each regression line represents the 95% confidence interval. Asterisks indicate statistical significance detected at the 0.001*** probability level.

This enzyme has a key role in the cellular micro-environment since malonyl-CoA generation is fundamental not only for fatty acids biosynthesis but also for the inhibition of carnitine palmitoyl-transferase enzyme which regulates the fatty acids beta oxidation pathway, catalyzing the transfer of acyl chains to carnitine with the consequent translocation of acyl-carnitine from the cytoplasm to the mitochondria (198). In order to block the *de novo* fatty acids synthesis, I treated the breast cancer cell lines used in this study with the ACC-alpha chemical inhibitor TOFA (5-tetradecyloxy-2-furoic acid). TOFA acts as an allosteric inhibitor of ACC-alpha since, once internalized by the cells, is converted to TOFyl-CoA, thus competing with acetyl-CoA for the binding (199).

Cells were evaluated for lipid droplet content at 48 hours post-treatment with 10 uM TOFA. Following treatment, I scored a reduction in the lipid droplet content of BT474, MCF7 and T47D cell lines in comparison to the control or the vehicle treated cells.

The lipid droplet content was evaluated both with Nile red staining, as shown in **Figure 3.12a**, and the previously described BODIPY-FACS (**Figure 3.12b).** Interestingly, the MDA-MB-231 cells, did not show a TOFA dependent drop in lipid droplets, suggesting that they may be more dependent on exogenous fatty acids, or conversely less dependent on mitochondrial Beta-oxidation as an energy source.

In order to test if the reduction in malonyl-CoA production was affecting also other lipid metabolic pathways, I also evaluated the capability of the cells to oxidize fatty acids taking advantage of a commercial fatty acid oxidation (FAO) assays. As shown in **Figure 3.11b**, with the exception of MDA-MB-231 cells, TOFA treated cells show a statistically significant reduction in fatty acids oxidation compared to the control cells, suggesting the existence of a futile cycle in these three cell lines. This could be due to the reduction of malonyl-CoA production that can lead to the inactivation of the carnitine-palmitoyl transferase enzyme.

Interestingly, MDA-MB-231 cells seem to not be affected by the TOFA treatments. Indeed, the lipid droplets content did not show any decrease and also fatty acid oxidation levels were not affected by the inhibitory effect of TOFA. This could be due to an intrinsic resistance to the inhibitor, for example, based on mutations at the TOFA binding site of ACC-alpha, or to the up-regulation of alternative pathways able to sustain fatty acids production. Further investigations are required to better characterize this phenomenon.

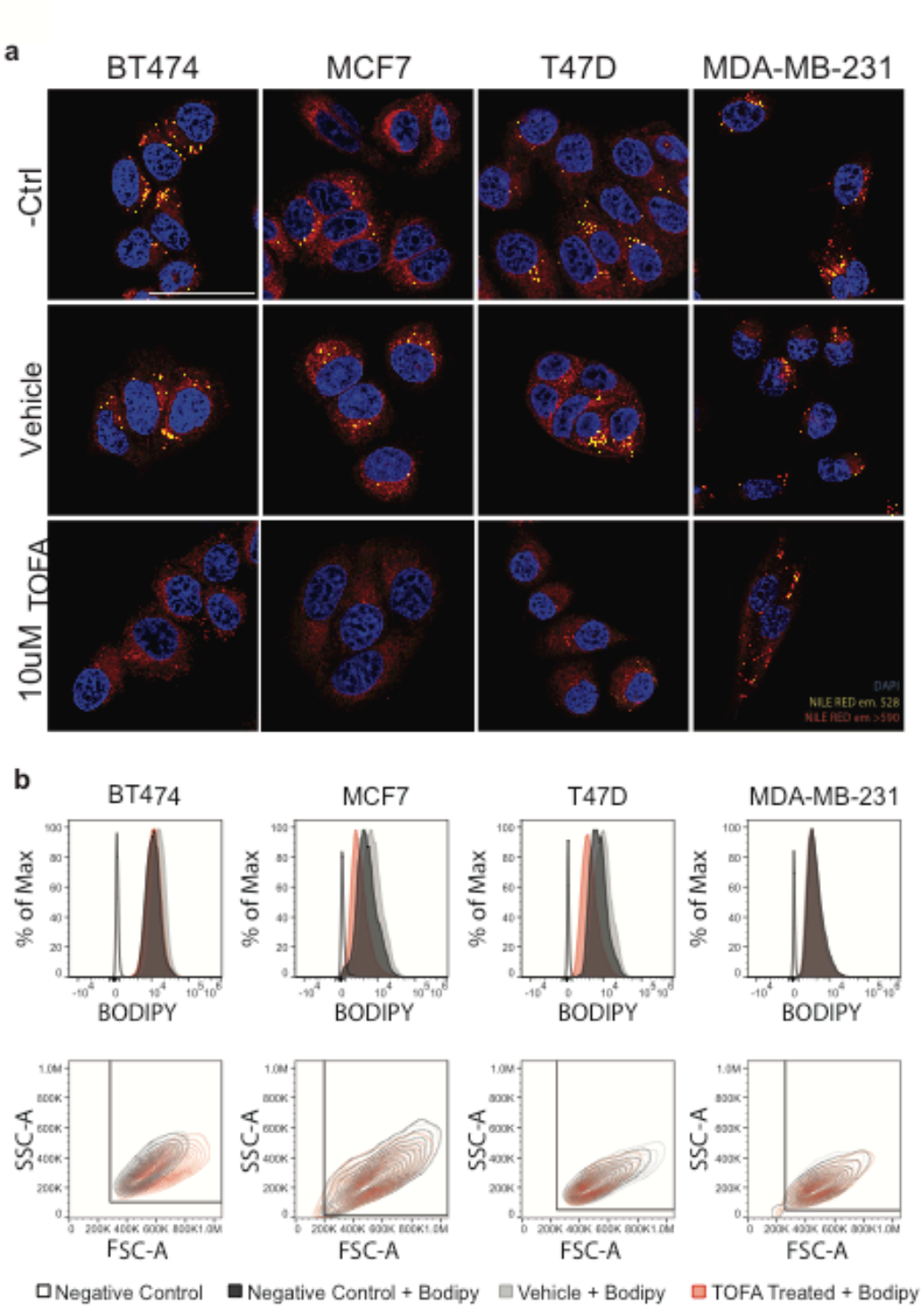

Figure 3.12. De novo fatty acids synthesis inhibition blocks lipid droplets accumulation. a Representative images of Nile red stainings in BT474, MCF7, T47D and MDA-MB-231 control cells, vehicle and TOFA treated for 48 hours with vehicle (DMSO) or 10 uM TOFA. Nuclei were stained with Dapi (in blue). Images were acquired using the Sp5 inverted confocal microscope, 63x oil immersion objective. Scale bar 50 µm. **b** BODIPY-FACS analysis of the cells treated with vehicle or TOFA for 48 hours. The upper panel represents the Bodipy signal for all the conditions analyzed; the bottom panel shows the side scatter vs forward scatter plots for total counted events in control, vehicle or TOFA treated cells.

Since I demonstrated that lipid droplets enriched cells show a cancer stem cells phenotype, I wanted to evaluate whether targeting the *de novo* fatty acids synthesis and thus the lipid droplets accumulation, I could score any difference in the tumorigenic capacity of the cells. To do so, I first wanted to evaluate the proliferation rates of the cells in the absence or presence of TOFA inhibitor. As shown in **Figure 3.13a**, with the exception of the MDA-MB-231 cell line, cells treated with 10 µM TOFA had a significant reduction in the cellular growth compared to the control or the vehicle treated cells.

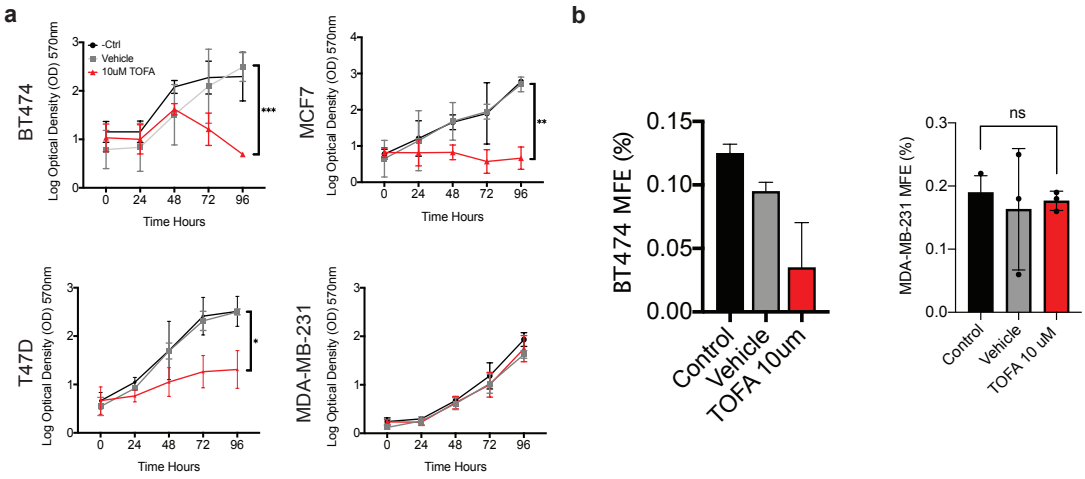

Figure 3.13. TOFA inhibits the proliferation potential. a Cellular growth for the breast cancer cell panel in control cells versus vehicle or TOFA treated cells. Significance was calculated using the multiple unpaired t-test. P value: *p<0.05, **p<0.01, ***p < 0.001. **b** Second generation mammospheres formation assay performed in BT474 and MDA-MB-231 cells after 5 days of vehicle or TOFA treatments (n=2).

Moreover, to assess whether the reduction of the LD content observed in the TOFA treated cells affected the cancer stem cells traits, I compared mammosphere formation between BT474 and MDA-MB-231 cells following an acute 5-day treatment with TOFA. Importantly, the assay was performed in free-TOFA media in order to avoid any possible effect on the cellular growth mediated by the presence of the inhibitor. In this way, I was able to observe the behaviour of cells that survived the TOFA treatment, with either (1) decreased LD content (as shown in **Figure 3.12**) (BT474) or (2) no effect (MDA-MB-231). Interestingly, I scored a reduction in the mammosphere formation efficiency in TOFA treated BT474 cells compared to the control cells (**Figure 3.13b**). Importantly, in line with their non-responsiveness to TOFA treatment, MDA-MB-231 cells did not show any difference in cellular proliferation rates or in the mammosphere formation capacity among the three groups (control, vehicle or TOFA). The observation that TOFA sensitive cells had reduced MFE strengthened the correlation between the LD content and the tumorigenic capacity.

Chapter IV

Results II

Results II: The biochemical interplay between glucose and lipid metabolism

4.1 PKM2 activity is differently regulated in a panel of breast cancer cell lines

Cellular metabolism includes all the biochemical reactions necessary to provide ATP based upon glucose, lipids or, in a lower fraction, proteins catabolism. According to the Randle cycle theory, also known as the "glucose-fatty acid cycle", there is a competitive mechanism between the usage of the two main cellular fuels, fatty acids and glucose. Specifically, Randle focused on the competition between glycolysis and fatty acid oxidation (FAO), since he observed that the accumulation of one of the two metabolites, glucose or fatty acid, at the cellular level was able to inhibit the other pathway. It is now known that Malonyl-CoA, a basic building block in *de novo* fatty acid biosynthesis, inhibits CPT1, thus blocking entry of fatty acids into the mitochondria for consumption via beta-oxidation. In addition to the work done by Randle, in the late 1960s several studies demonstrated that long and short chain fatty acids were able to inhibit glycolytic enzymes hexokinase and pyruvate kinase, although the mechanism behind the fatty acid mediated inhibition remains unknown (72, 200).

Pyruvate kinase M2 (PKM2) enzyme plays a key role in the regulation of the glycolytic flux, since it catalyses the terminal reaction of glycolysis. The previously mentioned observations regarding a potential role for fatty acids in regulating PKM2 activity and the important role played by PKM2 in cancer, led me to investigate whether there was a direct interaction between fatty acids and PKM2. To do so, I started analysing the expression and activity of PKM2 in a panel of ten breast cancer cell lines. As shown in **Figure 4.1a**, the protein expression levels are very similar in all the cells that I tested. Taking advantage of a previously published protocol from Worthington Biochemical, I measured the pyruvate kinase activity in a lactate dehydrogenase coupled assay system (**Figure 4.1b**).

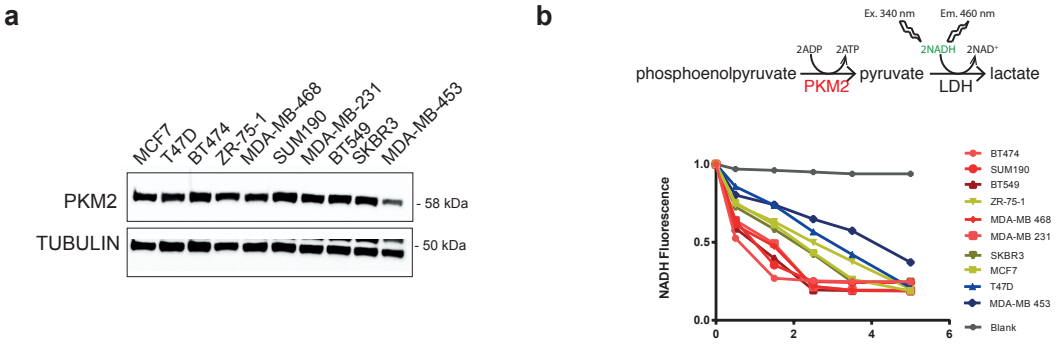

Figure 4.1. Pyruvate kinase M2 expression and activity. **a** Immunoblot analysis of PKM2 expression in a panel of ten breast cancer cell lines. **b** In vitro pyruvate kinase assay. The upper part shows the schematic representation of the in vitro assay used in our study. The lower panel shows the pyruvate kinase activity for the ten breast cancer cell lines.

Measuring the decrease in the absorbance at 340 nm coming from the NADH oxidation, I analysed the PKM2 activity across the cell line panel and I interestingly found that, despite similar levels of total protein, PKM2 activity differed significantly between the cell lines.

4.2 Specific interactions between PKM2 and fatty acids

Thus, I selected BT474 cell line, which showed the highest PKM2 glycolytic activity, and I assessed the PKM2 capability to bind to fatty acids by performing a fatty acid pull-down assay. Following a previously published protocol (184), I first conjugated the aminohexyl-agarose beads with fatty acids of various chain lengths (**Figure 4.2a**). Then, after evaluating the efficiency of the conjugation of the fatty acids to the agarose beads using the Kaiser test assay (185), I used whole cell protein extracts from exponentially growing BT474 cells to perform pull-down assay followed by immunoblotting analysis. As shown in **Figure 4.2b** (left upper-panel), using the cellular lysates, I observed a strong interaction between PKM2 and all the fatty-acids tested. Conversely, PKM2 did not interact with the unconjugated control beads, suggesting that PKM2 can bind to lipids.

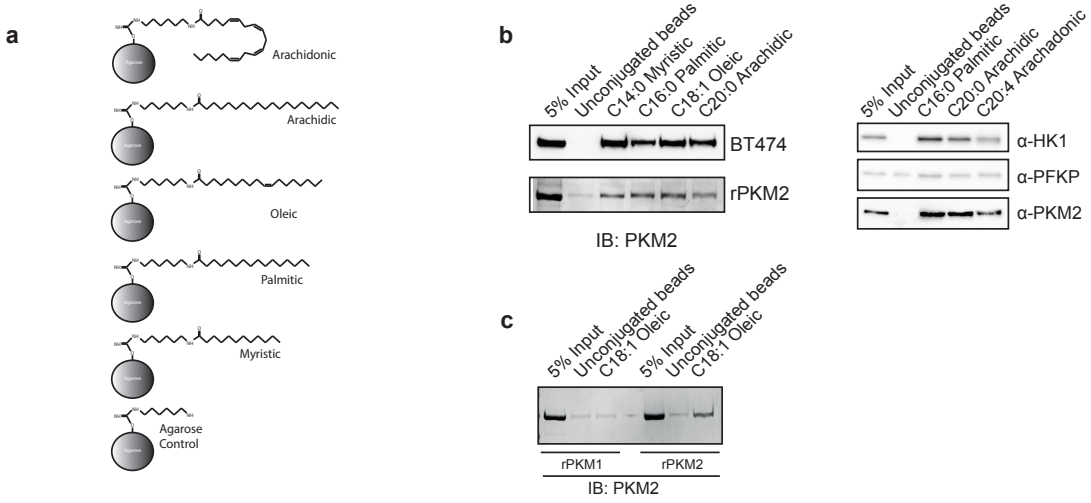

Figure 4.2. PKM2 binds fatty acids. a Schematic representation of the four different fatty-acyl beads used in this assay. The preparation of fatty-acyl co-Aminohexyl-agarose beads was performed as described by E. Beck-Garcia et al. 2013. **b** Western blot analysis for PKM2 after the fatty acid pull-down assay for BT474 cells (left panel - upper part), recombinant PKM2 protein (left panel - lower part) and Western blot analysis for Hexokinase, Phosphofructokinase and PKM2 post-pull down (right panel). **c** Western blot analysis for PKM2 after the fatty acid pull-down assay using recombinant PKM1 and PKM2 proteins.

I then expanded the analysis using the other two glycolytic enzymes considered glycolytic gatekeepers, since they catalyse the other two unidirectional reactions of glycolysis, Hexokinase 1 (HK1) and Phosphofructokinase P (PFKP). The *in vitro* pull-down assay showed an interaction between HK1 and medium-long chain fatty acids (**Figure 4.2b,** right

panel), suggesting a potential direct mechanism based on physical interaction behind the old observations made by Lea and collaborators concerning fatty-acids mediated hexokinase inhibition (200). PFKP was, instead, a-specifically binding in all conditions including the unconjugated control beads. In order to assess if the observed binding was due to a direct interaction or was modulated by co-factors, I decided to assess the lipid binding property of the recombinant PKM2 protein produced in *Escherichia coli*. Interestingly, the binding with the fatty acids was maintained, albeit reduced, by the recombinant PKM2 protein, confirming a direct interaction between the enzyme and the tested fatty acids (**Figure 4.2b**, lower panel).

PKM2 protein sequence arises from the same transcript that also generates Pyruvate Kinase M1 (PKM1) protein, through an alternative splicing event. The two proteins differ for the presence of exon 9 in PKM1 and exon 10 in PKM2. This important difference confers upon PKM2 the ability to tune its activity through allosteric regulation, while PKM1 is constitutively active (201). In order to test whether PKM1 was also able to bind lipids, I purified the recombinant protein and again performed the fatty acid pull-down assay using oleic acid and the two (PKM1 and PKM2) recombinant proteins. Interestingly, PKM1 did not appear to bind the oleic acid, while the interaction was confirmed for PKM2 (**Figure 4.2c**). I observed that, although the rPKM2 was able to bind to lipids, the binding was reduced in respect to that seen from lysates. This observation led me to ask why that might be. Focusing specifically on the potential lipid binding capacity, I used a published tool (202) to analyze the amino acids properties of PKM2 and to create a hydrophobicity plot. The analysis revealed that PKM2 harbors a specific region particularly enriched in hydrophobic residues (**Figure 4.3**), suggesting a potential region of interaction of the protein with hydrophobic molecules like lipids. This region lies within the inter-subunit contact region, within close proximity to the FBP binding site, suggesting that availability of PKM2 to bind to fatty acids may depend on its multimerization state.

From a structural point of view, the main difference between the two isozymes is that while PKM1 is a stable tetramer, PKM2 alternates two different conformations, switching from a less active dimer to a more active tetramer.

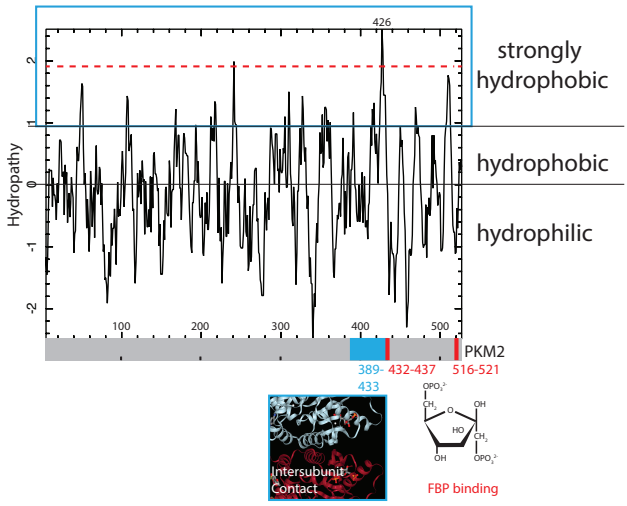

Figure 4.3. PKM2 sequence shows highly enriched hydrophobic regions. Hydropathy plot of PKM2 amino acids sequence. Sequences in the upper part are hydrophobic (>0), while sequences in the lower part are hydrophilic (<0). The hydrophobic peak at the 426 residue represents the highest hydrophobic region and belongs to PKM2 inter-subunit contact domain region. The hydropathy plot is based on the Kyte and Dolittle algorithm and was created using the EMBL-EBI sequence analysis tool APIs.

Therefore, I hypothesized that a possible interaction site could be exposed in the dimeric form of PKM2. This idea, reinforced by the hydropathy plot data, is further supported by analysis of the crystal structure from which one can appreciate the cluster of highly hydrophobic regions, showed in dark blue in **Figure 4.4** (RCSB Protein Data Bank: 3U2Z), positioned within the dimer:dimer interface.

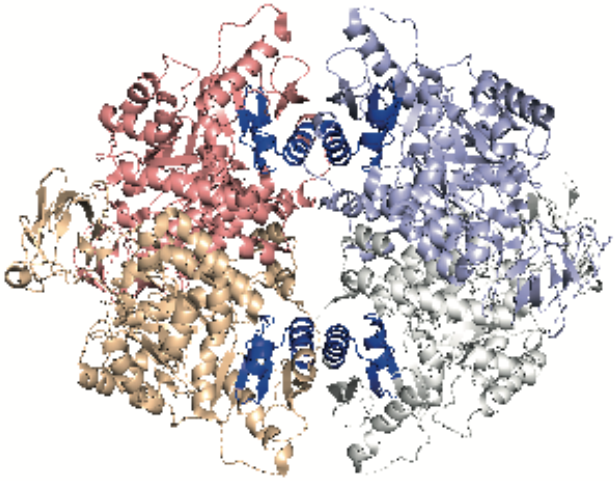

Figure 4.4. Crystal structure of PKM2 wildtype tetramer. Each monomer is displayed in a different color. In white, light purple, light yellow and salmon respectively chains A, B, C and D. Dimer 1 is formed by chains A and B, Dimer 2 by chains C and D. In dark blue are represented the highly hydrophobic regions at the dimer:dimer interface. Image was generated using Pymol.

4.3 Generation of recombinant PKM2 mutants in E. coli

Since the hydrophobic region is mostly present at the PKM2 dimer:dimer interface, I hypothesized that this region could regulate the stabilization of the dimeric or tetrameric form of PKM2. Therefore, based upon literature and structure-function analysis, I selected residues, that once mutated, might affect the quaternary structure of the protein. In particular, I focused on lysine 422 (K422) as its mutation to arginine has been previously shown to modulate the activity and to promote conformational changes on PKM2 structure (203). Indeed, it is a critical residue as it is located within the previously identified hydrophobic patch in the inter-subunit contact domain (**Figure 4.5b**). The second residue I selected was the arginine 489 (R489). The mutation of this arginine to leucine has been shown to abrogate the FBP binding capacity (204), thus altering the FBP mediated-allosteric regulation.

Conducting site directed mutagenesis of the parental WT_PKM2 coding sequence, I generated the PKM2_R489L mutant and two different PKM2_K442 mutants: PKM2_K422R and PKM2_K422E. As described before, the first one is characterized by the same mutation reported in patients K422R and, the second one, K422E, where the lateral amino acid chain of the glutamic acid imparts a negative charge to the patch.

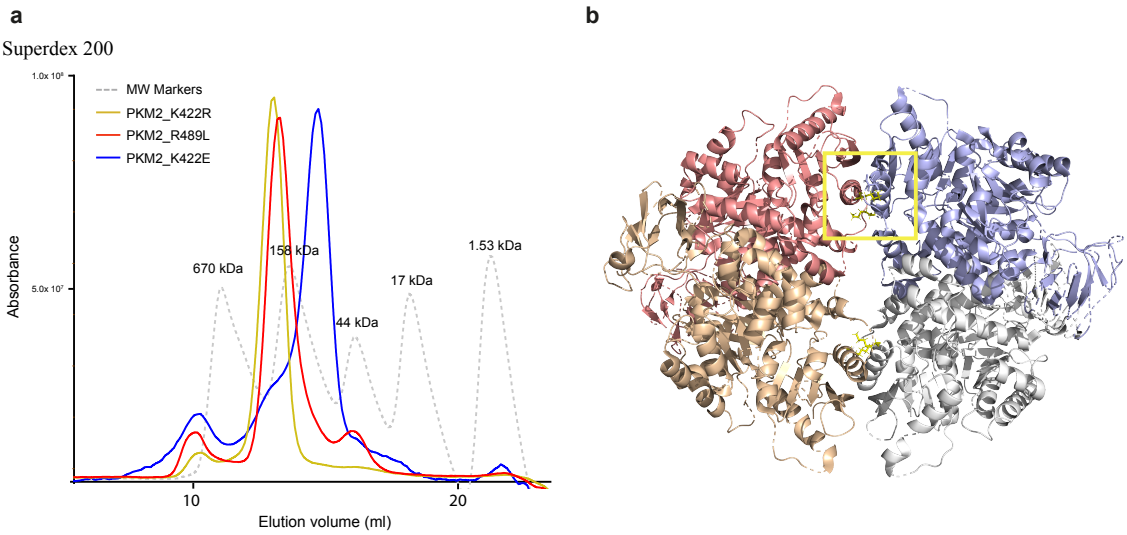

Figure 4.5. Size exclusion chromatography (SEC) analysis of PKM2 mutants. a Proteins were separated and analyzed using Superdex 200 Increase analytical SEC column. The chromatogram displays the UV at 280 nm curve for the three PKM2 mutants. The elution profile of globular markers is reported as dashed grey lines. **b** PKM2 crystal structure. The yellow lines represent the Lysine 422 residues for each chain (A, B, C, D).

Recombinant proteins have been expressed and purified in *E. coli*. Then, with the help of the Biochemistry and Structural Biology Unit of the European Institute of Oncology, we have analyzed their oligomeric state by analytical Size Exclusion Chromatography (SEC). As

shown in **Figure 4.5a**, SEC runs suggested that both the PKM2_K422R and PKM2_R489L assemble as tetramers (yellow and red curves respectively). On the other hand, PKM2_K422E was mainly present in a dimeric form, as shown by the blue curve in **Figure 4.5a**. Having assessed that among these mutants, the only one that purified as a stable dimer was PKM2_K422E, I choose this mutant to better characterize the putative PKM2:fatty acid interaction.

4.4 Biochemical characterization of PKM2_K422E mutant

In order to determine the oligomerization state of PKM2_Wild type and the K422E mutant and to check their homogeneity, we first ran an analytical gel filtration by loading the two proteins on a Superdex 200 Increase column. As shown in **Figure 4.6a**, both the samples eluted as a single peak, with PKM2_WT eluting slightly before the 158 kDa molecular weight marker and K422E mutant after the 158 kDa, suggesting that most likely they respectively elute as tetramer and dimer in solution. Yet, since SEC does not provide absolute values for molecular weight and elution profiles can be influenced by folding, in order to assess the absolute molecular weight, we performed a static light scattering analysis (SLS). This technique provides a measure of the specific molecular weight by recording the intensity of light scattered by the sample in solution. The SLS analysis confirmed that while PKM2_WT is a tetramer in solution, with a measured molecular weight of 236.4 kDa, PKM2_K422E is dimeric with a 121.5 kDa mass (**Figure 4.6b**). As shown in **Figure 4.6c**, the estimated molecular weights are very close to the theoretical predicted ones.

It has been reported that tetramerization is required for PKM2 to act as the canonical glycolytic enzyme. Given that the PKM2_K422E mutant purified as a dimer, I did not expect it to be able to convert phosphoenolpyruvate to pyruvate. To test this, I performed the previously described pyruvate kinase activity assay. Comparing a range of PKM2_WT concentrations from 12,5 ng-50 ng/reaction to 50 ng of K422E mutant activity, I observed a significant reduction of pyruvate kinase activity in the mutant (**Figure 4.6d**). All together our SEC and SLS data demonstrated that PKM2_K422E mutant is expressed as a stable monodisperse dimer in solution that lacks canonical kinase activity.

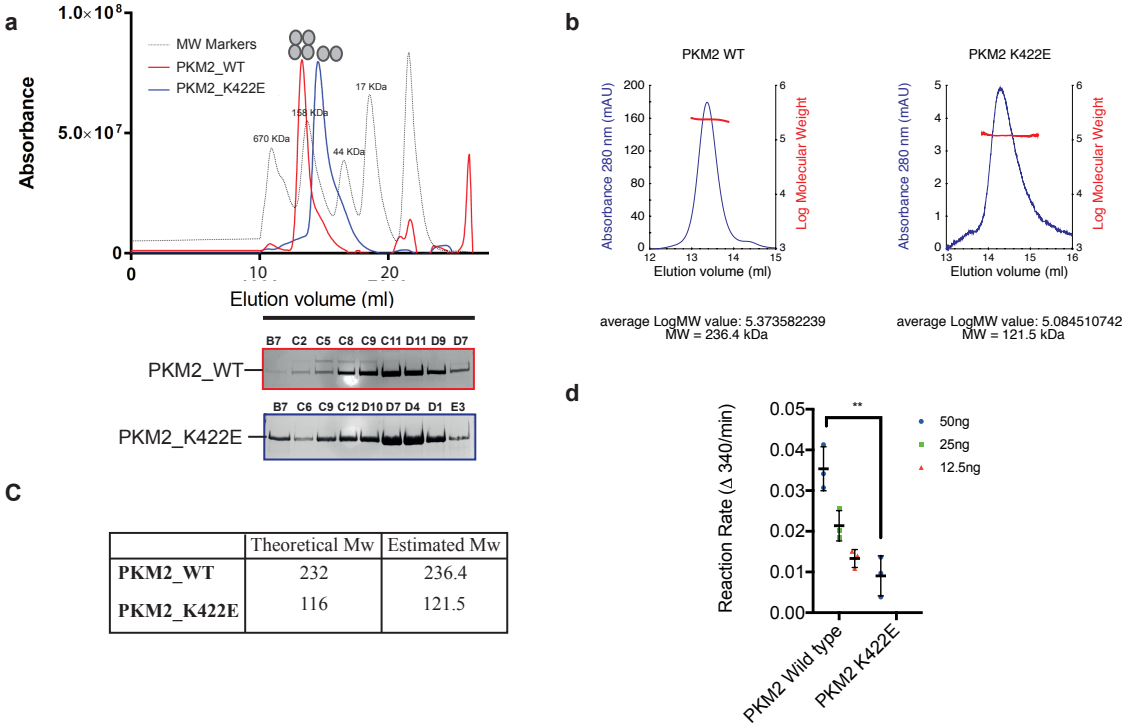

	Theoretical Mw	Estimated Mw
PKM2_WT	232	236.4
PKM2_K422E	116	121.5

Figure 4.6. Characterization of PKM2_K422E mutant. a SEC elution profile of PKM2_WT and PKM2_K422E run on a Superdex 200 increase. The chromatogram shows the UV at 280 nm. Molecular weight markers are shown in grey. In the lower part Coomassie stained of the SDS-page of the peak fractions corresponding to the horizontal black bar. **b** Static light scattering (SLS) analysis of PKM2_WT and K422E mutant. In blue is shown the UV Absorbance trace (left Y axis) and the measured molecular weight in red (right Y axis). The analyses show an average molecular mass of 236.4 kDa and 121.5 kDa along the peaks which are consistent with a tetramer for PKM2_WT and a dimer for PKM2_K422E. **c** Table showing the comparison between the theoretical molecular weights and the molecular weight measured by SLS. **d** Pyruvate kinase activity assay of PKM2_WT and K422E mutant. Significance was calculated using two-tailed Student t-test. P value: **p<0.01.

4.5 Dimeric PKM2 exhibits higher in vitro binding affinity to fatty acids

Since I demonstrated that PKM2_K422E mutant is a stable dimeric form of the enzyme, I decided to use this mutant to verify whether the dimeric form of the enzyme is, indeed, more prone to bind lipids compared to the tetrameric form, as our data suggested.

I reasoned that since I already observed a binding between PKM2_WT and palmitic acid in the fatty acid pull-down assay, also a chemical lipid probe C:16 should be able to bind the protein; then, thanks to the terminal alkyne group, C:16 can react with Alexa Fluor Picolyl Azide allowing me to detect the interaction. Hence, I set up an in vitro binding assay using the chemical lipid probe *prop-2-yn-1-yl-2-(3-tridecyl-3-diazirin-3-yl) acetate*. This lipid probe is an alkynyl-cis-palmitic acid (C 16:0) which contains a photoactivatable diazirine group and an alkyne handle and it represents a useful highly sensitive tool for studying lipid: protein interactions in *in vivo* and *in vitro* systems (**Figure 4.7a**). The alkyne group is able

to react with fluorescent azides through a copper-catalysed cycloaddition, known as "click chemistry" reaction allowing for visualization of probe binding both *in vitro* and *in vivo* (205). Using this tool, I compared the *in vitro* binding efficiency of the lipid probe with the WT tetrameric protein and the K422E dimeric mutant.

Thus, I incubated both the proteins with or without the lipid probe for 1 hour at 25 ˚C and then all the samples were subjected to UV light at 345 nm to activate the diazirine group. Samples were then incubated with Alexa Fluor Picolyl Azide reagents (Molecular Probes, C10641) for detection and processed for SDS-page. The *in vitro* binding assay with the chemical lipid probe showed that both the tetrameric WT protein and the dimeric mutant were able to bind the lipid (**Figure 4.7b**). Strikingly, the dimeric K422E mutant showed a stronger affinity compared to the WT protein, suggesting that the highly hydrophobic region included into the dimer:dimer interface can represent the region with the highest affinity towards hydrophobic molecules.

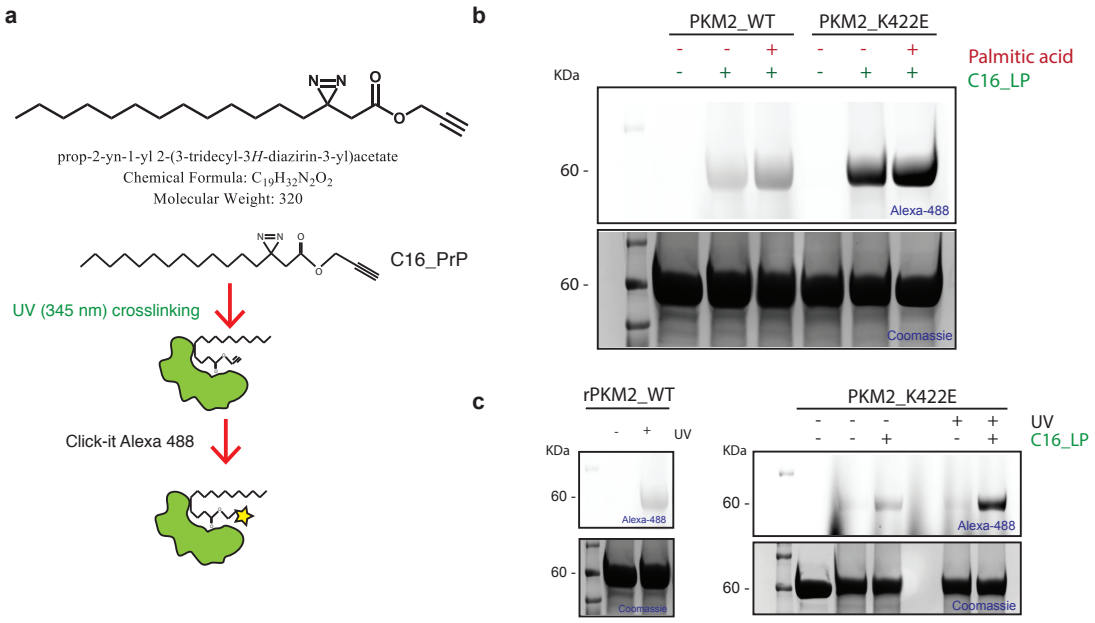

Figure 4.7. Fatty acids preferentially bind the dimeric form of PKM2. a Schematic representation of the in vitro binding assay used. A chemical synthesized lipid probe $C_{19}H_{32}N_2O_2$ (C16_LP) was used for a Click-IT chemistry reaction. PKM2_WT and K422E mutant were incubated with and without 30 uM C16_LP_N3 and 30 uM palmitic acid (1:3 ratio protein:lipids) and exposed to UV light at 345 nm. **b** Samples were subjected to SDS-page and visualized by a Chemidoc fluorescent acquisition for Alexa Fluor 488 (upper panel) or stained with Coomassie blue (lower panel). **c** Samples were subjected to the same procedure described before with and without UV light.

In order to assess whether I could observe a competitive mechanism between the chemical lipid probe C:16 and the fatty acid palmitic acid (C 16:0), I performed the same assay also in the presence of equimolar concentration of palmitic acid. Interestingly, while for the

dimeric K422E mutant I did not observe any significant difference in the chemical probe binding capacity in the absence or presence of palmitic acid, unexpectedly, for the WT tetrameric protein I observed a slightly increase in the binding capacity to the chemical probe in the presence of the fatty acid (**Figure 4.7b**). This enhancement of binding was confirmed for fatty acids of shorter chain lengths as well. These data suggest that exposure to fatty acids could facilitate the binding of the WT protein to the chemical probe. Thus, necessitating the need for further structural studies of fatty acid:PKM2 complexes.

Finally, as a technical internal control, I performed the *in vitro* binding assay with or without the UV light exposure, which leads to covalent attachment of the lipid probe to bound proteins through the diazirine group. As shown in **Figure 4.7c**, in the absence of UV light there is no binding between the tetrameric PKM2_WT protein and the chemical lipid probe (left panel), while a light band appears for the dimeric K422E mutant (right panel). This experiment confirms the specificity of the technique and shows that the dimer, even in the absence of the photo-activated diazirine group, displays a basal level of interaction with the chemical lipid probe.

4.6 Crystal structure of PKM2_WT

Understanding the properties and the function of the proteins and the interaction with other macromolecules is greatly facilitated by structural analysis. Thus, to better characterize the role of the Lys422 to Glu mutation at the structural level, and to map the residues coordinating the fatty acid binding to the PKM2_K422E mutant, in collaboration with the Biochemistry and Structural Biology Unit of the European Institute of Oncology (IEO), we initiated the structural investigation of the protein and its interaction with fatty acids.

As a starting point for the structural analysis, we both tried recapitulating the previously published crystallization conditions for the bacterially produced PKM2_WT protein (40) and, in parallel, set up a general screening of crystallization conditions using the commercial screen Peg/Ion and JSCG+ from Hampton Research. Commercial crystallization kits are designed to allow sampling of crystallization space by making use of several different conditions, which vary in pH, salts and type of precipitant reagents. We set up crystallisation trays with different protein concentrations and ratios of protein:reservoir volume, eventually managing to obtain crystals in about 30% of the commercial screen conditions. For the wild type protein, it was not necessary to further optimize the conditions, since the crystals obtained with the commercial screen were already single and of an appropriate size for diffraction studies (**Figure 4.8)**.

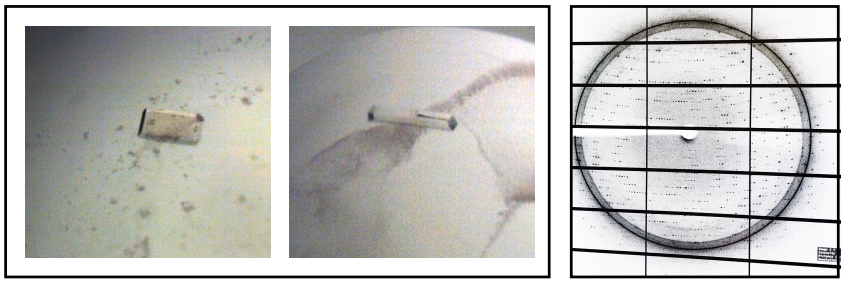

Figure 4.8. Crystals of PKM2_wild type. Crystals of PKM2 WT grown by sitting drop vapor diffusion using the commercial screen Peg/Ion. The first crystals appeared after two days of crystallization mixing the protein sample with 10 mM Hepes pH 7.5, 100 mM KCl, 5 mM MgCl2, 5% glycerol and 1 mM DTT (left). Crystals grew in the presence of 0.1 M HEPES pH 7.5, 10% PEG 8000, 8% ethylene glycol. On the right the diffraction of PKM2 WT crystals. 2.8 Å resolution X-ray diffraction pattern obtained using a synchrotron-radiation source on Beamline PXIII at Swiss Light Source.

Crystals grown in 0.1 M Hepes pH 7.5, 10% PEG 8000, 8% ethylene glycol were harvested and flash cooled in liquid nitrogen using a cryo-protectant solution containing 20% glycerol, to allow cryogenic X-ray diffraction data collection, which was performed at beamline X06DA (PXIII) of the Swiss Light Source synchrotron (Villigen, Switzerland). Crystals diffracted to 2.87 Å resolution, and belonged to $P2_1$ space group. The structure was solved by molecular replacement by our collaborators, and refinement is still ongoing. Table 5 reports the data collection statistics and the current state of model refinement.

Recent structural studies have described the existence of two different conformations for the tetrameric state of PKM2. The protein can assemble into an active state, named R-state, and a less active state, or T-state. Allosteric inhibitors, like phenylalanine, have been correlated with the stabilization of the less active T-state, while the allosteric activator FBP is involved in the stabilization of the active R-state (65). From a structural point of view, the T-state adopts a conformation in which a general rotation of 13˚ of all the four chains is observed in the comparison with the R-state. In my *in vitro* pyruvate kinase assays I have previously shown that the WT protein is active in glycolysis. In order to verify whether our PKM2_WT crystal structure adopted the active R-state conformation, we decided to align it with two different PKM2 crystal structures previously published as R-state structures. Alignment analyses were conducted with the help of Janine Weber, a postdoctoral fellow of the IFOM Molecular machines in signaling pathways laboratory headed by Simona Polo.

The two different crystals that we used for this comparison are deposited on the RCSB Protein Data Bank as 4FXF (65) and 4RPP (206) and represent respectively PKM2_WT and PKM2_K422R mutant, both in complex with FBP. The alignments showed that our PKM2

WT structure perfectly recapitulates the deposited R-state crystal structures (**Figure 4.9**), confirming the active state of the protein.

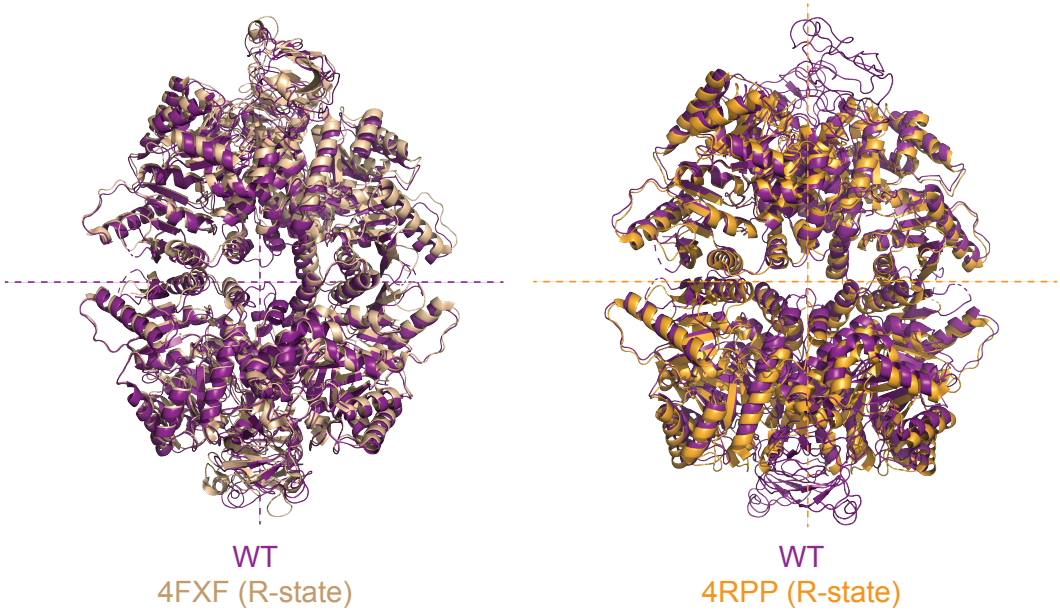

Figure 4.9. Structural comparison of PKM2 WT and PKM2 in R-state. Superimposed crystal structures of our PKM2 WT (magenta) with two previously published crystal structures of PKM2 WT and PKM2_K422R^{FBP} in the active R-state (light brown and orange). Alignments were created using the PyMOL software. The PDB code of the published PKM2 structures are 4FXF for the PKM2 WT and 4RPP for the PKM2_K422R mutant. Their atomic coordinates are deposited on the RCSB Protein Data Bank.

4.7 Crystal structure of PKM2_K422E mutant

Having identified the best conditions for the crystallization of the wild type PKM2 protein, we moved forward with our goal of crystallizing the K422E mutant in combination with Oleic acid. Thus, identifying the fatty acid binding pocket required to bind fatty acids, as demonstrated by my *in vitro* experiments. I proceeded in parallel to set up the crystallization of PKM2_K422E alone and in combination with Oleic acid. PKM2_K422E was prepared following the previously described protocol of PKM2_WT. Instead, for PKM2_K422E in combination with fatty acids, I incubated the protein with Oleic acid in a 1:10 molar ratio overnight at 18˚C. Both PKM2_K422E and the pre-incubated protein with Oleic acid, were then concentrated to 5 mg/ml. Crystallization trials were performed using the Peg/Ion and JCSG-plus screens from Molecular Dimension Ltd. After two days, we started to observe the first crystals in many conditions of the JCSG-plus screen, with the best crystals growing in the presence of 0.1 M HEPES and 10% PEG (**Figure 4.10**).

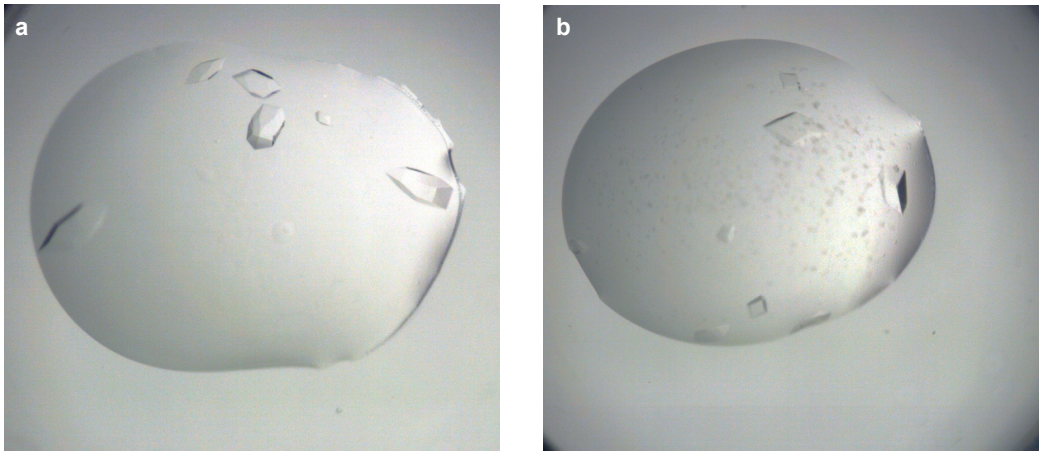

Figure 4.10. Crystals of PKM2_K422E mutant. Crystals of PKM2_K422E grown by sitting drop vapor diffusion. The protein sample at 5 mg/ml was mixed with 10 mM Hepes pH 7.5, 100 mM KCl, 5 mM MgCl2, 5% glycerol, 1 mM DTT, the same buffer conditions used for the WT protein. **a** B-04 condition of the JCSG-plus HT-96 MD1-40 screen containing 0.1 M HEPES pH 7.5, 10% PEG 8000 and 8% ethylene glycol. **b** C-04 condition of the same JCSG-plus screen containing 0.1 M HEPES pH7.0 and 10% PEG 6000.

Unfortunately, none of the obtained single crystals diffracted during the X-ray diffraction analysis. Thus, I started to optimize the crystallization conditions manually with the hanging drop method. I used the conditions where the best crystals grew as a starting point to set up grid screens where we tested various concentrations of PKM2_422E protein and PKM2_K422E+Oleic acid and different buffer conditions. To further increase the percentage of success of the crystallization procedure and to work with a more reproducible system, I also performed seeding. In this case, crystals can be originated by seeds added to the equilibrating drops and this process can help to obtain larger single crystals.

Seeding was always performed 24 hours after the preparation of the trays and we observed a higher efficiency of crystallization in the seeded wells (**Figure 4.11)**.

Sample concentration is a key factor for protein crystallization. PKM2 high concentrations have been shown to correlate with an increase in the tetramer formation in both the wild type and the mutants previously described (206). In order to avoid a concentration related configuration, we used the same concentration for both the WT and the K422E mutant corresponded to 5 mg/ml. Among the several conditions screened, we tested different concentrations of PEG-3350 (from 17% to 23%) and di-ammonium tartrate (from 225 mM to 275 mM). Moreover, we also added different additives commonly used to favor the crystallization process, like glycine, proline, phenol or urea.

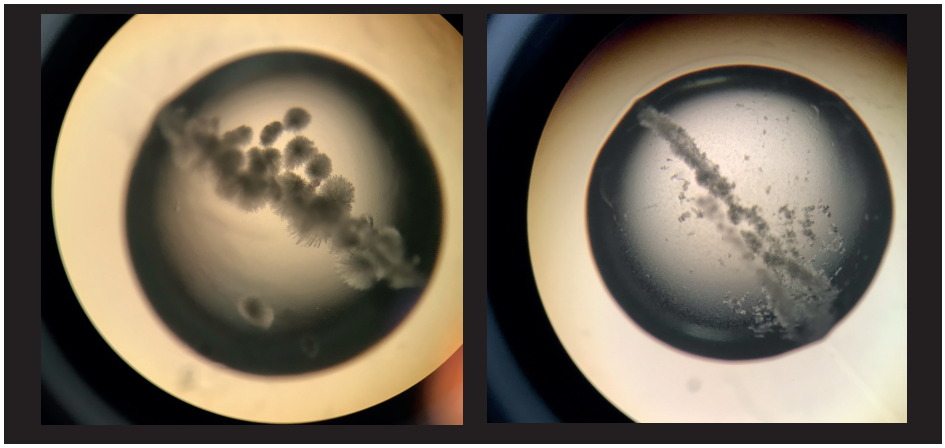

Figure 4.11. PKM2_K422E crystals growing on seeding lines. Representative images acquired after seven days from the seeding process. Streak seeding was performed using micro-seeds obtained by pre-formed crystals previously crushed to be used as a seed stock. A cat whisker was used as a transfer tool for the seeds.

PKM2 crystals morphology appeared to be highly modulated by additive concentration. Single crystals suitable for diffraction studies were obtained in the presence of different concentration of PEG-3350, glycine and proline (**Figure 4.12**).

Crystals were harvested and flash cooled in liquid nitrogen in a cryo-protectant solution containing 20% glycerol and their X-ray diffraction was collected at beamline X06DA (PXIII) of the Swiss Light Source synchrotron (Villigen, Switzerland).

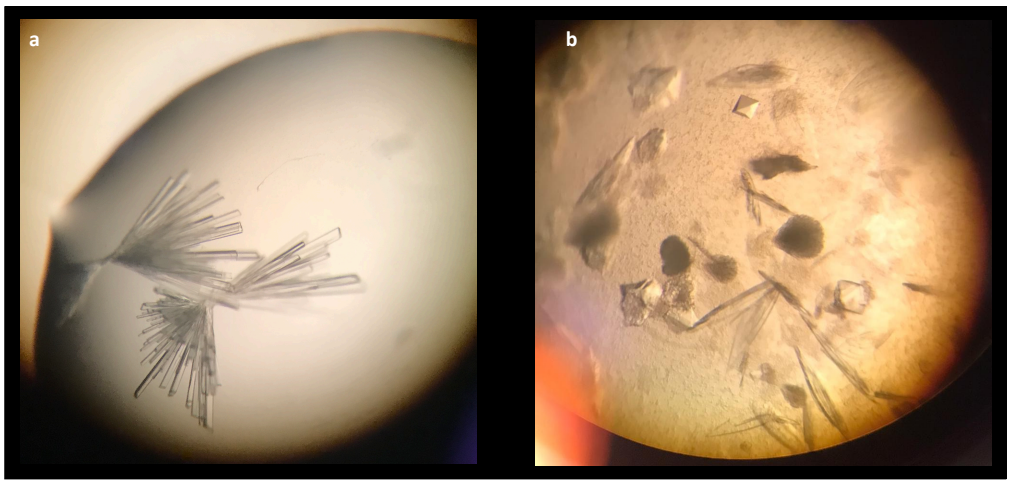

Figure 4.12. PKM2_K422E crystals. PKM2_K422E crystals obtained after 7 days using the hanging drop method. **a** Crystals grown in the presence of 18% PEG-3350, 275 mM di-ammonium tartrate, 17% proline. **b** Crystals grown with 21% PEG-3350, 275 mM di-ammonium tartrate, 12% glycine.

Despite obtaining single crystals suitable for diffraction for both PKM2_K422E and PKM2_K422E+Oleic acid, diffracting crystals were obtained only with protein incubated with Oleic acid. Hence, I focused exclusively on the refinement of the crystals grew in the presence of oleic acid. We were able to collect data for crystals belonging to two different space groups: *P*1 and $P2_1$, which diffracted with resolution limits of 1.89 and 2.00 Å, respectively. The *P*1 crystal grew in presence of 18% PEG-3350 and 7% phenol, 0.8 mM Oleic acid, while the $P2_1$ crystal grew in 10% PEG-3350 and 16% Glycine and 0.8 mM Oleic acid. The structures were solved by molecular replacement by our collaborators of the Biochemistry and Structural Biology Unit of the IEO, and refinement is still ongoing. Table 5 reports the data collection statistics and the current state of model refinement.

	PKM2 wild type	**PKM2 K422E**	**PKM2 K422E**
Data Collection			
Space group	$P2_1$	*P*1	$P2_1$
Wavelength	1.00 Å	1.00 Å	1.00 Å
Cell dimensions *a, b, c* (Å) *α, β, γ* (°)	81.28, 152.85, 94.10 90, 102.99, 90	93.87, 108.72, 125.68 88.59, 70.97, 66.29	96.06, 70.82, 167.62 90, 105.34, 90
Resolution	70.32-2.87 (2.92-2.87)	118.89-1.89 (1.92-1.89)	161.73-2.00 (2.03-2.00)
R_{sym} or R_{merge}	0.084 (0.701)	0.097 (0.994)	0.179 (2.962)
$CC_{1/2}$	0.996 (0.749)	0.988 (0.169)	0.997 (0.356)
I/σI	11.7 (2.1)	4.1 (0.2)	4.9 (0.2)
Completeness (%)	99.0 (100.0)	97.7 (96.3)	100.0 (100.0)
Unique reflections	50586 (2549)	335311 (16522)	147132 (7324)
Multiplicity	4.2 (4.3)	3.4 (3.4)	6.6 (6.8)
Refinement			
Resolution (Å)	45.85-2.87	53.19-1.89	91.52-2.00
R_{work}/R_{free}	0.343/0.376	0.213/0.238	0.230/0.280
No. atoms Proteins Water	 15732 78	 31441 1648	 15489 261
B-factor protein/water	85.51/30.00	45.20/43.14	62.39/49.22
R.m.s. deviations Bond lengths (Å) Bond angles (°)	 0.016 2.33	 0.020 3.12	 0.003 0.68
Ramachandran values Favoured (%) Allowed (%) Outliers (%)	 88.2 10.5 1.3	 96.4 2.4 1.3	 95.1 4.2 0.7

Table 5. Data collection and refinement statistics for PKM2 WT and the two PKM2_K422E crystal structures.

The structures of PKM2_K422E in two different space groups are both arranged in the crystal packing as tetramers. However, two very different tetrameric assemblies are formed (see below). Indeed, the dimers assembling the two space groups are very different (**Figure 4.13**), suggesting that the dimeric arrangement of PKM2_K422E is very open and allows a fairly large movement of one monomer with respect to the other.

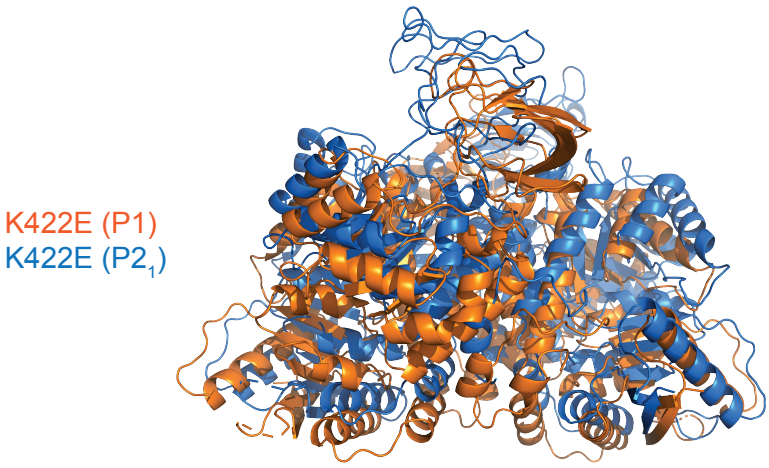

Figure 4.13. Structural comparison of PKM2 K422E crystals belonging to two different space groups. Superimposed crystal structures of the dimeric units of PKM2_K422E belonging to the P1 space group (orange) and to the $P2_1$ space group (light blue). Alignments were created with PyMOL software.

In order to understand whether the different conformations assumed by the K422E mutant could correlate with the previously described T and R-states, we superposed the two crystal structures with two different PKM2 structures previously shown as T (PDB: 4QGC) and R-state (PDB: 4RPP). The comparison showed us that PKM2_K422E *P*1 structure corresponds to the R-state, while the $P2_1$ structure, instead, matches with the T-state (**Figure 4.14**). Interestingly, while preliminary data suggests that the allosteric activator FPB is present in our WT structure, no density for FBP was observed in either the K422E structures. This suggests that, unlike the situation described for other mutants, with this mutant FBP is dispensable for R (active) state assembly. These observations open new perspectives for the study of the dimeric form of PKM2 enzyme that plays an important role in cancer progression.

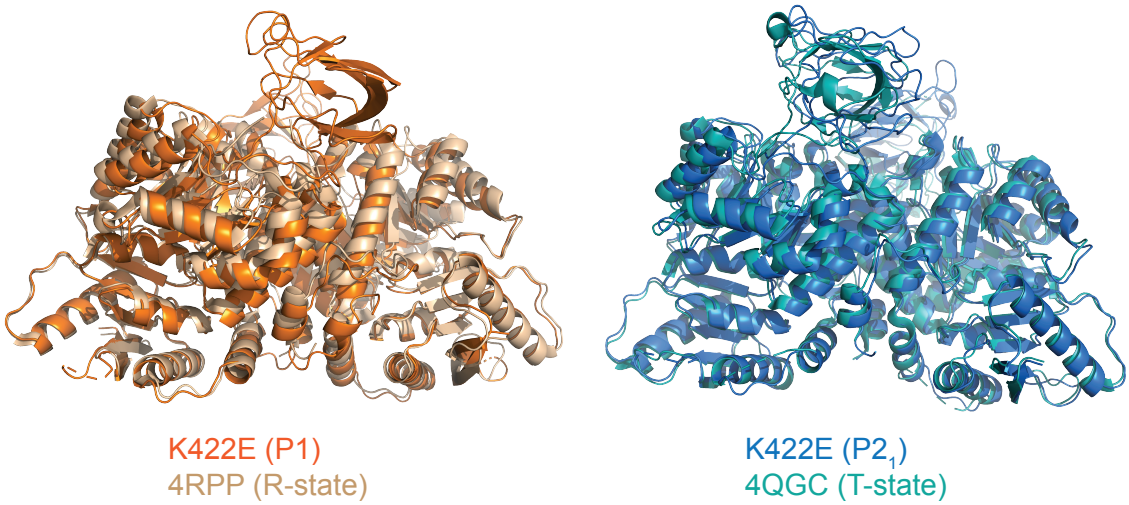

Figure 4.14. Structural comparison of PKM2 K422E P1 and P2$_1$ crystals with PKM2 in R and T-states. Superimposed crystal structures of the dimeric units of PKM2_K422E belonging to the P1 space group (left) with PKM2 R-state (PDB: 4RPP) respectively in orange and beige. On the right superimposed crystal structures of PKM2_K422E belonging to the P2$_1$ space group with PKM2 T-state (PDB: 4QGC) respectively in blue and green. Alignments created with PyMOL software.

Chapter V

Discussion and Conclusions

Deregulation of lipid metabolism belongs to a more general metabolic reprogramming that is often observed in cancer cells that is required to satisfy the increased energy demands. Due to the important role dysregulated metabolism plays in supporting cell proliferation and cancer progression, there is an emergent interest in understanding the molecular mechanisms leading to the reprogramming.

Recent studies highlighted the role of lipid metabolism in the maintenance of stemness properties in cancer cells. Cancer stem cells (CSC) represent a small percentage of the tumour mass and are characterized by high self-renewal capacity and tumour-initiating features. Importantly, they are considered to be refractory to most therapeutic treatments, thus an important target for effective therapeutic intervention. Interestingly, a recent metabolomic profiling of CSC has shown that CSC have specific metabolic alterations (151), particularly in lipid biosynthesis. Thus, a better understanding of the aberrant lipid metabolism could provide a strategy to better tackle this sub-population of cancer cells.

An accumulation of lipid droplets in the subpopulation of cells that survived therapeutic intervention, the so-called minimal residual disease, has recently been described (179). Lipid droplets (LD) are cytosolic organelles constituted by triacyclglycerols and sterol esters surrounded by a phospholipidic monolayer. LDs number varies in response to the metabolic profile of the cells and the accumulation of LDs has been observed in many diseases, including cancer. Despite that, very little is known about the role of their accumulation in cancer onset and progression. Considering the important contribution of CSC to tumour progression (177) and the recent evidence that they have an aberrant lipid metabolic profile, I investigated whether there was any correlation between the accumulation of lipid droplets and stemness traits in breast cancer.

Initially, I searched for a possible correlation between the expression of one of the most abundant lipid droplet associated proteins, PLIN2, and relapse free survival (R.F.S.) in breast cancer patients. Using Kaplan-Meyer plotter, I scored a significant negative correlation between PLIN2 expression and R.F.S., suggesting a potential role of lipid droplets accumulation and a worse clinical outcome.

Analysing the LDs content of four different cell lines, I observed a remarkable heterogeneity both among the different cell lines and, surprisingly, also in the context of the same cell line, with some cells highly enriched in LDs while others were almost devoid. In regards to the observed differences in LD content between the cell lines could be explained by the different metabolic profiles of the four cell lines. Intriguingly these differences persist despite their being grown and maintained in the same media conditions. The differences observed in the same cell line, instead, could be explained by the intra-tumoural heterogeneity that has been

recently shown in cancer cell lines (207) and could be a sign of metabolically different clones inside the same population.

Taking advantage of the *in vitro* approach developed to identify CSC that relies on their capability to survive form spheroids in non-adherent conditions (192), I observed that all the cell lines were able to form mammospheres, even if with a different efficiency. Importantly, a higher efficiency was observed in BT474 and MDA-MB-231, the cell lines most enriched for LDs, suggesting a possible correlation between LD accumulation and stemness. Moreover, in the second generation mammospheres, I observed, using confocal microscopy, that in the context of the single mammosphere, only one or two cells were highly enriched in LDs. Taken together, I could speculate that the cells which are highly enriched for LDs could represent the potential stem/progenitor cells. While the intracellular heterogeneity in the lipid droplets content could be associated with a more general cellular heterogeneity.

Through the FACS-based method that we established to isolate the different subpopulations of cells according to the lipid droplets content, I demonstrated that the LD enriched subpopulation was indeed characterized by stem cell traits as shown by the higher expression of stemness markers, the higher propensity to form mammospheres and the colocalization in the FACS analysis with the $CD44^{high}/CD24^{low}$ cells. All together these data demonstrated that the lipid droplets enriched sub-population of cells show a stem-like phenotype that is not shared with the LD^{low} population. Similar observations have been previously shown in colon-rectal cancer and glioblastoma (173, 175), suggesting a conserved common mechanism among different cancer types.

Moreover, using xenotransplantation, I observed a higher tumorigenic potential of lipid droplets enriched cells that, when injected in mice, had an earlier onset in comparison to the LD^{low} cells. I can hypothesize that the accumulation of lipid droplets can have a role in breast cancer onset, confirming the important role of these organelles already described in other tumour types. Although the general implications of LDs accumulation in breast CSC require further investigation, I can postulate that LDs enrichment represents an important energy reservoir that can allow cells to survive under nutrient deprivation, as previously shown in colon cancer (208).

Another interesting aspect of my study is that I provide evidence that LD enriched subpopulations of cells have an increased cytosolic complexity that is detectable in a label free manner by evaluating the SSC at FACS. This important aspect can be used as a new parameter to distinguish and isolate cancer stem cells from the population, providing a new tool for clinical diagnosis.

As a further demonstration of the role played by lipid droplets, I provide evidence that targeting lipid droplets formation negatively impact upon cellular proliferation and

tumorigenesis in breast cancer cells. Despite the lack of specific LDs inhibitors, many chemical compounds targeting lipid metabolic pathways have been shown to affect LD formation (209). Among them, the Acetyl CoA Carboxylase alpha (ACC-alpha) chemical inhibitor TOFA (5-tetradecyloxy-2-furoic acid) has been previously shown to induce apoptosis in lung and colon cancer cells through targeting the *de novo* fatty acids synthesis pathway (210). My data is in line with those previous observations, showing that also breast cancer cell lines proliferation is affected by TOFA treatment, suggesting an addiction to *de novo* fatty acid biosynthesis is a feature of tumours derived from multiple tissue types. Moreover, I also showed that in BT474 cells the inhibition of LDs formation leads to a decreased mammospheres formation efficiency, suggesting an effect on the stem-like phenotype of LDs enriched cells described before. Although further studies are required to better characterize the molecular mechanism underpinning the correlation between LD accumulation and stemness traits, the possibility that targeting lipid metabolism and LDs formation impact on tumorigenesis, open important scenarios for the development of new therapeutic strategies.

Interestingly, my data showed that MDA-MB-231 cells, representing triple negative breast cancer, were not affected by TOFA treatment, being the only exception in our panel of breast cancer cell lines. Indeed, they did not show any decrease in the LD amount upon TOFA treatments compared to the control cells; additionally, proliferation rates and mammosphere formation capacity were not affected by the inhibition of ACC. These findings suggest that MDA-MB-231 cells could rely on compensatory mechanisms that sustain their lipid biosynthetic pathways.

Lipid metabolic reprogramming is emerging as an important contributor to cancer onset and progression. This is not surprising, since lipids play a role in multiple aspects of the cellular physiology from energy storage, to the generation of the cellular membranes and as signaling molecules. An additional role for lipids as modulators of the activity and function of proteins and enzymes, is another key function of lipids. In the late 60s', Randle and collaborators demonstrated for the first time an hormone independent mechanism by which lipid and glucose metabolism regulated each other according to their availability (71). The Randle cycle, also known as glucose-fatty acid cycle, provided a mechanistic explanation for the observed decrease in glycolysis when high levels of fatty acids are available. Reciprocally, the increased glycolysis in the presence of high glucose availability, leads to decreased fatty acid oxidation. Moreover, a decreased activity of some glycolytic enzymes, such as phosphofructokinase (PFK) and pyruvate kinase (PK), was also described to correlate with increased levels of citrate, an essential metabolite upstream of FA biosynthesis (69, 180). The inhibition of glycolytic enzymes activity means a shift of the cellular metabolism from

catabolism to anabolism, a mechanism that is very often observed in cancer cells. Indeed, the enhanced tumour proliferation rates require an intense production of nucleic acids, proteins and lipids that is sustained by the carbon sources provided by the glycolytic intermediates such as glucose-6-phosphate and 3-phosphoglycerate (211). Despite the increased interest in the field, there are still many gaps in the understanding of the cross talk between lipid and glycolytic metabolism.

In this study, I focused on the role of lipids as possible regulators of glycolysis and glycolytic enzymes opening new perspectives for this old field. Several studies have previously suggested a role for free fatty acids and lipids as regulators of glycolytic enzymes. Particularly, this was proposed for pyruvate kinase whose inhibition was reported to be regulated by long and short chain fatty acids as described by Weber and collaborators (72, 200). These controversial studies done over 50 years ago described the potential for regulation but did not go as far as to describe a mechanism behind this phenomenon. More recently, quantitative mass spectrometry analysis of fatty acid associated proteins revealed that PKM2 was able to bind Palmitic acid, suggesting an interaction between the two as a possible mechanism of protein stabilization or re-localization, since palmitic acid represents one of the most abundant fatty acids in the cellular membranes (184). Given the aforementioned observations, I hypothesized that fatty acids themselves, might directly regulate Pyruvate kinase M2 (PKM2) activity by acting as an allosteric modulator of the protein. Pyruvate kinase catalyzes the terminal reaction of glycolysis and, as such, is believed to be one of the key regulators of glycolytic flux. While normal tissues express Pyruvate kinase M1 isoform, most tumours express the M2 isoform that arises from alternative splicing of one exon. Whereas PKM1 is constitutively active, PKM2 is allosterically regulated allowing for more efficient regulation of glycolytic flux. Therefore, I began by analyzing the expression and the activity of PKM2, in a panel of ten breast cancer cell lines. Although, I found similar levels of expression, the enzymatic activity of PKM2 differed significantly between the 10 lines, suggesting an additional layer of regulation.

Intrigued by these observations, I decided to analyze PKM2 aminoacidic sequence to better understand if it was possible an interaction with hydrophobic lipids. The hydropathy plot of PKM2 aminoacidic sequence, highlighted a region particularly enriched in hydrophobic residues that could be involved in the protein-lipids interaction. Performing a fatty acid pull-down assay with cellular lysates using, as a bait, agarose beads coupled with fatty acids of different lengths and saturation states, I detected by western blot a strong interaction between PKM2 and all fatty acids tested. This interaction was maintained when the bacterial produced recombinant human PKM2 protein (rPKM2) was used in the place of whole cell lysates, suggesting a direct interaction between the PKM2 protein and fatty acids.

I noticed that although the rPKM2 bound the fatty acids, the binding efficiency appeared to be lower compared to that from the lysates, therefore I decided to further analyze the sequence to try to gain additional insight into the binding. Comparing the information retrieved by the hydropathy plot with the previously resolved PKM2 crystal structure, I realized that the region of the protein characterized by an enrichment in hydrophobic residues localized to the inter-subunit contact domain. This was not unexpected if we consider that proteins usually fold in the most thermodynamically stable state in which, hydrophilic regions are exposed to the polar environment and hydrophobic portions are instead enclosed within water-free domains. But, the most interesting aspect of this observation was that those hydrophobic alpha-helixes that mapped to the inter-subunit contact domain represent the contact site where two dimers of PKM2 interact to form the tetrameric form of PKM2 that is active in glycolysis. In contrast to PKM1 which is constitutively active, PKM2 activity is allosterically regulated. Thus, regulating the conversion between the dimeric (putative protein kinase) and tetrameric (glycolytic) forms of PKM2. Cells use this mechanism to tune the glycolytic flux according to the specific circumstances (212). Considering that within a cellular context PKM2 is found both in dimeric and tetrameric forms, I hypothesized that the dimer may be the lipid interacting form of PKM2.

In order to test this hypothesis, I generated and characterized a set of bacterially produced PKM2 mutants. This characterization revealed lysine K422 as a key residue in regulating tetramer formation. Indeed, replacement of the Lysine with Glutamic Acid resulted in the production of a stable dimer as demonstrated by SLS. Performing lipid binding assays using the recombinant wildtype and dimeric form of PKM2, I demonstrated that dimeric PKM2 bound fatty acids with a higher affinity than the tetrameric protein. Excitingly, these results suggest a potential role of fatty acids as modulators of PKM2 structure and activity, opening new scenarios for the understanding of the complex allosteric regulation of PKM2 enzyme. The idea of fatty acids as allosteric regulators was also recently proposed by Pinkosky and colleagues, who demonstrated that long-chain fatty acyl-CoA regulate AMPK activity (213) (214). In this case fatty acyl-CoA binding activates AMPK leading to phosphorylation and inactivation of ACC1, thus contributing to AMPK mediated metabolic reprograming. This work provides further evidence that fatty acid binding participates in metabolic reprogramming by tuning enzyme activity.

My next goal was to understand whether structural studies could help me to better characterize the hypothetical fatty acid binding site in my PKM2_K422E dimer. In an attempt to identify the residues that coordinate the fatty acyl binding, all crystallization trials were done in the presence of oleic acid. Initial structural analysis revealed that, despite

purifying as a dimer, the PKM2 K422E mutant crystalized as a tetramer. Regardless, structural studies of PKM2_K422E mutant revealed that, in comparison with the wild type protein, the mutant could assemble into two different conformations, corresponding with the previously published active (R) and inactive state (T). Interestingly, the ability to form the R state has previously been described to require the binding of FBP, yet I found no evidence for an FBP density in the refined structures. Suggesting that this mutant is able to form an active state in the absence of FBP. Further studies are ongoing to confirm its ability to catalyze the conversion of PEP to pyruvate. The ability of the dimer to form these two tetrameric assemblies suggests that, with respect to the wildtype, the dimeric arrangement of PKM2_K422E is more fluid, and allows movement of one monomer with respect to the other. Despite the presence of Oleic acid during the crystallization, I was not able to detect a density for oleic acid in the refined structure. Yet, interestingly, although I also sent crystals of PKM2_K422E formed in the absence of oleic acid for diffraction analysis, they were unable to diffract. Collectively, this data suggests that the presence of oleic acid could stabilize the structure of PKM2_K422E, since in its absence, I do not obtain ordered structures able to diffract. The absence of oleic acid density in my crystals of course represents an important aspect to consider. It is a well-recognized concept that fatty acids in solution tend to form micelles, changing their chemical properties, for this reason it's usually not possible to use concentrations higher than 0.5-1 mM since this aspect can interfere with the formation of the complex protein-fatty acid. Previous studies have shown that these low concentrations used for fatty acid binding protein crystallization trials might have been too low to allow the detection of the presence of fatty acid electron density (215).

In this study, taking advantage of *in vitro* assays, I showed that medium and long-chain fatty acids can bind the glycolytic gatekeeper PKM2. Moreover, preliminary data from my structural investigation, suggested that fatty acids can regulate the dimer/tetramer transition, acting as allosteric regulator. While further functional and crystallization studies are ongoing, my findings pave the way towards uncovering fatty acids as a novel regulator of PKM2 activity. As direct regulators of glycolysis, fatty acids could have a direct role on the balance between catabolism and anabolism, which, together with the recent description of the role of fatty acids in regulating AMPK, add a new chapter in our knowledge of the cellular metabolism. The functional implications of this mechanism could be multiple, since the allosteric regulation of PKM2 plays an important role in cancer onset and progression. One could speculate that the metabolic reprogramming observed in cancer could include another level of complexity connecting the highly active *de novo* fatty acid synthesis with the regulation of PKM2 activity, considered a fundamental player in cancer metabolism. The binding of lipids to PKM2 could lead to the stabilization of the dimer thus representing a

way to sustain the anabolic growth in cancer cells. Another possibility one could contemplate is the possible role of medium-long fatty acids as activators of PKM2. A recent study demonstrated a role of the short chain fatty acid butyrate in promoting PKM2 tetramerization, thus inhibiting the Warburg effect and proliferation of colon-rectal cancer cells (216). Although the exact mechanism is still not understood, my findings open new perspectives on the role of lipid metabolism in the regulation of the cellular proliferation and cancer progression.

Multiple studies have demonstrated an upregulation of PKM2 in solid tumours, including breast (217), liver (218) and colon-rectal cancers (219), as well as a role for PKM2 in therapeutic resistance (220), suggesting that it could be a viable therapeutic target. Among the different regulators of glycolysis or PKM2 inhibitors introduced into the clinics, including Metformin (221) and Temozolomide (222), Shikonin represents a good candidate due to the high specificity towards PKM2 (223). Yet, it has limited success due to reported high toxicity and low solubility (224). Thus, the identification of effective to modulate PKM2 activity in cancer represents an unmet clinical need. Due to the interplay between glucose and lipid metabolism, we could target the main lipid metabolic pathways, thus impacting indirectly the glycolytic flux by regulating both PKM2 and AMPK activity. For example, as already shown in cortical neurons, the use of C75, a specific Fatty acid synthase (FASN) inhibitor, has an impact on glucose metabolism (225). Moreover, the use of the antibiotic Platensimycin, another inhibitor of FASN, has also shown to induce an increase of glucose oxidation in mouse models of diabetes (226). High levels of free fatty acids have been described in breast cancer (227) as key players of the metabolic reprogramming of cancer cells. Thus, a better characterization of their role in the regulation of the glycolytic flux could open the avenue towards the development of new therapeutic strategies since the use of specific lipid metabolic inhibitors in cancer therapy could also impact on the regulation of glucose metabolism, as shown in non-tumoural tissues.

References

1. H. Sung *et al.*, Global cancer statistics 2020: GLOBOCAN estimates of incidence and mortality worldwide for 36 cancers in 185 countries. *CA Cancer J Clin* 10.3322/caac.21660 (2021).
2. M. Escala-Garcia *et al.*, Breast cancer risk factors and their effects on survival: a Mendelian randomisation study. *BMC Med* **18**, 327 (2020).
3. I. Alvarado Cabrero, M. Carrera Alvarez, D. Perez Montiel, F. A. Tavassoli, Metastases to the breast. *Eur J Surg Oncol* **29**, 854-855 (2003).
4. J. Ferlay *et al.*, Cancer incidence and mortality worldwide: sources, methods and major patterns in GLOBOCAN 2012. *Int J Cancer* **136**, E359-386 (2015).
5. A. Goldhirsch *et al.*, Strategies for subtypes--dealing with the diversity of breast cancer: highlights of the St. Gallen International Expert Consensus on the Primary Therapy of Early Breast Cancer 2011. *Ann Oncol* **22**, 1736-1747 (2011).
6. P. J. O'Donovan, D. M. Livingston, BRCA1 and BRCA2: breast/ovarian cancer susceptibility gene products and participants in DNA double-strand break repair. *Carcinogenesis* **31**, 961-967 (2010).
7. D. Hanahan, R. A. Weinberg, Hallmarks of cancer: the next generation. *Cell* **144**, 646-674 (2011).
8. M. M. Zarou, A. Vazquez, G. Vignir Helgason, Folate metabolism: a re-emerging therapeutic target in haematological cancers. *Leukemia* 10.1038/s41375-021-01189-2 (2021).
9. S. Ali, R. C. Coombes, Endocrine-responsive breast cancer and strategies for combating resistance. *Nat Rev Cancer* **2**, 101-112 (2002).
10. D. Zhang *et al.*, Proteomic study reveals that proteins involved in metabolic and detoxification pathways are highly expressed in HER-2/neu-positive breast cancer. *Mol Cell Proteomics* **4**, 1686-1696 (2005).
11. Y. H. Zhao *et al.*, Upregulation of lactate dehydrogenase A by ErbB2 through heat shock factor 1 promotes breast cancer cell glycolysis and growth. *Oncogene* **28**, 3689-3701 (2009).
12. L. Shen *et al.*, Metabolic reprogramming in triple-negative breast cancer through Myc suppression of TXNIP. *Proc Natl Acad Sci U S A* **112**, 5425-5430 (2015).
13. J. O'Neal *et al.*, Inhibition of 6-phosphofructo-2-kinase (PFKFB3) suppresses glucose metabolism and the growth of HER2+ breast cancer. *Breast Cancer Res Treat* **160**, 29-40 (2016).
14. Y. Zhao *et al.*, Overcoming trastuzumab resistance in breast cancer by targeting dysregulated glucose metabolism. *Cancer Res* **71**, 4585-4597 (2011).
15. D. S. Wishart, Is Cancer a Genetic Disease or a Metabolic Disease? *EBioMedicine* **2**, 478-479 (2015).
16. O. Warburg, F. Wind, E. Negelein, The Metabolism of Tumors in the Body. *J Gen Physiol* **8**, 519-530 (1927).
17. M. G. Vander Heiden, L. C. Cantley, C. B. Thompson, Understanding the Warburg effect: the metabolic requirements of cell proliferation. *Science* **324**, 1029-1033 (2009).
18. N. N. Pavlova, C. B. Thompson, The Emerging Hallmarks of Cancer Metabolism. *Cell Metab* **23**, 27-47 (2016).
19. R. J. DeBerardinis, N. S. Chandel, Fundamentals of cancer metabolism. *Sci Adv* **2**, e1600200 (2016).
20. O. Warburg, On the origin of cancer cells. *Science* **123**, 309-314 (1956).
21. N. Majewski *et al.*, Hexokinase-mitochondria interaction mediated by Akt is required to inhibit apoptosis in the presence or absence of Bax and Bak. *Mol Cell* **16**, 819-830 (2004).

22. S. P. Mathupala, Y. H. Ko, P. L. Pedersen, Hexokinase II: cancer's double-edged sword acting as both facilitator and gatekeeper of malignancy when bound to mitochondria. *Oncogene* **25**, 4777-4786 (2006).
23. K. C. Patra *et al.*, Hexokinase 2 is required for tumor initiation and maintenance and its systemic deletion is therapeutic in mouse models of cancer. *Cancer Cell* **24**, 213-228 (2013).
24. X. Y. Zhang *et al.*, Hexokinase 2 confers resistance to cisplatin in ovarian cancer cells by enhancing cisplatin-induced autophagy. *Int J Biochem Cell Biol* **95**, 9-16 (2018).
25. A. Wolf *et al.*, Hexokinase 2 is a key mediator of aerobic glycolysis and promotes tumor growth in human glioblastoma multiforme. *J Exp Med* **208**, 313-326 (2011).
26. T. Atsumi *et al.*, High expression of inducible 6-phosphofructo-2-kinase/fructose-2,6-bisphosphatase (iPFK-2; PFKFB3) in human cancers. *Cancer Res* **62**, 5881-5887 (2002).
27. S. Mazurek, Pyruvate kinase type M2: a key regulator of the metabolic budget system in tumor cells. *Int J Biochem Cell Biol* **43**, 969-980 (2011).
28. M. S. Jurica *et al.*, The allosteric regulation of pyruvate kinase by fructose-1,6-bisphosphate. *Structure* **6**, 195-210 (1998).
29. W. J. Israelsen *et al.*, PKM2 isoform-specific deletion reveals a differential requirement for pyruvate kinase in tumor cells. *Cell* **155**, 397-409 (2013).
30. T. Noguchi, H. Inoue, T. Tanaka, The M1- and M2-type isozymes of rat pyruvate kinase are produced from the same gene by alternative RNA splicing. *J Biol Chem* **261**, 13807-13812 (1986).
31. C. V. Clower *et al.*, The alternative splicing repressors hnRNP A1/A2 and PTB influence pyruvate kinase isoform expression and cell metabolism. *Proc Natl Acad Sci U S A* **107**, 1894-1899 (2010).
32. C. J. David, M. Chen, M. Assanah, P. Canoll, J. L. Manley, HnRNP proteins controlled by c-Myc deregulate pyruvate kinase mRNA splicing in cancer. *Nature* **463**, 364-368 (2010).
33. B. Chaneton, E. Gottlieb, Rocking cell metabolism: revised functions of the key glycolytic regulator PKM2 in cancer. *Trends Biochem Sci* **37**, 309-316 (2012).
34. J. D. Dombrauckas, B. D. Santarsiero, A. D. Mesecar, Structural basis for tumor pyruvate kinase M2 allosteric regulation and catalysis. *Biochemistry* **44**, 9417-9429 (2005).
35. H. R. Christofk *et al.*, The M2 splice isoform of pyruvate kinase is important for cancer metabolism and tumour growth. *Nature* **452**, 230-233 (2008).
36. S. Mazurek, W. Zwerschke, P. Jansen-Durr, E. Eigenbrodt, Effects of the human papilloma virus HPV-16 E7 oncoprotein on glycolysis and glutaminolysis: role of pyruvate kinase type M2 and the glycolytic-enzyme complex. *Biochem J* **356**, 247-256 (2001).
37. T. L. Dayton, T. Jacks, M. G. Vander Heiden, PKM2, cancer metabolism, and the road ahead. *EMBO Rep* **17**, 1721-1730 (2016).
38. K. E. Keller, I. S. Tan, Y. S. Lee, SAICAR stimulates pyruvate kinase isoform M2 and promotes cancer cell survival in glucose-limited conditions. *Science* **338**, 1069-1072 (2012).
39. E. Eigenbrodt, D. Basenau, S. Holthusen, S. Mazurek, G. Fischer, Quantification of tumor type M2 pyruvate kinase (Tu M2-PK) in human carcinomas. *Anticancer Res* **17**, 3153-3156 (1997).
40. D. Anastasiou *et al.*, Pyruvate kinase M2 activators promote tetramer formation and suppress tumorigenesis. *Nat Chem Biol* **8**, 839-847 (2012).
41. G. M. Oremek, S. Teigelkamp, W. Kramer, E. Eigenbrodt, K. H. Usadel, The pyruvate kinase isoenzyme tumor M2 (Tu M2-PK) as a tumor marker for renal carcinoma. *Anticancer Res* **19**, 2599-2601 (1999).

42. G. M. Oremek, E. Eigenbrodt, J. Radle, S. Zeuzem, U. B. Seiffert, Value of the serum levels of the tumor marker TUM2-PK in pancreatic cancer. *Anticancer Res* **17**, 3031-3033 (1997).
43. H. Cerwenka *et al.*, TUM2-PK (pyruvate kinase type tumor M2), CA19-9 and CEA in patients with benign, malignant and metastasizing pancreatic lesions. *Anticancer Res* **19**, 849-851 (1999).
44. Q. Sun *et al.*, Mammalian target of rapamycin up-regulation of pyruvate kinase isoenzyme type M2 is critical for aerobic glycolysis and tumor growth. *Proc Natl Acad Sci U S A* **108**, 4129-4134 (2011).
45. K. E. Keller, Z. M. Doctor, Z. W. Dwyer, Y. S. Lee, SAICAR induces protein kinase activity of PKM2 that is necessary for sustained proliferative signaling of cancer cells. *Mol Cell* **53**, 700-709 (2014).
46. W. Ying, NAD+/NADH and NADP+/NADPH in cellular functions and cell death: regulation and biological consequences. *Antioxid Redox Signal* **10**, 179-206 (2008).
47. R. Possemato *et al.*, Functional genomics reveal that the serine synthesis pathway is essential in breast cancer. *Nature* **476**, 346-350 (2011).
48. G. M. DeNicola *et al.*, NRF2 regulates serine biosynthesis in non-small cell lung cancer. *Nat Genet* **47**, 1475-1481 (2015).
49. X. Gao, H. Wang, J. J. Yang, X. Liu, Z. R. Liu, Pyruvate kinase M2 regulates gene transcription by acting as a protein kinase. *Mol Cell* **45**, 598-609 (2012).
50. L. Lv *et al.*, Mitogenic and oncogenic stimulation of K433 acetylation promotes PKM2 protein kinase activity and nuclear localization. *Mol Cell* **52**, 340-352 (2013).
51. W. Yang *et al.*, ERK1/2-dependent phosphorylation and nuclear translocation of PKM2 promotes the Warburg effect. *Nat Cell Biol* **14**, 1295-1304 (2012).
52. X. Gao *et al.*, Reciprocal regulation of protein kinase and pyruvate kinase activities of pyruvate kinase M2 by growth signals. *J Biol Chem* **288**, 15971-15979 (2013).
53. W. Yang *et al.*, PKM2 phosphorylates histone H3 and promotes gene transcription and tumorigenesis. *Cell* **150**, 685-696 (2012).
54. S. R. Hwang *et al.*, Pyrimidine tract-binding protein 1 mediates pyruvate kinase M2-dependent phosphorylation of signal transducer and activator of transcription 3 and oncogenesis in anaplastic large cell lymphoma. *Lab Invest* **97**, 962-970 (2017).
55. P. Yang, Z. Li, R. Fu, H. Wu, Z. Li, Pyruvate kinase M2 facilitates colon cancer cell migration via the modulation of STAT3 signalling. *Cell Signal* **26**, 1853-1862 (2014).
56. W. Yang *et al.*, Nuclear PKM2 regulates beta-catenin transactivation upon EGFR activation. *Nature* **480**, 118-122 (2011).
57. J. Lee, H. K. Kim, Y. M. Han, J. Kim, Pyruvate kinase isozyme type M2 (PKM2) interacts and cooperates with Oct-4 in regulating transcription. *Int J Biochem Cell Biol* **40**, 1043-1054 (2008).
58. W. Luo *et al.*, Pyruvate kinase M2 is a PHD3-stimulated coactivator for hypoxia-inducible factor 1. *Cell* **145**, 732-744 (2011).
59. Y. Ikeda, T. Noguchi, Allosteric regulation of pyruvate kinase M2 isozyme involves a cysteine residue in the intersubunit contact. *J Biol Chem* **273**, 12227-12233 (1998).
60. K. Ashizawa, M. C. Willingham, C. M. Liang, S. Y. Cheng, In vivo regulation of monomer-tetramer conversion of pyruvate kinase subtype M2 by glucose is mediated via fructose 1,6-bisphosphate. *J Biol Chem* **266**, 16842-16846 (1991).
61. E. Bailey, F. Stirpe, C. B. Taylor, Regulation of rat liver pyruvate kinase. The effect of preincubation, pH, copper ions, fructose 1,6-diphosphate and dietary changes on enzyme activity. *Biochem J* **108**, 427-436 (1968).
62. A. Dabrowska, J. Pietkiewicz, K. Dabrowska, E. Czapinska, R. Danielewicz, Interaction of M1 and M2 isozymes pyruvate kinase from human tissues with phospholipids. *Biochim Biophys Acta* **1383**, 123-129 (1998).

63. G. Sparmann, J. Schulz, E. Hofmann, Effects of L-alanine and fructose (1,6-diphosphate) on pyruvate kinase from ehrlich ascites tumour cells. *FEBS Lett* **36**, 305-308 (1973).
64. B. Chaneton *et al.*, Serine is a natural ligand and allosteric activator of pyruvate kinase M2. *Nature* **491**, 458-462 (2012).
65. H. P. Morgan *et al.*, M2 pyruvate kinase provides a mechanism for nutrient sensing and regulation of cell proliferation. *Proc Natl Acad Sci U S A* **110**, 5881-5886 (2013).
66. T. Hitosugi *et al.*, Tyrosine phosphorylation inhibits PKM2 to promote the Warburg effect and tumor growth. *Sci Signal* **2**, ra73 (2009).
67. D. Anastasiou *et al.*, Inhibition of pyruvate kinase M2 by reactive oxygen species contributes to cellular antioxidant responses. *Science* **334**, 1278-1283 (2011).
68. L. Lv *et al.*, Acetylation targets the M2 isoform of pyruvate kinase for degradation through chaperone-mediated autophagy and promotes tumor growth. *Mol Cell* **42**, 719-730 (2011).
69. P. B. Garland, D. Shepherd, D. G. Nicholls, J. Ontko, Energy-dependent control of the tricarboxylic acid cycle by fatty acid oxidation in rat liver mitochondria. *Adv Enzyme Regul* **6**, 3-30 (1968).
70. E. A. Newsholme, P. J. Randle, K. L. Manchester, Inhibition of the phosphofructokinase reaction in perfused rat heart by respiration of ketone bodies, fatty acids and pyruvate. *Nature* **193**, 270-271 (1962).
71. P. J. Randle, P. B. Garland, C. N. Hales, E. A. Newsholme, The glucose fatty-acid cycle. Its role in insulin sensitivity and the metabolic disturbances of diabetes mellitus. *Lancet* **1**, 785-789 (1963).
72. G. Weber, M. A. Lea, N. B. Stamm, Sequential feedback inhibition and regulation of liver carbohydrate metabolism through control of enzyme activity. *Adv Enzyme Regul* **6**, 101-123 (1968).
73. C. Depre, S. Ponchaut, J. Deprez, L. Maisin, L. Hue, Cyclic AMP suppresses the inhibition of glycolysis by alternative oxidizable substrates in the heart. *J Clin Invest* **101**, 390-397 (1998).
74. N. H. Jeoung, R. A. Harris, Pyruvate dehydrogenase kinase-4 deficiency lowers blood glucose and improves glucose tolerance in diet-induced obese mice. *Am J Physiol Endocrinol Metab* **295**, E46-54 (2008).
75. A. P. Bhatt *et al.*, Dysregulation of fatty acid synthesis and glycolysis in non-Hodgkin lymphoma. *Proc Natl Acad Sci U S A* **109**, 11818-11823 (2012).
76. E. S. Reckzeh *et al.*, Inhibition of Glucose Transporters and Glutaminase Synergistically Impairs Tumor Cell Growth. *Cell Chem Biol* **26**, 1214-1228 e1225 (2019).
77. H. Lin *et al.*, Fatty acid oxidation is required for the respiration and proliferation of malignant glioma cells. *Neuro Oncol* **19**, 43-54 (2017).
78. J. A. Menendez, R. Lupu, Fatty acid synthase regulates estrogen receptor-alpha signaling in breast cancer cells. *Oncogenesis* **6**, e299 (2017).
79. J. V. Swinnen *et al.*, Overexpression of fatty acid synthase is an early and common event in the development of prostate cancer. *Int J Cancer* **98**, 19-22 (2002).
80. W. Zhao *et al.*, Fatty acid synthase: a novel target for antiglioma therapy. *Br J Cancer* **95**, 869-878 (2006).
81. D. Innocenzi *et al.*, Fatty acid synthase expression in melanoma. *J Cutan Pathol* **30**, 23-28 (2003).
82. J. V. Swinnen, K. Brusselmans, G. Verhoeven, Increased lipogenesis in cancer cells: new players, novel targets. *Curr Opin Clin Nutr Metab Care* **9**, 358-365 (2006).
83. C. Postic, J. Girard, The role of the lipogenic pathway in the development of hepatic steatosis. *Diabetes Metab* **34**, 643-648 (2008).
84. Q. Liu, Q. Luo, A. Halim, G. Song, Targeting lipid metabolism of cancer cells: A promising therapeutic strategy for cancer. *Cancer Lett* **401**, 39-45 (2017).

85. N. Koundouros, G. Poulogiannis, Reprogramming of fatty acid metabolism in cancer. *Br J Cancer* **122**, 4-22 (2020).
86. E. Audet-Walsh *et al.*, SREBF1 Activity Is Regulated by an AR/mTOR Nuclear Axis in Prostate Cancer. *Mol Cancer Res* **16**, 1396-1405 (2018).
87. G. Lee *et al.*, Post-transcriptional Regulation of De Novo Lipogenesis by mTORC1-S6K1-SRPK2 Signaling. *Cell* **171**, 1545-1558 e1518 (2017).
88. H. Q. Wang *et al.*, Positive feedback regulation between AKT activation and fatty acid synthase expression in ovarian carcinoma cells. *Oncogene* **24**, 3574-3582 (2005).
89. D. Guo *et al.*, An LXR agonist promotes glioblastoma cell death through inhibition of an EGFR/AKT/SREBP-1/LDLR-dependent pathway. *Cancer Discov* **1**, 442-456 (2011).
90. D. Guo *et al.*, EGFR signaling through an Akt-SREBP-1-dependent, rapamycin-resistant pathway sensitizes glioblastomas to antilipogenic therapy. *Sci Signal* **2**, ra82 (2009).
91. R. A. Saxton, D. M. Sabatini, mTOR Signaling in Growth, Metabolism, and Disease. *Cell* **168**, 960-976 (2017).
92. T. Porstmann *et al.*, SREBP activity is regulated by mTORC1 and contributes to Akt-dependent cell growth. *Cell Metab* **8**, 224-236 (2008).
93. Y. Guri *et al.*, mTORC2 Promotes Tumorigenesis via Lipid Synthesis. *Cancer Cell* **32**, 807-823 e812 (2017).
94. A. Nath, I. Li, L. R. Roberts, C. Chan, Elevated free fatty acid uptake via CD36 promotes epithelial-mesenchymal transition in hepatocellular carcinoma. *Sci Rep* **5**, 14752 (2015).
95. A. Ladanyi *et al.*, Adipocyte-induced CD36 expression drives ovarian cancer progression and metastasis. *Oncogene* **37**, 2285-2301 (2018).
96. Z. Madak-Erdogan *et al.*, Free Fatty Acids Rewire Cancer Metabolism in Obesity-Associated Breast Cancer via Estrogen Receptor and mTOR Signaling. *Cancer Res* **79**, 2494-2510 (2019).
97. E. Rysman *et al.*, De novo lipogenesis protects cancer cells from free radicals and chemotherapeutics by promoting membrane lipid saturation. *Cancer Res* **70**, 8117-8126 (2010).
98. R. Watanabe, L. Wei, J. Huang, mTOR signaling, function, novel inhibitors, and therapeutic targets. *J Nucl Med* **52**, 497-500 (2011).
99. D. Wang, R. N. Dubois, Eicosanoids and cancer. *Nat Rev Cancer* **10**, 181-193 (2010).
100. L. L. Listenberger *et al.*, Triglyceride accumulation protects against fatty acid-induced lipotoxicity. *Proc Natl Acad Sci U S A* **100**, 3077-3082 (2003).
101. M. T. Accioly *et al.*, Lipid bodies are reservoirs of cyclooxygenase-2 and sites of prostaglandin-E2 synthesis in colon cancer cells. *Cancer Res* **68**, 1732-1740 (2008).
102. R. V. Farese, Jr., T. C. Walther, Lipid droplets finally get a little R-E-S-P-E-C-T. *Cell* **139**, 855-860 (2009).
103. S. Yasuda *et al.*, Gene polymorphisms of tissue plasminogen activator and plasminogen activator inhibitor-1 in patients with antiphospholipid antibodies. *J Rheumatol* **29**, 1192-1197 (2002).
104. K. Tauchi-Sato, S. Ozeki, T. Houjou, R. Taguchi, T. Fujimoto, The surface of lipid droplets is a phospholipid monolayer with a unique Fatty Acid composition. *J Biol Chem* **277**, 44507-44512 (2002).
105. J. A. Olzmann, P. Carvalho, Dynamics and functions of lipid droplets. *Nat Rev Mol Cell Biol* **20**, 137-155 (2019).
106. M. J. Robenek *et al.*, Lipids partition caveolin-1 from ER membranes into lipid droplets: updating the model of lipid droplet biogenesis. *FASEB J* **18**, 866-868 (2004).

107. H. L. Ploegh, A lipid-based model for the creation of an escape hatch from the endoplasmic reticulum. *Nature* **448**, 435-438 (2007).
108. V. Choudhary, N. Jacquier, R. Schneiter, The topology of the triacylglycerol synthesizing enzyme Lro1 indicates that neutral lipids can be produced within the luminal compartment of the endoplasmatic reticulum: Implications for the biogenesis of lipid droplets. *Commun Integr Biol* **4**, 781-784 (2011).
109. V. Choudhary, N. Ojha, A. Golden, W. A. Prinz, A conserved family of proteins facilitates nascent lipid droplet budding from the ER. *J Cell Biol* **211**, 261-271 (2015).
110. A. R. Thiam, L. Foret, The physics of lipid droplet nucleation, growth and budding. *Biochim Biophys Acta* **1861**, 715-722 (2016).
111. N. T. Nettebrock, M. Bohnert, Born this way - Biogenesis of lipid droplets from specialized ER subdomains. *Biochim Biophys Acta Mol Cell Biol Lipids* **1865**, 158448 (2020).
112. P. R. Cullis, B. de Kruijff, Lipid polymorphism and the functional roles of lipids in biological membranes. *Biochim Biophys Acta* **559**, 399-420 (1979).
113. K. Ben M'barek *et al.*, ER Membrane Phospholipids and Surface Tension Control Cellular Lipid Droplet Formation. *Dev Cell* **41**, 591-604 e597 (2017).
114. Y. Y. Zaytseva *et al.*, Increased expression of fatty acid synthase provides a survival advantage to colorectal cancer cells via upregulation of cellular respiration. *Oncotarget* **6**, 18891-18904 (2015).
115. A. K. Cotte *et al.*, Lysophosphatidylcholine acyltransferase 2-mediated lipid droplet production supports colorectal cancer chemoresistance. *Nat Commun* **9**, 322 (2018).
116. B. Taib *et al.*, Lipid accumulation and oxidation in glioblastoma multiforme. *Sci Rep* **9**, 19593 (2019).
117. E. Clement *et al.*, Adipocyte extracellular vesicles carry enzymes and fatty acids that stimulate mitochondrial metabolism and remodeling in tumor cells. *EMBO J* **39**, e102525 (2020).
118. Y. Y. Wang *et al.*, Mammary adipocytes stimulate breast cancer invasion through metabolic remodeling of tumor cells. *JCI Insight* **2**, e87489 (2017).
119. E. Jarc *et al.*, Lipid droplets induced by secreted phospholipase A2 and unsaturated fatty acids protect breast cancer cells from nutrient and lipotoxic stress. *Biochim Biophys Acta Mol Cell Biol Lipids* **1863**, 247-265 (2018).
120. A. Pucer *et al.*, Group X secreted phospholipase A(2) induces lipid droplet formation and prolongs breast cancer cell survival. *Mol Cancer* **12**, 111 (2013).
121. C. Corbet *et al.*, TGFbeta2-induced formation of lipid droplets supports acidosis-driven EMT and the metastatic spreading of cancer cells. *Nat Commun* **11**, 454 (2020).
122. A. M. Giudetti *et al.*, A specific lipid metabolic profile is associated with the epithelial mesenchymal transition program. *Biochim Biophys Acta Mol Cell Biol Lipids* **1864**, 344-357 (2019).
123. H. J. Wright *et al.*, CDCP1 drives triple-negative breast cancer metastasis through reduction of lipid-droplet abundance and stimulation of fatty acid oxidation. *Proc Natl Acad Sci U S A* **114**, E6556-E6565 (2017).
124. R. Gushima *et al.*, Expression of adipophilin in gastric epithelial neoplasia is associated with intestinal differentiation and discriminates between adenoma and adenocarcinoma. *Virchows Arch* **468**, 169-177 (2016).
125. X. D. Zhang *et al.*, Identification of adipophilin as a potential diagnostic tumor marker for lung adenocarcinoma. *Int J Clin Exp Med* **7**, 1190-1196 (2014).
126. M. Fujimoto *et al.*, Adipophilin expression in cutaneous malignant melanoma. *J Cutan Pathol* **44**, 228-236 (2017).
127. K. Wang *et al.*, PLIN3 is up-regulated and correlates with poor prognosis in clear cell renal cell carcinoma. *Urol Oncol* **36**, 343 e349-343 e319 (2018).

128. M. Fujimoto *et al.*, Adipophilin expression in lung adenocarcinoma is associated with apocrine-like features and poor clinical prognosis: an immunohistochemical study of 328 cases. *Histopathology* **70**, 232-241 (2017).
129. M. Yao *et al.*, Expression of adipose differentiation-related protein: a predictor of cancer-specific survival in clear cell renal carcinoma. *Clin Cancer Res* **13**, 152-160 (2007).
130. A. Herms *et al.*, AMPK activation promotes lipid droplet dispersion on detyrosinated microtubules to increase mitochondrial fatty acid oxidation. *Nat Commun* **6**, 7176 (2015).
131. J. Zhu *et al.*, Phosphorylation of PLIN3 by AMPK promotes dispersion of lipid droplets during starvation. *Protein Cell* **10**, 382-387 (2019).
132. B. Englinger *et al.*, Lipid droplet-mediated scavenging as novel intrinsic and adaptive resistance factor against the multikinase inhibitor ponatinib. *Int J Cancer* **147**, 1680-1693 (2020).
133. R. Dubey *et al.*, Lipid droplets can promote drug accumulation and activation. *Nat Chem Biol* **16**, 206-213 (2020).
134. A. Carnero *et al.*, The cancer stem-cell signaling network and resistance to therapy. *Cancer Treat Rev* **49**, 25-36 (2016).
135. M. Todaro *et al.*, Colon cancer stem cells dictate tumor growth and resist cell death by production of interleukin-4. *Cell Stem Cell* **1**, 389-402 (2007).
136. R. Bjerkvig, B. B. Tysnes, K. S. Aboody, J. Najbauer, A. J. Terzis, Opinion: the origin of the cancer stem cell: current controversies and new insights. *Nat Rev Cancer* **5**, 899-904 (2005).
137. Y. Cho *et al.*, Cleaved CD44 intracellular domain supports activation of stemness factors and promotes tumorigenesis of breast cancer. *Oncotarget* **6**, 8709-8721 (2015).
138. J. Cui, P. Li, X. Liu, H. Hu, W. Wei, Abnormal expression of the Notch and Wnt/beta-catenin signaling pathways in stem-like ALDH(hi)CD44(+) cells correlates highly with Ki-67 expression in breast cancer. *Oncol Lett* **9**, 1600-1606 (2015).
139. A. N. Seo *et al.*, Expression of breast cancer stem cell markers as predictors of prognosis and response to trastuzumab in HER2-positive breast cancer. *Br J Cancer* **114**, 1109-1116 (2016).
140. C. Joseph *et al.*, Overexpression of the cancer stem cell marker CD133 confers a poor prognosis in invasive breast cancer. *Breast Cancer Res Treat* **174**, 387-399 (2019).
141. C. Bock *et al.*, Strong correlation between N-cadherin and CD133 in breast cancer: role of both markers in metastatic events. *J Cancer Res Clin Oncol* **140**, 1873-1881 (2014).
142. F. Brugnoli *et al.*, Up-modulation of PLC-beta2 reduces the number and malignancy of triple-negative breast tumor cells with a CD133(+)/EpCAM(+) phenotype: a promising target for preventing progression of TNBC. *BMC Cancer* **17**, 617 (2017).
143. T. Hiraga, S. Ito, H. Nakamura, EpCAM expression in breast cancer cells is associated with enhanced bone metastasis formation. *Int J Cancer* **138**, 1698-1708 (2016).
144. C. Hadjimichael *et al.*, Common stemness regulators of embryonic and cancer stem cells. *World J Stem Cells* **7**, 1150-1184 (2015).
145. D. Wang *et al.*, Oct-4 and Nanog promote the epithelial-mesenchymal transition of breast cancer stem cells and are associated with poor prognosis in breast cancer patients. *Oncotarget* **5**, 10803-10815 (2014).
146. F. Yang, J. Zhang, H. Yang, OCT4, SOX2, and NANOG positive expression correlates with poor differentiation, advanced disease stages, and worse overall

survival in HER2(+) breast cancer patients. *Onco Targets Ther* **11**, 7873-7881 (2018).
147. C. Zhang, C. Li, F. He, Y. Cai, H. Yang, Identification of CD44+CD24+ gastric cancer stem cells. *J Cancer Res Clin Oncol* **137**, 1679-1686 (2011).
148. G. Mannelli, O. Gallo, Cancer stem cells hypothesis and stem cells in head and neck cancers. *Cancer Treat Rev* **38**, 515-539 (2012).
149. J. Dou, N. Gu, Emerging strategies for the identification and targeting of cancer stem cells. *Tumour Biol* **31**, 243-253 (2010).
150. M. Peiris-Pages, U. E. Martinez-Outschoorn, R. G. Pestell, F. Sotgia, M. P. Lisanti, Cancer stem cell metabolism. *Breast Cancer Res* **18**, 55 (2016).
151. M. Sun, Z. Yang, Metabolomic Studies of Live Single Cancer Stem Cells Using Mass Spectrometry. *Anal Chem* **91**, 2384-2391 (2019).
152. R. Mancini *et al.*, Metabolic features of cancer stem cells: the emerging role of lipid metabolism. *Oncogene* **37**, 2367-2378 (2018).
153. K. Song *et al.*, Active glycolytic metabolism in CD133(+) hepatocellular cancer stem cells: regulation by MIR-122. *Oncotarget* **6**, 40822-40835 (2015).
154. P. P. Liu *et al.*, Metabolic regulation of cancer cell side population by glucose through activation of the Akt pathway. *Cell Death Differ* **21**, 124-135 (2014).
155. C. Dong *et al.*, Loss of FBP1 by Snail-mediated repression provides metabolic advantages in basal-like breast cancer. *Cancer Cell* **23**, 316-331 (2013).
156. Y. Zhou *et al.*, Metabolic alterations in highly tumorigenic glioblastoma cells: preference for hypoxia and high dependency on glycolysis. *J Biol Chem* **286**, 32843-32853 (2011).
157. B. L. Emmink *et al.*, The secretome of colon cancer stem cells contains drug-metabolizing enzymes. *J Proteomics* **91**, 84-96 (2013).
158. J. Liao *et al.*, Ovarian cancer spheroid cells with stem cell-like properties contribute to tumor generation, metastasis and chemotherapy resistance through hypoxia-resistant metabolism. *PLoS One* **9**, e84941 (2014).
159. Y. A. Shen, C. Y. Wang, Y. T. Hsieh, Y. J. Chen, Y. H. Wei, Metabolic reprogramming orchestrates cancer stem cell properties in nasopharyngeal carcinoma. *Cell Cycle* **14**, 86-98 (2015).
160. P. Sancho *et al.*, MYC/PGC-1alpha Balance Determines the Metabolic Phenotype and Plasticity of Pancreatic Cancer Stem Cells. *Cell Metab* **22**, 590-605 (2015).
161. M. Janiszewska *et al.*, Imp2 controls oxidative phosphorylation and is crucial for preserving glioblastoma cancer stem cells. *Genes Dev* **26**, 1926-1944 (2012).
162. E. D. Lagadinou *et al.*, BCL-2 inhibition targets oxidative phosphorylation and selectively eradicates quiescent human leukemia stem cells. *Cell Stem Cell* **12**, 329-341 (2013).
163. T. Simsek *et al.*, The distinct metabolic profile of hematopoietic stem cells reflects their location in a hypoxic niche. *Cell Stem Cell* **7**, 380-390 (2010).
164. W. Zhao *et al.*, Candidate Antimetastasis Drugs Suppress the Metastatic Capacity of Breast Cancer Cells by Reducing Membrane Fluidity. *Cancer Res* **76**, 2037-2049 (2016).
165. H. Ye *et al.*, Leukemic Stem Cells Evade Chemotherapy by Metabolic Adaptation to an Adipose Tissue Niche. *Cell Stem Cell* **19**, 23-37 (2016).
166. C. L. Chen *et al.*, NANOG Metabolically Reprograms Tumor-Initiating Stem-like Cells through Tumorigenic Changes in Oxidative Phosphorylation and Fatty Acid Metabolism. *Cell Metab* **23**, 206-219 (2016).
167. I. Samudio *et al.*, Pharmacologic inhibition of fatty acid oxidation sensitizes human leukemia cells to apoptosis induction. *J Clin Invest* **120**, 142-156 (2010).
168. M. Humbert *et al.*, Reducing FASN expression sensitizes acute myeloid leukemia cells to differentiation therapy. *Cell Death Differ* 10.1038/s41418-021-00768-1 (2021).

169. Y. Yasumoto *et al.*, Inhibition of Fatty Acid Synthase Decreases Expression of Stemness Markers in Glioma Stem Cells. *PLoS One* **11**, e0147717 (2016).
170. A. Noto *et al.*, Stearoyl-CoA desaturase-1 is a key factor for lung cancer-initiating cells. *Cell Death Dis* **4**, e947 (2013).
171. A. Noto *et al.*, Stearoyl-CoA-desaturase 1 regulates lung cancer stemness via stabilization and nuclear localization of YAP/TAZ. *Oncogene* **36**, 4573-4584 (2017).
172. J. Li *et al.*, Lipid Desaturation Is a Metabolic Marker and Therapeutic Target of Ovarian Cancer Stem Cells. *Cell Stem Cell* **20**, 303-314 e305 (2017).
173. L. B. Hoang-Minh *et al.*, Infiltrative and drug-resistant slow-cycling cells support metabolic heterogeneity in glioblastoma. *EMBO J* **37** (2018).
174. R. Mitra, O. Chao, Y. Urasaki, O. B. Goodman, T. T. Le, Detection of lipid-rich prostate circulating tumour cells with coherent anti-Stokes Raman scattering microscopy. *BMC Cancer* **12**, 540 (2012).
175. L. Tirinato *et al.*, Lipid droplets: a new player in colorectal cancer stem cells unveiled by spectroscopic imaging. *Stem cells* **33**, 35-44 (2015).
176. S. R. Singh *et al.*, The lipolysis pathway sustains normal and transformed stem cells in adult Drosophila. *Nature* **538**, 109-113 (2016).
177. J. A. Ajani, S. Song, H. S. Hochster, I. B. Steinberg, Cancer stem cells: the promise and the potential. *Semin Oncol* **42 Suppl 1**, S3-17 (2015).
178. A. Recasens, L. Munoz, Targeting Cancer Cell Dormancy. *Trends Pharmacol Sci* **40**, 128-141 (2019).
179. K. M. Havas *et al.*, Metabolic shifts in residual breast cancer drive tumor recurrence. *J Clin Invest* **127**, 2091-2105 (2017).
180. P. J. Randle, Regulatory interactions between lipids and carbohydrates: the glucose fatty acid cycle after 35 years. *Diabetes Metab Rev* **14**, 263-283 (1998).
181. L. L. Listenberger, D. A. Brown, Fluorescent detection of lipid droplets and associated proteins. *Curr Protoc Cell Biol* **Chapter 24**, Unit 24 22 (2007).
182. F. L. Shaw *et al.*, A detailed mammosphere assay protocol for the quantification of breast stem cell activity. *J Mammary Gland Biol Neoplasia* **17**, 111-117 (2012).
183. B. Gyorffy, A. Lanczky, Z. Szallasi, Implementing an online tool for genome-wide validation of survival-associated biomarkers in ovarian-cancer using microarray data from 1287 patients. *Endocr Relat Cancer* **19**, 197-208 (2012).
184. E. Beck-Garcia, K. Beck-Garcia, A. Schlosser, W. W. Schamel, Analysis of interactions between proteins and fatty acids or cholesterol using a fatty acid/cholesterol pull-down assay. *Anal Biochem* **436**, 75-77 (2013).
185. E. Kaiser, R. L. Colescott, C. D. Bossinger, P. I. Cook, Color test for detection of free terminal amino groups in the solid-phase synthesis of peptides. *Anal Biochem* **34**, 595-598 (1970).
186. P. D. Adams *et al.*, PHENIX: building new software for automated crystallographic structure determination. *Acta Crystallogr D Biol Crystallogr* **58**, 1948-1954 (2002).
187. P. Emsley, B. Lohkamp, W. G. Scott, K. Cowtan, Features and development of Coot. *Acta Crystallogr D Biol Crystallogr* **66**, 486-501 (2010).
188. B. J. Hershey, R. Vazzana, D. L. Joppi, K. M. Havas, Lipid Droplets Define a Sub-Population of Breast Cancer Stem Cells. *J Clin Med* **9** (2019).
189. R. M. Neve *et al.*, A collection of breast cancer cell lines for the study of functionally distinct cancer subtypes. *Cancer Cell* **10**, 515-527 (2006).
190. A. Prat *et al.*, Phenotypic and molecular characterization of the claudin-low intrinsic subtype of breast cancer. *Breast Cancer Res* **12**, R68 (2010).
191. P. Greenspan, E. P. Mayer, S. D. Fowler, Nile red: a selective fluorescent stain for intracellular lipid droplets. *J Cell Biol* **100**, 965-973 (1985).
192. G. Dontu *et al.*, In vitro propagation and transcriptional profiling of human mammary stem/progenitor cells. *Genes Dev* **17**, 1253-1270 (2003).

193. D. Ponti *et al.*, Isolation and in vitro propagation of tumorigenic breast cancer cells with stem/progenitor cell properties. *Cancer Res* **65**, 5506-5511 (2005).
194. J. Kasurinen, A novel fluorescent fatty acid, 5-methyl-BDY-3-dodecanoic acid, is a potential probe in lipid transport studies by incorporating selectively to lipid classes of BHK cells. *Biochem Biophys Res Commun* **187**, 1594-1601 (1992).
195. D. S. Wishart *et al.*, HMDB 4.0: the human metabolome database for 2018. *Nucleic Acids Res* **46**, D608-D617 (2018).
196. M. Al-Hajj, M. S. Wicha, A. Benito-Hernandez, S. J. Morrison, M. F. Clarke, Prospective identification of tumorigenic breast cancer cells. *Proc Natl Acad Sci U S A* **100**, 3983-3988 (2003).
197. R. W. Brownsey, A. N. Boone, J. E. Elliott, J. E. Kulpa, W. M. Lee, Regulation of acetyl-CoA carboxylase. *Biochem Soc Trans* **34**, 223-227 (2006).
198. J. P. Bonnefont *et al.*, Carnitine palmitoyltransferases 1 and 2: biochemical, molecular and medical aspects. *Mol Aspects Med* **25**, 495-520 (2004).
199. D. L. Halvorson, S. A. McCune, Inhibition of fatty acid synthesis in isolated adipocytes by 5-(tetradecyloxy)-2-furoic acid. *Lipids* **19**, 851-856 (1984).
200. M. A. Lea, G. Weber, Inhibition of glycolytic enzymes of normal and neoplastic liver by free fatty acids. *Biochem J* **104**, 37P (1967).
201. Z. Zhang *et al.*, PKM2, function and expression and regulation. *Cell Biosci* **9**, 52 (2019).
202. F. Madeira *et al.*, The EMBL-EBI search and sequence analysis tools APIs in 2019. *Nucleic Acids Res* **47**, W636-W641 (2019).
203. J. German, Bloom's syndrome. XX. The first 100 cancers. *Cancer Genet Cytogenet* **93**, 100-106 (1997).
204. J. A. Macpherson *et al.*, Functional cross-talk between allosteric effects of activating and inhibiting ligands underlies PKM2 regulation. *Elife* **8** (2019).
205. V. V. Rostovtsev, L. G. Green, V. V. Fokin, K. B. Sharpless, A stepwise huisgen cycloaddition process: copper(I)-catalyzed regioselective "ligation" of azides and terminal alkynes. *Angew Chem Int Ed Engl* **41**, 2596-2599 (2002).
206. P. Wang, C. Sun, T. Zhu, Y. Xu, Structural insight into mechanisms for dynamic regulation of PKM2. *Protein Cell* **6**, 275-287 (2015).
207. S. Wu *et al.*, Cellular, transcriptomic and isoform heterogeneity of breast cancer cell line revealed by full-length single-cell RNA sequencing. *Comput Struct Biotechnol J* **18**, 676-685 (2020).
208. F. Francescangeli *et al.*, Proliferation state and polo-like kinase1 dependence of tumorigenic colon cancer cells. *Stem Cells* **30**, 1819-1830 (2012).
209. M. J. Thun, S. J. Henley, C. Patrono, Nonsteroidal anti-inflammatory drugs as anticancer agents: mechanistic, pharmacologic, and clinical issues. *J Natl Cancer Inst* **94**, 252-266 (2002).
210. C. Wang *et al.*, Acetyl-CoA carboxylase-alpha inhibitor TOFA induces human cancer cell apoptosis. *Biochem Biophys Res Commun* **385**, 302-306 (2009).
211. M. G. Vander Heiden *et al.*, Evidence for an alternative glycolytic pathway in rapidly proliferating cells. *Science* **329**, 1492-1499 (2010).
212. D. Y. Gui, C. A. Lewis, M. G. Vander Heiden, Allosteric regulation of PKM2 allows cellular adaptation to different physiological states. *Sci Signal* **6**, pe7 (2013).
213. S. L. Pinkosky *et al.*, Long-chain fatty acyl-CoA esters regulate metabolism via allosteric control of AMPK beta1 isoforms. *Nat Metab* **2**, 873-881 (2020).
214. B. Viollet *et al.*, AMPK inhibition in health and disease. *Crit Rev Biochem Mol Biol* **45**, 276-295 (2010).
215. B. van den Berg, P. N. Black, W. M. Clemons, Jr., T. A. Rapoport, Crystal structure of the long-chain fatty acid transporter FadL. *Science* **304**, 1506-1509 (2004).

216. Q. Li *et al.*, Butyrate Suppresses the Proliferation of Colorectal Cancer Cells via Targeting Pyruvate Kinase M2 and Metabolic Reprogramming. *Mol Cell Proteomics* **17**, 1531-1545 (2018).
217. C. Benesch *et al.*, The clinicopathological and prognostic relevance of pyruvate kinase M2 and pAkt expression in breast cancer. *Anticancer Res* **30**, 1689-1694 (2010).
218. Q. Zheng *et al.*, Long noncoding RNA MEG3 suppresses liver cancer cells growth through inhibiting beta-catenin by activating PKM2 and inactivating PTEN. *Cell Death Dis* **9**, 253 (2018).
219. K. Taniguchi *et al.*, MicroRNA-124 inhibits cancer cell growth through PTB1/PKM1/PKM2 feedback cascade in colorectal cancer. *Cancer Lett* **363**, 17-27 (2015).
220. H. S. Shi *et al.*, Silencing of pkm2 increases the efficacy of docetaxel in human lung cancer xenografts in mice. *Cancer Sci* **101**, 1447-1453 (2010).
221. D. Shang *et al.*, Metformin increases sensitivity of osteosarcoma stem cells to cisplatin by inhibiting expression of PKM2. *Int J Oncol* **50**, 1848-1856 (2017).
222. I. Park *et al.*, Changes in pyruvate metabolism detected by magnetic resonance imaging are linked to DNA damage and serve as a sensor of temozolomide response in glioblastoma cells. *Cancer Res* **74**, 7115-7124 (2014).
223. J. Chen *et al.*, Shikonin and its analogs inhibit cancer cell glycolysis by targeting tumor pyruvate kinase-M2. *Oncogene* **30**, 4297-4306 (2011).
224. J. C. Boulos, M. Rahama, M. F. Hegazy, T. Efferth, Shikonin derivatives for cancer prevention and therapy. *Cancer Lett* **459**, 248-267 (2019).
225. L. E. Landree *et al.*, C75, a fatty acid synthase inhibitor, modulates AMP-activated protein kinase to alter neuronal energy metabolism. *J Biol Chem* **279**, 3817-3827 (2004).
226. M. Wu *et al.*, Antidiabetic and antisteatotic effects of the selective fatty acid synthase (FAS) inhibitor platensimycin in mouse models of diabetes. *Proc Natl Acad Sci U S A* **108**, 5378-5383 (2011).
227. D. Jia, J. H. Park, K. H. Jung, H. Levine, B. A. Kaipparettu, Elucidating the Metabolic Plasticity of Cancer: Mitochondrial Reprogramming and Hybrid Metabolic States. *Cells* **7** (2018).

Appendix - List of collaborations

This Ph.D. thesis includes results carried out with the support of valuable collaborations:

- Flow cytometry and qPCR analyses were performed by the Scientific Service of Cogentech, IFOM, Milan (Italy);

- The chemical synthesis of the lipid probe *prop-2-yn-1-yl-2-(3-tridecyl-3-diazirin-3-yl) acetate* was conducted by Dmytro Yushchenko of the Institute of Organic Chemistry and Biochemistry of Prague (Czech Republic);

- Structural and crystallization studies were conducted in by Dr. Sebastiano Pasqualato at the Biochemistry and Structural Biology Unit of the European Institute of Oncology (IEO) of Milan (Italy).